











A Fresh Look at AGB stars in Galactic Open Clusters with *Gaia*: Impact on Stellar Models and the Initial-Final Mass Relation

PAOLA MARIGO ¹, DIEGO BOSSINI ², MICHELE TRABUCCHI ³, FRANCESCO ADDARI ⁴, LÉO GIRARDI ⁵,
JEFFREY CUMMINGS ⁶, GIADA PASTORELLI ⁷, PIERO DAL TIO ¹, GUGLIELMO COSTA ¹ AND
ALESSANDRO BRESSAN ⁴

¹*Department of Physics and Astronomy G. Galilei, University of Padova, Vicolo dell'Osservatorio 3, I-35122, Padova, Italy*

²*Instituto de Astrofísica e Ciências do Espaço, Universidade do Porto CAUP, Rua das Estrelas, PT4150-762 Porto, Portugal*

³*Astronomy Department, Geneva University Ch. Pegasi 51, CH-1290 Versoix, Switzerland*

⁴*SISSA, via Bonomea 265, I-34136 Trieste, Italy*

⁵*INAF-Osservatorio Astronomico di Padova Vicolo dell'Osservatorio 5, I-35122 Padova, Italy*

⁶*Department of Astronomy, Indiana University, 727 E 3rd Street, Bloomington, IN 47405, USA*

⁷*STScI, 3700 San Martin Drive, Baltimore, MD 21218, USA*

(Received September, 2021; Revised xxx, 2021; Accepted November 8, 2021)

Submitted to ApJ

ABSTRACT

Benefiting from the *Gaia* second and early third releases of photometric and astrometric data we examine the population of asymptotic giant branch (AGB) stars that appear in the fields of intermediate-age and young open star clusters. We identify 49 AGB star candidates, brighter than the tip of the red giant branch, with a good-to-high cluster membership probability. Among them we find 19 TP-AGB stars with known spectral type: 4 M stars, 3 MS/S stars and 12 C stars. By combining observations, stellar models, and radiative transfer calculations that include the effect of circumstellar dust, we characterize each star in terms of initial mass, luminosity, mass-loss rate, core mass, period and mode of pulsation. The information collected helps us shed light on the TP-AGB evolution at solar-like metallicity, placing constraints on the third dredge-up process, the initial masses of carbon stars, stellar winds, and the initial-final mass relation (IFMR). In particular, we find that two bright carbon stars, MSB 75 and BM IV 90, members of the clusters NGC 7789 and NGC 2660 (with similar ages of $\simeq 1.2 - 1.6$ Gyr and initial masses $2.1 \gtrsim M_i/M_\odot \gtrsim 1.9$), have unusually high core masses, $M_c \approx 0.67 - 0.7 M_\odot$. These results support the findings of a recent work (Marigo et al. 2020) that identified a kink in the IFMR, which interrupts its monotonic trend just at the same initial masses. Finally, we investigate two competing scenarios to explain the M_c data: the role of stellar winds in single-star evolution, and binary interactions through the blue-straggler channel.

Keywords: Open star clusters — Asymptotic giant branch stars — Carbon stars — Long period variable stars — Stellar winds — Circumstellar dust — Stellar evolution

1. INTRODUCTION

The final stages of the evolution of low and intermediate mass stars, the so-called thermally-pulsing asymptotic giant branch (TP-AGB) phase, are important drivers of the evolution of galaxies, contributing to their

integrated light (e.g., Bruzual 2007; Maraston et al. 2006) and chemical enrichment in the form of gas and dust expelled by stellar winds (e.g., Ventura et al. 2018; Slemer et al. 2017; Nanni et al. 2014; Cristallo et al. 2011; Ferrarotti & Gail 2006; Karakas et al. 2002; Marigo 2001). The complexity of the physical processes that characterize the TP-AGB phase makes stellar modeling particularly difficult and the predictions are sometimes very uncertain. For example, the predicted efficiency of the third dredge-up (3DU) or of the hot-bottom burning

(HBB) process still does not find an agreement among the different evolution codes, due to the rough treatment of convection and mixing, and the sensitivity to numerical details (e.g., Wagstaff et al. 2020; Marigo et al. 2013; Ventura & D’Antona 2005; Frost & Lattanzio 1996)

In this context, observations play a key role, as they can place constraints on processes whose physics are still poorly defined (Marigo 2015). Moreover, through observations of AGB stars in different environments it is possible to study their dependence on metallicity (Marigo & Girardi 2007).

The Magellanic Clouds are fundamental calibrators of the intermediate-metallicity regime ($-0.2 \lesssim [\text{Fe}/\text{H}] \lesssim -0.4$) thanks to their large population of AGB stars both in the field (Boyer et al. 2011; Meixner et al. 2006; Blum et al. 2006), and in massive globular clusters (Frogel et al. 1990; Maraston 2005; Pessev et al. 2008; Noël et al. 2013). Various works have focused on Magellanic Clouds in the attempt to calibrate mass loss, third dredge-up and hot-bottom burning either through the population synthesis technique (Pastorelli et al. 2020, 2019; Girardi & Marigo 2007; Marigo et al. 1999), or using single AGB tracks (Wagstaff et al. 2020; Ventura et al. 2015; Dell’Aglì et al. 2015; Kamath et al. 2012, 2010; Lebzelter et al. 2008; Ventura et al. 2000), or with radiative transfer calculations across dusty circumstellar envelopes (Nanni et al. 2019, 2018; Groenewegen & Sloan 2018; Gullieuszik et al. 2012; Sargent et al. 2011; Srinivasan et al. 2011; Groenewegen et al. 2009). The Magellanic Clouds have also been serving as ideal laboratories for studying the variability of AGB stars (e.g. Feast et al. 1989; Wood et al. 1999; Wood 2000; Cioni et al. 2003; Whitelock et al. 2008; Soszyński et al. 2009, 2011, 2013; Riebel et al. 2015; Ita et al. 2018; Goldman et al. 2019), and in particular for modeling their pulsation (e.g. Wood & Sebo 1996; Wood et al. 1999; Soszyński et al. 2007; Wood 2015; Trabucchi et al. 2017, 2019, 2021b). At low metallicities ($[\text{Fe}/\text{H}] \lesssim -0.9$), the calibration has been extended to AGB star samples in dwarf galaxies (Rosenfield et al. 2014; Girardi et al. 2010) from the ANGST survey (Dalcanton et al. 2009).

In the solar-like metallicity regime, a relevant source of information comes from the Andromeda galaxy (M31) thanks to the extraordinary photometric data provided by the PHAT survey (Dalcanton et al. 2012; Boyer et al. 2013), which also made it possible to identify 2753 star clusters with $\simeq 294$ candidate AGB stars (Girardi et al. 2020). Another valuable tool is the semi-empirical IFMR which links the initial mass of low- and intermediate-mass stars with the final mass of white dwarfs left behind on their death (e.g., Barnett et al. 2021; Cummings et al. 2018; El-Badry et al. 2018; Salaris

et al. 2009). Recent studies have shown the great potential of the IFMR in placing constraints on mass loss, third dredge-up, and hot-bottom burning of the progenitor stars (e.g., Althaus et al. 2021; Marigo et al. 2020; Kalirai et al. 2014). In the IFMR context, it is worth mentioning the work by Fragkou et al. (2019) who measured the central star mass of a planetary nebula, member of the open cluster Andrews–Lindsay 1.

The solar-metallicity calibration based on Milky Way AGB stars has so far been hampered by the severe uncertainties on their distances, and by the fact that the TP-AGB population in star clusters is very small, except for some notable exceptions, such as the old globular clusters 47 Tuc (Lebzelter & Wood 2005; McDonald et al. 2011a; Momany et al. 2012; Lebzelter et al. 2014) and ω Cen (Boyer et al. 2008; McDonald et al. 2009, 2011b).

The situation is now remarkably improving thanks to the advent of the *Gaia* satellite and its data releases, in particular Gaia Collaboration et al. (2018, *Gaia* DR2) and Gaia Collaboration et al. (2021, *Gaia* EDR3). Despite some intrinsic issues related to the variability and surface dynamics of AGB stars (Chiavassa et al. 2018), we can rely on much better parallaxes than ever, which paves the way for detailed studies also in the Milky Way. When combined with near-infrared (NIR) data, the full-sky, multi-epoch optical photometry provided by *Gaia* is especially promising for characterizing the chemistry and evolutionary stage of evolved red giants, in particular AGB stars (Lebzelter et al. 2018, 2019). Recently, Abia et al. (2020) derived the luminosity function and the kinematic properties of a sample of 210 field carbon stars in the solar neighborhood, having measured parallaxes with relative errors of less than 20%.

A limitation in using field stars is that the ages, and therefore the initial masses of the progenitors, are not easily known. This weakness can potentially be overcome if AGB stars belong to star clusters, which are routinely dated with stellar isochrones. In this respect, Milky Way open clusters are potentially suitable targets, as they cover a wide age range ($\approx 0.001 - 10$ Gyr) where AGB stars can be found. It is dutiful to recall the early efforts made in the past to visually identify AGB stars on photographic plates and report them as probable cluster members: some of the carbon stars analyzed in this work were discovered roughly 50 years ago! The interested reader may refer to the papers of Gaustad & Conti (1971); Hartwick & Hesser (1971, 1973); Catchpole & Feast (1973); Kalinowski et al. (1974); Jorgensen & Westerlund (1988); Eggen & Iben (1991).

Since those first studies until today, AGB stars in open clusters have been largely neglected due to two main

problems: the small-number statistics (in the best cases no more than one or two TP-AGB stars are expected per cluster, and very often none), and the difficulty to assess reliable cluster membership.

With *Gaia* this last limitation has been overcome and we now have large catalogs available that provide astrometric data and membership probabilities for the stars of many open clusters (Monteiro et al. 2020; Castro-Ginard et al. 2020; Ferreira et al. 2020; Cantat-Gaudin & Anders 2020; Liu & Pang 2019; Castro-Ginard et al. 2019; Cantat-Gaudin et al. 2018). Using the data from *Gaia* DR2, Pal & Worthey (2021) recently identified 9 carbon stars, likely members of open clusters covering a large age range, $\simeq 0.03 - 3.20$ Gyr, and studied their frequency normalized to the integrated luminosity of the host cluster, N_C/L_V , as a function of the turn-off mass M_{TO} , or equally of the cluster age. Their study indicates that the normalized frequency of carbon stars peaks at $M_{TO} \simeq 1.7 M_\odot$, and drops to zero for $M_{TO} < 1.24 M_\odot$. This piece of information is useful to constrain the AGB contribution to the integrated light of galaxies.

Spurred by the new perspective offered by *Gaia* (DR2 and EDR3), in this study we aim to carry out a systematic analysis of AGB stars in open clusters and to characterize them as much as possible by exploiting the observational data (parallax and proper motion, spectral type, spectral energy distribution, light curve and pulsation period) and coupling them with stellar models and radiative transfer calculations that include the effect of circumstellar dust.

The paper is structured as follows. In Sect. 2 we select a sample of bright near-infrared evolved giants and supergiants, likely members of open clusters, using membership data and cluster ages from *Gaia* DR2-based catalogs (Cantat-Gaudin & Anders 2020; Cantat-Gaudin et al. 2020), and the diagnostic *Gaia*-2MASS diagram, originally designed by Lebzelter et al. (2018). Starting from this sample, in Sect. 3 we extract the candidate AGB stars by means of suitable photometric and age criteria, and discuss their main characteristics as a function of spectral type (M, S, C) and initial stellar mass. Sect. 4 reviews the main information available for the 19 identified TP-AGB stars with assigned spectral type. We add, whenever possible, variability information and new period estimates from the analysis of available light curves. In Sect. 4.2 we introduce and discuss the AGB star parallaxes from *Gaia* EDR3, and apply two different prescriptions for the zero-point correction, namely Lindegren et al. (2021a), and Groenewegen 2021. We use the new *Gaia* EDR3 astrometric and kinematic data (including the zero-point corrections) to re-evaluate the cluster membership of the TP-AGB stars

with known spectroscopic type. The procedure is described in Sect. 4.3. By using the individual distances, obtained from the parallax inversion, and the extinction A_V from the catalogs of cluster ages, we fit the spectral energy distribution (SED) of each TP-AGB star by means of radiative transfer models that account for the presence of circumstellar dust. The details are given in Sect. 4.4. From the SED fitting we derive the bolometric luminosity and the present-day dust-mass loss rate. From the luminosity we infer the current mass of the core, M_c , by means of TP-AGB stellar models available in the literature. Sect. 4.5 provides a full description of the method. The entire Sect. 5 is devoted to present and analyze the results of this study, addressing several aspects of the TP-AGB evolution (e.g, onset of the 3DU and carbon star formation, stellar winds and dust production, long-period variability). In Sect. 5.2 we compare the values of the current core mass inferred from the luminosity with the initial-final mass relation of white dwarfs in the Milky Way. In Sect. 5.3 we investigate two competitive scenarios for the formation of carbon stars with high M_c in old open clusters: the single stellar evolution mode and the blue straggler channel. Finally, Sect. 6 closes the paper.

2. IDENTIFICATION OF NEAR-INFRARED BRIGHT STARS

To investigate the near-infrared bright stellar populations in Galactic open clusters we start with the catalog of Cantat-Gaudin & Anders (2020), which provides main parameters and lists of star members for 1481 open star clusters based on the second *Gaia* data release (DR2, Gaia Collaboration et al. 2018). Each star in the catalog is assigned the *Gaia* DR2 photometry, the distance from parallax inversion, and its membership probability.

Then, we select the brightest near-infrared stars by adopting the following four criteria: 1) stars have 2MASS photometry in the J , H , K_s pass-bands (Cutri et al. 2003), in addition to the *Gaia* ones; 2) they have an absolute magnitude $M_{K_s} < -5$; 3) they belong to the associated clusters with a membership probability $p \geq 0.5$; 4) the age of the host cluster is estimated from recent studies, mostly based on *Gaia* DR2 (Dias et al. 2021; Cantat-Gaudin & Anders 2020; Bossini et al. 2019; Cummings et al. 2018).

To cross-match *Gaia* DR2 and 2MASS catalogs we adopt a search radius of $3''$, which avoids spurious duplicates. The absolute magnitude of each star M_{K_s} is obtained by subtracting the true distance modulus from the apparent magnitude K_s and then applying the extinction correction A_{k_s} . In general, the same is done for any relevant pass-band i using the transformation

coefficients A_i/A_V^1 , provided that the visual extinction A_V is known. This latter is taken to be the same A_V of the host cluster, available from the age-estimation studies based on the best-fit isochrone technique (Dias et al. 2021; Cantat-Gaudin & Anders 2020; Bossini et al. 2019; Cummings et al. 2018). We note that some stars may be also affected by circumstellar extinction due the presence of dust shells; this aspect will be discussed in Sect. 4.4.

We consider stars brighter than $M_{K_s} = -5$. This value is roughly 2 magnitudes fainter than the tip of the red giant branch (RGB) at solar-like metallicities, $M_{K_s}^{\text{RGBtip}} \simeq -7$ (Freedman et al. 2020). We end up with a sample of 543 stars that satisfy the four constraints listed above. To obtain a more informative characterization of the selected stars we search for those of known spectroscopic type with the aid of the SIMBAD astronomical database (Wenger et al. 2000). In total the spectroscopic sample contains 191 objects. Among them we find 14 O stars, 26 B stars, 11 A stars, 16 F stars, 18 G stars, 54 K stars, 4 Wolf-Rayet stars, 35 M stars, 1 MS star, 2 S stars, 9 C stars, and 1 peculiar star, classified as LBV. We consider 2 additional carbon stars, not present in the catalog of Cantat-Gaudin & Anders (2020). More details about these objects are provided in Sect. 3.

2.1. The *Gaia*-2MASS diagram

Once the cross-identification and dereddening operations are completed, we construct the *Gaia*-2MASS diagram (see Fig. 1), originally designed by Lebzelter et al. (2018, 2019, hereinafter L18, L19), that is especially suitable to highlight the presence of AGB stars. In this diagram the K_s magnitude is correlated with a particular combination of *Gaia* and 2MASS pass-bands, through the quantity $W_{\text{BR}} - W_{\text{JK}_s}$. Here W_{BR} and W_{JK_s} are reddening-free Wesenheit functions (Madore 1982; Soszynski et al. 2005), defined as $W_{\text{BR}} = G_{\text{RP}} - 1.3 \times (G_{\text{BP}} - G_{\text{RP}})$ and $W_{\text{JK}_s} = K_s - 0.686 \times (J - K_s)$, respectively. L18 first demonstrated that this diagram is a powerful tool to analyze and identify sub-classes of AGB stars, as a function of chemical type and initial mass.

Figure 1 shows three versions of the same *Gaia*-2MASS diagram, in which the stars are flagged by their spectroscopic type, age and turn-off mass of the host cluster. To guide the analysis we mark with letters the regions of the four main stellar branches as introduced by L18 (see their figures 1-3), namely: (a) low-mass O-

rich AGB stars, RGB and faint AGB stars; (b) carbon stars; (c) intermediate-mass O-rich AGB stars; (d) red super giants (RSG) and massive O-rich AGB stars.

In this respect, we should note that some important differences exist between the stellar populations examined by L18, L19 and our study. In the original L18, L19 works the data mainly refer to long-period variables (LPVs) in the Magellanic Clouds (LMC), identified with *Gaia* DR2 data, while in this study we consider *all* stars of Galactic open clusters satisfying the four criteria given in Sect. 2. As a consequence, the *Gaia*-2MASS diagrams of Fig. 1 are populated also by stars not belonging to the AGB star population. Let us discuss the main features of each region, as a function of spectral type (top panel), age (middle panel) and turn-off mass (hereafter also M_{TO} ; bottom panel).

2.1.1. Region (a)

The main differences between L18 and this study show up in the mixture of stars that populate the region (a). In our diagram we identify a group of O-B-A stars, mostly of I luminosity class (light blue diamonds in the top-left panel). They draw a sort of vertical sequence leftward of the main branch at $W_{\text{BR}} - W_{\text{JK}_s} \approx 0.5$, where most of the K stars (green triangles) and some faint M stars (blue circles) are found. The O-B-A stars are associated to young open clusters, with $7.0 \lesssim \log(\text{age/yr}) \lesssim 7.5$, likely corresponding to core H-burning massive stars of initial mass $M_i > 10 M_{\odot}$ (bottom panel). Slightly to the right of the O-B-A type group we find F-G stars (purple diamonds) of older ages, with $\log(\text{age/yr}) > 8$. These should mainly correspond to core He-burning stars. Intermediate-age K stars, with $8 \lesssim \log(\text{age/yr}) \lesssim 9$, appear to populate the main branch at $W_{\text{BR}} - W_{\text{JK}_s} \approx 0.5$ as E-AGB stars, together with the old RGB K stars, with $\log(\text{age/yr}) > 9$. Finally, we note that the region (a) hosts also M-type stars distributed over a wide age range, typically with $\log(\text{age/yr}) > 8$. These stars are mainly O-rich AGB star candidates. Among them there are 3 stars of spectral type S and MS, which are particularly interesting since they witness the occurrence of the 3DU. A more in-depth discussion about AGB stars in the region (a) is given in Sect. 3.

In addition to the groups of stars just mentioned, we find a few peculiar objects in region (a). We identify a faint carbon star, NIKC 3-81, located at $W_{\text{BR}} - W_{\text{JK}_s} \simeq 0.65$ and $M_{K_s} \simeq -5.63$ on the main branch of RGB K stars. Following the recent work by Abia et al. (2020) on field Galactic carbon stars, we suggest that NIKC 3-81 might belong to the class of R-hot carbon stars. These objects are faint carbon stars, without s-process

¹ The transformation coefficients for the different filters are derived from the extinction curve of Cardelli et al. (1989) and O'Donnell (1994) with a total-to-selective extinction ratio of $R_V = 3.1$.

enhancement, whose origin is still a matter of debate. One hypothesis is that the carbon enrichment occurs during the He-flash at the tip of the RGB, but other channels are also invoked (see [Abia et al. 2020](#), and references therein for a thorough discussion). The star NIKC 3-81 has an age of 2.7 Gyr, and $M_i \simeq 1.53 M_\odot$ assuming it is in a post-He-flash stage.

At the bottom of the same sequence there are five Wolf-Rayet stars (orange pentagons), belonging to young open clusters (Hogg 15, NGC 6231, NGC 6871, Negueruela 1, and Teutsch 127), with $6.3 \lesssim \log(\text{age}/\text{yr}) \lesssim 7.2$. In particular, the star HD 311884, member of Hogg 15, is assigned a spectral type WN6+O5V with an age of 2.2 Myr, and hence it is consistent with a very massive progenitor, $M_i \gtrsim 100 M_\odot$. Following recent stellar evolution calculations, this object may end up its life as a pulsation pair-instability supernova ([Goswami et al. 2021](#); [Costa et al. 2021](#); [Chen et al. 2015](#)).

On the left side of the region (a), at $W_{\text{BR}} - W_{\text{JK}_s} \simeq -1.64$ and $M_{K_s} \simeq -6.22$, there is an intriguing object, MR 35, (asterisk), which is attributed the spectral type of Luminous Blue Variable (LBV), typical of very massive and bright stars near the Humphreys-Davidson limit ([Humphreys & Davidson 1979](#)). This classification appears in conflict with the age of about 1.1 Gyr of the host cluster Teutsch 143a, which has $M_{\text{TO}} \simeq 2 M_\odot$. A closer inspection reveals that this star is included in the atlas of post-AGB stars and planetary nebulae selected from IRAS point source catalogue ([Suárez et al. 2006](#)). MR 35 is classified as a peculiar star (neither a genuine planetary nebula, nor a post-AGB star), with an optical spectrum showing a few emission lines including H α . It is suggested to be a very young proto-planetary nebula. This configuration better matches with the intermediate age of MR 35.

2.1.2. Region (b)

It should correspond to the domain of intrinsic carbon stars. In fact, we count 11 spectroscopically identified C stars in this region, which have a good probability of being cluster members. We devote an extensive analysis of their properties in Sect. 3. They span an age range from about 0.2 Gyr to 4.3 Gyr. We note that only 2 carbon stars have $W_{\text{BR}} - W_{\text{JK}_s} > 1.7$, the approximate boundary beyond which stars are expected to experience significant mass loss driven by carbonaceous dust. The remaining 9 carbon stars are located to the left of this limit where dust should be inefficiently produced. We will deepen this aspect with the aid of radiative transfer models in Sect. 4.4.

2.1.3. Regions (c) and (d)

The region (c) should contain intermediate-mass O-rich AGB stars. Though it appears barely populated, we find three stars consistent with this expectation, having $8.0 \lesssim \log(\text{age}/\text{yr}) \lesssim 8.4$, and initial masses $5.0 \gtrsim M_i/M_\odot \gtrsim 3.5$. They are likely E-AGB stars (based on PARSEC stellar isochrones of [Pastorelli et al. 2020](#), triangles). Two of them have spectral type K (blue triangles in the top-right panel of Fig. 1).

M-type red supergiants, evolved from massive stars with $7.0 \lesssim \log(\text{age}) \lesssim 7.8$, are detected close to the bright edge of the region (c), and mostly in region (d) where they draw a nearly vertical branch. This finding is fully consistent with the analysis of L18. In the same region we identify a younger bright star (at $W_{\text{BR}} - W_{\text{JK}_s} \simeq 0.66$ and $M_{K_s} \simeq -9.19$) with an age of 0.34 Gyr. This object, 2MASS J07570972-2553064, is also a candidate TP-AGB star (with $M_i^{\text{AGB}} \simeq 3.3 M_\odot$), perhaps undergoing a mild HBB.

3. AGB STARS IN OPEN CLUSTERS

From the sample of bright near-infrared stars we aim to extract a sub-sample of AGB star candidates. This is done by combining the *Gaia*-2MASS diagram with the age estimates of the clusters. The AGB star candidates are selected according to the following criteria: 1) they must be brighter than the RGB tip, i.e. $M_{K_s} < -7$; 2) they must be older than about 100 Myr, corresponding to an upper limit of the initial post-main sequence mass of about $6 M_\odot$; 3) they are assigned a spectral type among K, M, MS, S, C, when known.

The lower age limit is chosen on the basis of stellar evolution models. At solar metallicity, PARSEC models predict a maximum mass for the development of a degenerate carbon-oxygen core, $M_{\text{up}} \simeq 6 M_\odot$, corresponding to a main-sequence lifetime of roughly 100 Myr. Stars with $M_i < M_{\text{up}}$ experience the standard double-shell AGB phase, that includes both the Early-AGB (E-AGB) and the TP-AGB phases. In total, we identified 49 candidate AGB stars: 17 are expected to be on the E-AGB and the remaining 32 are interpreted as evolving on the TP-AGB. This distinction is made using the information stored in the PARSEC isochrones filtered through 2MASS pass-bands.

The main properties of the host clusters and the *Gaia* DR2 and 2MASS photometry of the individual AGB candidates are summarized in Table 1. For about half of the AGB sample (24 sources) we also know the spectral type from the SIMBAD database: 5 stars are of K type, 7 stars are of M type, 1 star is of MS type, 2 stars are of S type, and 8 stars are of type C. The group of spectroscopic C stars is complemented with 2 additional sources, namely: the TP-AGB stars MSB 75 and Wray

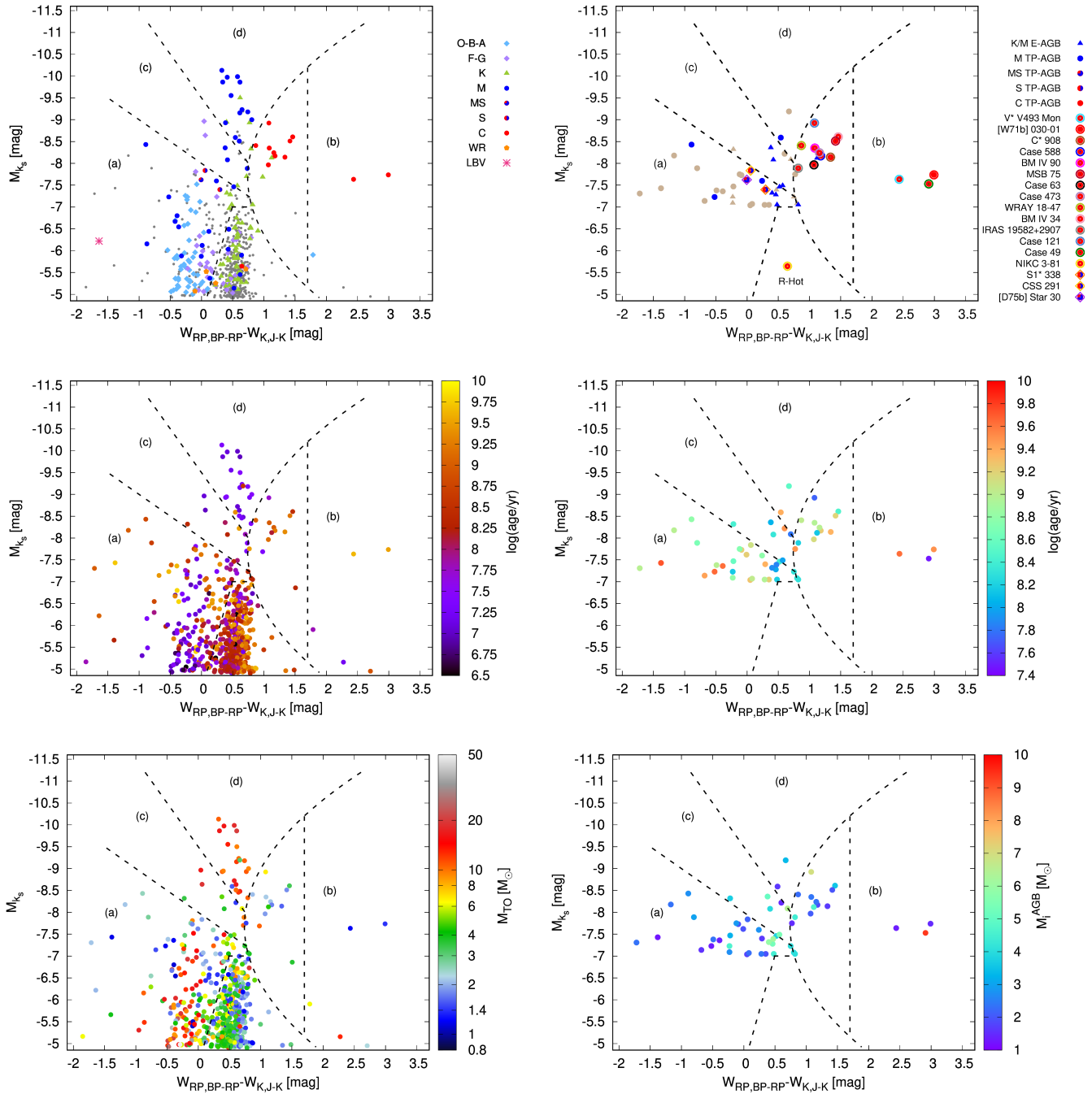


Figure 1. Near-infrared bright stars of open clusters in the *Gaia*-2MASS diagram. The absolute M_{K_s} magnitude is corrected for interstellar extinction, derived from A_V of each cluster. Dashed lines show the approximate boundaries of main stellar branches, defined by (Lebzelter et al. 2018). *Left panels:* all stars from the catalog of Cantat-Gaudin & Anders (2020) with cluster membership probability ($p \geq 0.5$). The stars are marked according to their spectral type if known (otherwise they are indicated by grey dots), age and turn-off mass of the host cluster. *Right panels:* AGB star candidates in open clusters, brighter than the RGB tip. From top to bottom the stars are color-coded as a function of the spectral type (when unknown the gray color is used), cluster’s age, and initial mass. The top panel distinguishes between E-AGB (triangles) and TP-AGB (circles) stars, based on PARSEC stellar isochrones. It also includes the full list of MS, S, and C stars. See the text for more details.

18-47, not included in the catalog of Cantat-Gaudin & Anders (2020). Analyzed with *Gaia* EDR3 data (see

Sect. 4.3), they turn out to be likely members of the open clusters NGC 7789 and NGC 2533, respectively.

The data for the AGB stars with known spectral type are summarized in Table 2. For comparison we report the age of their associated cluster from two different sources, namely: Cantat-Gaudin et al. (2020), and Dias et al. (2021). Both catalogs use *Gaia* DR2 photometric data and membership information.

All AGB star candidates are plotted in the *Gaia*-2MASS diagram (Fig. 1). In Sect. 2.1 we already analyzed the main features of the different regions of the diagram introduced by L18 and L19. Here we focus on some specific aspects of the AGB population that still deserve to be properly taken into consideration.

3.1. O-rich AGB stars

L18 pointed out that in the region (a) the branch extending towards negative $W_{\text{BR}} - W_{\text{JK}_s}$ primarily contains low-mass O-rich AGB stars (with $M_i^{\text{AGB}} \gtrsim 2 M_\odot$), while more massive objects are found in regions (c) and (d). In our sample the region (a) contains a few stars, with ages exceeding 1 Gyr, that are consistent with that indication, though also younger, and more massive ($M_i^{\text{AGB}} \gtrsim 3 M_\odot$) stars are present. This is a substantial difference with respect to the Magellanic Clouds populations analyzed by L18 and L19. In practice, we do not detect a clear separation between low- and intermediate-mass stars in regions (a) and (c), though our conclusions might be conditioned by the small size of the sample. However, this does not seem to be the case. In fact, the lack of a well-defined gap between branches (a) and (c) stands out quite clearly if we consider the rich LPVs population in the Milky Way observed with *Gaia* DR2, as well as the corresponding synthetic populations that include AGB stars with solar-like metallicity (Pastorelli et al., in preparation). As discussed in that study, the disappearance of the gap between regions (a) and (c) is driven by a metallicity effect, mainly reflecting i) the reduction of the initial-mass range for carbon-star formation at increasing metallicity, and ii) the specific behaviour of spectra for O-rich AGB stars as a function of effective temperature and metallicity (Pastorelli et al., in preparation).

Quite interesting is the case of the three stars of spectral type S and MS detected in region (a). To our knowledge this is the first time that AGB stars of this spectral type are confirmed to be members of open clusters. An early study (Jaschek & Keenan 1985) adopted a statistical approach to examine 15 S stars found along the line of sight of open clusters, but concluded that such configuration could be just explained as the result of a random field distribution of stars. Thanks to *Gaia* data, this negative conclusion has now been importantly revised. We note that the 1 MS and 2 S stars are located

in the vicinity of the bright side of the region (c), supporting the predictions of evolutionary models for the TP-AGB phase in which repeated 3DU events increase the photospheric C/O approaching unity (Marigo et al. 2013, more details in Pastorelli et al., in prep.).

By using the estimated ages of the host clusters we can characterize the stellar progenitors: the two S stars, S1* 338 and CSS 291, belong to the old open clusters BH 55 and Tombaugh 1, and correspond to initial masses $M_i^{\text{AGB}} \simeq 1.65 M_\odot$ and $M_i^{\text{AGB}} \simeq 2.13 M_\odot$, respectively. The only MS star, [D75b] Star 30, member of the cluster NGC 1798, is associated with $M_i^{\text{AGB}} \simeq 1.93 M_\odot$. These objects may set useful constraints on the onset of the 3DU, as discussed in Sect. 5, **M and S stars: the onset of the 3DU**.

Moving to intermediate-mass stars, we identify in regions (c) and (d) few AGB stars with initial masses $M_i^{\text{AGB}} > 3 M_\odot$, which are in principle compatible with the occurrence of HBB. However, we note that they are not particularly bright ($K_s > -9.5$) and their evolutionary stage is expected to correspond to the E-AGB. Therefore these objects still have to enter the TP-AGB phase.

3.2. Carbon stars

We find 10 spectroscopically confirmed carbon stars, all falling inside region (b), as expected from the studies by L18, L19 and Abia et al. (2020). Among them, 8 carbon stars derive from the *Gaia* DR2 catalog of Cantat-Gaudin & Anders (2020), having a membership probability $p \geq 0.5$. We add 2 stars, MSB 75 and Wray 18-47, likely members of the open clusters NGC 7789 and NGC 2533, according to a new membership analysis based on *Gaia* EDR3 (Sect. 4.3).

Pal & Worthey (2021) recently analyzed the frequency of carbon stars in open clusters using the data from *Gaia* DR2. They obtained a list of 9 objects possibly associated to star clusters (their table 2), of which 6 are in common with our 10-star sample, namely: V493 Mon, C* 908, V* BI Per², BM IV 90, Case 473, and BM IV 34. The remaining 3 carbon stars considered by Pal & Worthey (2021, namely IRAS 19582+2907, Case 121, Case 49) are not included in our initial selection as their cluster membership probability is rather low, $p = 0.4$, according to Cantat-Gaudin et al. (2020). However, for the purpose of comparison we add these 3 doubtful cases at the bottom of Table 2 and in Fig. 1. We just note that these carbon stars are related to relatively young star clusters, with $29 \lesssim (\text{age}/\text{Myr}) \lesssim 158$ and turn-off masses in the range $8.97 \gtrsim (M_{\text{TO}}/M_\odot) \gtrsim 4.20$. We ana-

² In this work V* BI Per is indicated also with the name Case 63.

lyze the cluster membership of these sources in Sect. 4.3, and the evolutionary status in Sect. 5.

4. BASIC INFORMATION ON INDIVIDUAL M, S AND C STARS

Table 2 summarizes a few relevant properties of the AGB stars with known spectroscopic type. Clusters ages are extracted from two recent works, both based on *Gaia* DR2, namely: Cantat-Gaudin et al. (2020) and Dias et al. (2021). The analysis that follows is limited to the stars that are expected to be on the TP-AGB phase, according to the PARSEC evolutionary tracks. Some of the evolved giants in our sample, the carbon stars in particular, were already discovered and associated to open clusters by early studies in the past century. Here we review the relevant literature about these historical TP-AGB stars and include basic data for other, less studied, M, S and C stars. The information about long-period variability, including our new analysis, is provided in Sect. 4.1 and in Tables 3 and 7.

M stars: IRAS 23455+6819, HD 292921, IRAS 09251-5101, 2MASS J00161695+5958115—We identify 4 M-type stars in the sample that are expected to be on the TP-AGB phase. Two of them are low-mass stars (IRAS 23455+6819 and HD 292921) with $M_i^{\text{AGB}} \simeq 1.3 M_\odot$ and $1.6 M_\odot$, and the other two (IRAS 09251-5101 and 2MASS J00161695 + 5958115) are intermediate-mass stars with similar initial mass, $M_i^{\text{AGB}} \simeq 2.7 M_\odot$. To our knowledge there is no specific literature on these stars, except for some information on their variability, which we find in the *Gaia* DR2 catalog dedicated to LPVs (Mowlavi et al. 2018). More details can be found in Sect. 4.1.

S stars: [D75b] Star 30, S1 338, CSS 291*—The MS star [D75b] Star 30 is a member of the cluster NGC 1798, with an estimated age of $\simeq 1.66$ Gyr (Cantat-Gaudin et al. 2020), and a slightly sub-solar metallicity $[\text{Fe}/\text{H}] = -0.18$ (Carrera et al. 2019). The progenitor initial mass is $M_i^{\text{AGB}} \simeq 1.79 M_\odot$. This star has experienced a few dredge-up episodes and should become a carbon star according to current TP-AGB stellar models (Cristallo et al. 2011; Marigo et al. 2013). The S star S1* 338 belongs to the old cluster BH 55, which is assigned an age of $\simeq 2$ Gyr (Cantat-Gaudin et al. 2020). A spectroscopic measure of $[\text{Fe}/\text{H}]$ is missing for this cluster, so we assume it to be solar. Under this assumption, its S-star witnesses the occurrence of the 3DU at $M_i^{\text{AGB}} \simeq 1.60 - 1.65 M_\odot$. A younger S star, CSS 291, is associated to the star cluster Tombaugh 1 with an estimated age of $\simeq 1.26$ Gyr. Also for this cluster no metallicity estimate is available. The initial mass

of the progenitor is $M_i^{\text{AGB}} \simeq 2.1 M_\odot$ at solar metallicity. The spectral type is S4/2, which would correspond to $\text{C}/\text{O} \simeq 0.95$ according to the classification of Keenan & Boeshaar (1980).

V V493 Mon*—This carbon star belongs to the old open cluster Trumpler 5, with an estimated age of $\simeq 4.3$ Gyr (Cantat-Gaudin et al. 2020), or $\simeq 3.5$ Gyr (Dias et al. 2021). The initial mass of the progenitor is $M_i^{\text{AGB}} \simeq 1.3 - 1.4 M_\odot$. We note that this cluster has a relatively low metallicity, $[\text{Fe}/\text{H}] \simeq -0.4$ according to the APOGEE and GALAH spectroscopic surveys (Carrera et al. 2019). Therefore, V* V493 Mon cannot be used to set constraints of carbon star formation at solar metallicity, rather it is useful to characterize an intermediate metallicity regime, similar to that of the Small Magellanic Cloud. In this respect, we note that $M_i^{\text{AGB}} \simeq 1.3 - 1.4 M_\odot$ is broadly consistent with the calibration of the 3DU, in particular in terms of the minimum mass for carbon star formation, carried out by Pastorelli et al. (2019) from a detailed analysis of the AGB star populations in the Small Magellanic Cloud.

[W71b] 030-01—It is a carbon star belonging to the intermediate-age open cluster Pismis 3, with an estimated age of $\simeq 3.2$ Gyr (Cantat-Gaudin et al. 2020), or $\simeq 1$ Gyr (Dias et al. 2021). Following the former age indication the initial mass of the progenitor is $M_i^{\text{AGB}} \simeq 1.5 M_\odot$, which lies towards the low-mass end of the interval for C star formation. Instead, adopting the latter age, the progenitor is more massive with $M_i^{\text{AGB}} \simeq 2.3 M_\odot$. The metal content of the host cluster is not available from spectroscopic measurements. Indirect estimates of the metallicity were derived by reproducing the morphology of color-magnitude diagrams with traditional best-isochrone fitting methods. The results suggested metallicities ranging from subsolar (Carraro & Ortolani 1994) to solar (Salaris et al. 2004), but it should be noted that these works predate the significant revision of the Sun metallicity (Asplund et al. 2009; Caffau et al. 2011).

C 908*—This star has no genuine spectral classification, but it is considered a possible carbon star and is listed in the General Catalog of Galactic Carbon Stars (Alksnis et al. 2001), as already noted by Pal & Worthey (2021). Its photometric properties match those of carbon stars very well: it has a red near-IR color ($J - K_{s0} \simeq 1.8$) and in the *Gaia*-2MASS diagram it is placed inside the region b) where all TP-AGB stars of spectral type C are found. C* 908 is a likely member of the cluster Ruprecht 37, which is assigned an age of $\simeq 2.2$ Gyr (Cantat-Gaudin et al. 2020), or $\simeq 3.1$ Gyr (Dias et al. 2021). Taking into account both age esti-

Table 1. Open cluster parameters and properties of AGB star candidate members, based on *Gaia* DR2.

2MASS ID	Cluster	log(age)	M_{TO}	D	A_V	p	$(J - K_s)_0$	$W_{\text{BR}} - W_{\text{JK}_s}$	M_{K_s}	M_i^{AGB}	stage
		dex	[M_{\odot}]	[pc]	[mag]		[mag]	[mag]	[mag]	[M_{\odot}]	
09551489 + 5633003	FSR 1521	9.72	1.16	4933	2.72	0.7	1.40	-1.38	-7.43	1.25	TP-AGB
23475728 + 6835426	King 11	9.65	1.18	3097	2.67	0.8	1.17	-0.52	-7.23	1.31	TP-AGB
07263860 + 4739437	Melotte 66	9.63	1.19	4830	0.25	0.9	1.28	-0.39	-7.36	1.33	TP-AGB
06363268 + 0925393	Trumpler 5	9.63	1.19	3047	1.20	0.7	2.94	+2.44	-7.64	1.33	TP-AGB
08310560 + 3838107	Pismis 3	9.50	1.40	2349	2.35	0.9	3.17	+2.99	-7.74	1.47	TP-AGB
06525082 + 1655289	Berkeley 29	9.49	1.42	12604	0.24	0.5	1.06	+0.60	-8.22	1.48	TP-AGB
10593792 + 5936032	Teutsch 106	9.48	1.44	7184	1.74	0.6	1.17	+0.77	-7.75	1.50	TP-AGB
21030493 + 4021370	Berkeley 54	9.43	1.51	6680	2.24	1.0	1.27	-0.68	-7.14	1.56	TP-AGB
07002883 + 0014204	Berkeley 34	9.38	1.56	7609	1.64	1.0	0.77	+0.54	-8.59	1.62	TP-AGB
08561346 + 3930429	BH 55	9.36	1.59	4783	1.22	0.8	1.26	+0.29	-7.40	1.65	TP-AGB
07494578 + 1715141	Ruprecht 37	9.35	1.60	4526	0.30	0.5	1.80	+1.34	-8.14	1.66	TP-AGB
05482764 + 0715292	Collinder 74	9.28	1.69	2498	0.85	0.7	1.30	+0.05	-7.04	1.76	TP-AGB
06090764 + 0436414	Dias 2	9.24	1.74	4009	0.47	0.9	2.05	+1.18	-8.17	1.84	TP-AGB
05113360 + 4740468	NGC 1798	9.22	1.77	5124	1.12	0.6	1.24	-0.01	-7.62	1.93	TP-AGB
08003039 + 1047532	NGC 2506	9.22	1.77	3191	0.09	1.0	1.18	+0.35	-7.05	1.93	TP-AGB
07030677 + 2050128	Tombaugh 2	9.21	1.79	9316	0.83	0.7	1.33	-0.09	-7.73	1.94	TP-AGB
03325580 + 5244137	Berkeley 9	9.14	1.89	1814	2.69	1.0	1.49	+1.07	-7.97	2.06	TP-AGB
07001366 + 2033294	Tombaugh 1	9.10	1.95	2554	0.66	0.8	1.19	+0.06	-7.84	2.13	TP-AGB
10092236 + 5718402	FSR 1530	9.03	2.06	5421	3.90	1.0	2.08	+0.08	-7.07	2.26	TP-AGB
20541769 + 5039128	Berkeley 53	8.99	2.13	3415	4.42	0.7	1.28	-1.72	-7.31	2.33	TP-AGB
20553632 + 5100498	Berkeley 53	8.99	2.13	3415	4.42	0.9	1.44	-1.17	-8.18	2.33	TP-AGB
20560804 + 5104316	Berkeley 53	8.99	2.13	3415	4.42	0.6	1.56	+1.16	-8.24	2.33	TP-AGB
20560894 + 5059071	Berkeley 53	8.99	2.13	3415	4.42	1.0	1.17	-0.49	-7.38	2.33	TP-AGB
08423384 + 4712252	NGC 2660	8.97	2.17	2788	1.19	1.0	1.70	+1.08	-8.35	2.36	TP-AGB
20104694 + 4110170	IC 1311	8.96	2.18	6167	1.34	0.7	1.13	+0.28	-7.05	2.38	TP-AGB
21104859 + 4832062	Berkeley 91	8.80	2.49	6057	4.04	0.7	1.09	-0.23	-7.09	2.70	E-AGB
09264885 + 5114107	BH 67	8.79	2.51	8167	3.00	0.8	1.35	-0.89	-8.43	2.72	TP-AGB
00161695 + 5958115	Juchert Saloran 1	8.78	2.53	5383	2.82	0.9	1.20	+0.24	-7.60	2.74	TP-AGB
14573523 + 6235349	Ruprecht 112	8.73	2.64	2733	2.07	0.7	1.12	-0.12	-7.75	2.85	TP-AGB
14543493 + 6233265	Ruprecht 112	8.73	2.64	2733	2.07	0.8	1.22	+7.68	-7.33	2.85	E-AGB
19474773 + 2328064	FSR 0154	8.68	2.76	3594	3.52	0.6	1.24	-0.80	-7.89	2.97	TP-AGB
17532024 + 2721185	Czernik 37	8.58	3.00	2314	3.43	0.9	1.14	-0.22	-7.47	3.21	TP-AGB
07570972 + 2553064	Ruprecht 42	8.53	3.13	6560	0.96	0.5	0.98	+0.67	-9.19	3.34	TP-AGB
07444463 + 2824077	Haffner 14	8.46	3.33	4108	1.52	0.6	1.44	+1.46	-8.61	3.54	TP-AGB
01292302 + 6316584	NGC 559	8.41	3.48	2884	2.19	0.9	1.17	-0.22	-8.32	3.69	E-AGB
07593754 + 6035134	NGC 2516	8.38	3.57	423	0.11	0.6	1.09	+0.52	-7.46	3.79	E-AGB
10190419 + 5625014	BH 92	8.33	3.74	2384	1.33	0.9	1.13	+0.42	-8.08	3.95	E-AGB
07082701 + 1312329	NGC 2345	8.32	3.77	2663	1.04	0.9	1.08	+0.80	-7.08	3.98	E-AGB
13193042 + 6454484	Ruprecht 107	8.31	3.80	3464	1.01	0.9	1.14	+0.75	-7.23	4.02	E-AGB
14350882 + 5633453	NGC 5662	8.30	3.84	761	0.60	0.8	1.19	+0.82	-7.05	4.05	E-AGB
23244485 + 6120384	NGC 7654	8.19	4.24	1653	1.85	1.0	0.79	+0.48	-7.05	4.46	E-AGB
01331401 + 6041111	Gulliver 16	8.15	4.40	4886	1.39	0.9	-0.13	-0.23	-7.23	4.63	E-AGB
10473842 + 5728027	Ruprecht 91	8.14	4.44	1070	0.19	0.6	1.28	+1.12	-8.12	4.67	E-AGB
09490713 + 5434130	Ruprecht 83	8.05	4.84	3706	2.38	0.5	1.10	+0.38	-8.36	5.07	E-AGB
01574017 + 6013079	NGC 743	8.00	5.07	1169	1.40	0.7	1.00	+0.46	-7.28	5.32	E-AGB
10384498 + 5910584	BH 99	7.98	5.17	467	0.34	1.0	0.92	+0.57	-7.49	5.42	E-AGB
16553781 + 3930177	NGC 6242	7.89	5.65	1246	1.03	1.0	0.76	+0.40	-7.32	5.92	E-AGB
18332658 + 1025317	NGC 6649	7.85	5.89	2124	3.90	0.8	0.94	+0.47	-7.39	6.15	E-AGB
05241683 + 4218238	SAI 47	7.80	6.20	4683	1.40	0.7	1.01	+0.70	-8.09	6.45	E-AGB

Notes: The table is sorted by cluster’s age decreasing downwards. From left to right the columns show: the star’s 2MASS identifier (1), the cluster’s name (2), age (3), turn-off mass M_{TO} (4), distance D (5), visual extinction A_V (6), the star’s membership probability p (7), intrinsic $(J - K_s)_0$ color (8), the difference of *Gaia*-2MASS Wasenheit functions (9), the absolute dereddened M_{K_s} magnitude (10), the initial mass M_i^{AGB} (11) and the evolutionary stage (12). Cluster’s parameters (age, A_V and distance D) are taken from Cantat-Gaudin et al. (2020), while the turn-off mass M_{TO} is extracted from the library of PARSEC stellar isochrones, assuming solar metallicity. For each star, the membership probability p is from Cantat-Gaudin & Anders (2020), intrinsic $(J - K_s)_0$ color, absolute magnitude M_{K_s} , initial mass M_i^{AGB} , and evolutionary stage (E-AGB or TP-AGB) are derived from the library of PARSEC stellar isochrones.

mates the initial mass of the progenitor should lie in the range $1.5 \lesssim M_i^{\text{AGB}}/M_{\odot} \lesssim 1.7M_{\odot}$. The spectroscopic metallicity of the cluster is unknown. By using the *Gaia* DR2 astrometric data for individual stars and matching the observed CMD with synthetic simple stellar populations, Piatti et al. (2019) derived for Ruprecht 37 an age of $\simeq 4.5 \pm 0.5$ Gyr and a metallicity $[\text{Fe}/\text{H}] = -0.32 \pm 0.24$.

MSB 75, BM IV 90, Case 588—The carbon star MSB 75 was first pointed out by Gaustad & Conti (1971) as a likely member of the intermediate-age open cluster NGC 7789, on the basis of the good consistency be-

tween its radial velocity and the measurements for a few K giants. NGC 7789 has an estimated age of $\simeq 1.6$ Gyr (Cantat-Gaudin et al. 2020; Cummings et al. 2018). The metallicity is almost solar, $[\text{Fe}/\text{H}] \simeq +0.06$ (Carrera et al. 2019), or $[\text{Fe}/\text{H}] \simeq -0.06$ (Zhong et al. 2020).

The carbon star BM IV 90 was identified within $1'$ of the center of the cluster NGC 2660 by Hartwick & Hesser (1973, 1971), while its evolutionary status was discussed by Eggen & Iben (1991). NGC 2660 is almost coeval of NGC 7789, with an age of $\simeq 1.6$ Gyr (Rain et al. 2021; Jeffery et al. 2016). We note that Cantat-

Table 2. Main properties of spectroscopically identified AGB stars, based on *Gaia* DR2.

2MASS ID	SIMBAD	Cluster	p	Cantat-G. 20		Dias 21		$(J - K_s)_0$	$W_{BR} - W_{JKs}$	M_{K_s}	type	stage
				$\log(\text{age})^a$	M_i^{AGB}	$\log(\text{age})^b$	M_i^{AGB}					
				dex	[M_\odot]	dex	[M_\odot]	[mag]	[mag]	[mag]		
23475728 + 6835426	IRAS 23455+6819	King 11	0.8	9.65	1.31	9.55	1.41	1.17	-0.52	-7.23	M	TP-AGB
06363268 + 0925393	V* V493 Mon	Trumpler 5	0.7	9.63	1.33	9.54	1.42	2.94	+2.44	-7.64	C	TP-AGB
08310560 - 3838107	[W71b] 030-01	Pismis 3	0.9	9.50	1.47	9.00	2.32	3.17	+2.99	-7.74	C	TP-AGB
07002883 - 0014204	HD 292921	Berkeley 34	1.0	9.38	1.62	-	-	0.77	+0.54	-8.59	M	TP-AGB
08561346 - 3930429	S1* 338	BH 55	0.8	9.36	1.65	9.40	1.60	1.26	+0.29	-7.40	S	TP-AGB
07494578 - 5115141	C* 908	Ruprecht 37	0.5	9.35	1.66	9.49	1.49	1.80	+1.34	-8.14	C	TP-AGB
06090764 + 0436414	Case 588	Dias 2	0.9	9.24	1.84	9.11	2.12	2.05	+1.18	-8.17	C	TP-AGB
05113360 + 4740468	[D75b] Star 30	NGC 1798	0.6	9.22	1.93	9.14	2.07	1.24	-0.01	-7.62	MS	TP-AGB
08423384 - 4712252	BM IV 90	NGC 2660 ^c	1.0	9.21	1.94	9.08	2.17	1.70	+1.08	-8.35	C	TP-AGB
05113360 + 4740468	MSB 75	NGC 7789	- ^d	9.19	1.97	9.21	1.94	1.90	+1.42	-8.51	C	TP-AGB
03325580 + 5244137	V* Case 63	Berkeley 9	1.0	9.14	2.06	9.18	1.99	1.49	+1.07	-7.97	C	TP-AGB
07001366 - 2033294	CSS 291	Tombaugh 1	0.8	9.10	2.13	9.11	2.12	1.19	+0.06	-7.84	S	TP-AGB
20560804 + 5104316	Case 473	Berkeley 53	0.6	8.99	2.33	-	-	1.56	+1.16	-8.24	C	TP-AGB
08070513 - 2947435	Wray 18-47	NGC 2533	- ^d	8.85	2.59	8.87	2.56	1.62	+0.87	-8.41	C	TP-AGB
09264885 - 5114107	IRAS 09251-5101	BH 67	0.8	8.79	2.72	-	-	1.35	-0.89	-8.43	M	TP-AGB
00161695 + 5958115	-	Juchert Saloran 1	0.9	8.78	2.74	8.81	2.69	1.20	+0.24	-7.60	M	TP-AGB
07444463 - 2824077	BM IV 34	Haffner 14	0.6	8.46	3.54	8.56	3.25	1.44	+1.46	-8.61	C	TP-AGB
07593754 - 6035134	V* V460 Car	NGC 2516	0.6	8.38	3.79	8.44	3.59	1.09	+0.52	-7.46	M	E-AGB
10190419 - 5625014	HD 300666	BH 92	0.9	8.33	3.95	7.46	9.02	1.13	+0.42	-8.08	M	E-AGB
14350882 - 5633453	HD 127753	NGC 5662	0.8	8.30	4.05	8.02	5.20	1.19	+0.82	-7.05	K	E-AGB
23244485 + 6120384	BD+60 2534	NGC 7654	1.0	8.19	4.46	7.72	6.74	0.79	+0.48	-7.05	K	E-AGB
10473842 - 5728027	HD 93662	Ruprecht 91	0.6	8.14	4.67	8.05	5.07	1.28	+1.12	-8.12	K	E-AGB
09490713 - 5434130	IRAS 09473-5420	Ruprecht 83	0.5	8.05	5.07	8.19	4.48	1.10	+0.38	-8.36	M	E-AGB
01574017 + 6013079	HD 11800	NGC 743	0.7	8.00	5.32	8.04	5.11	1.00	+0.46	-7.28	K	E-AGB
10384498 - 5910584	* t02 Car	BH 99	1.0	7.98	5.42	7.79	6.23	0.92	+0.57	-7.49	K	E-AGB
16553781 - 3930177	HD 152524	NGC 6242	1.0	7.89	5.92	7.77	6.37	0.76	+0.4	-7.32	K	E-AGB
Doubtful cases												
20001359 + 2915413	IRAS 19582+2907	FSR 0172	0.4	8.20	4.42	-	-	1.84	+0.82	-7.89	C	TP-AGB
05500040 + 2216113	Case 121	Berkeley 72	0.4	7.73	6.96	8.73	2.86	1.56	+1.27	-8.92	C	S-/TP-AGB ^(e)
01443756 + 6049533	Case 49	NGC 663	0.4	7.47	9.37	7.40	9.74	2.85	+2.91	-7.53	C	S-AGB ^(e)

Notes: Similar to Table 1, but restricted to AGB star candidates (SIMBAD designation in column 2) with known spectroscopic type (column 12). Note that compared to Table 1, here we include 5 additional C stars: MSB 75, Wray 18-47, IRAS 19582+2907, Case 121, and Case 49. The first two stars are not present in the original catalog of Cantat-Gaudin & Anders (2020). The latter three objects are doubtful cases as their *Gaia* DR2-based cluster membership probability is rather low, $p = 0.4$. See the text for more explanation.

(a) Cluster ages from Cantat-Gaudin et al. (2020) with M_i^{AGB} derived accordingly (next column).

(b) Cluster ages from Dias et al. (2021) with M_i^{AGB} derived accordingly (next column). A dash (-) means that the cluster is not present in the catalog.

(c) Age and M_i^{AGB} for NGC 2660 are reported according to the Bayesian analysis of Jeffery et al. (2016) and the recent work of Rain et al. (2021), in place of the Cantat-Gaudin et al. (2020) estimate. The reason of this choice is related to the dual morphology of the red clump of core He-burning stars, as explained in Sect. 4.

(d) Membership probability absent from the *Gaia* DR2 catalog of Cantat-Gaudin & Anders (2020). The inclusion in the list of C-star cluster members follows from our new analysis based on *Gaia* EDR3 (Sect. 4.3).

(e) S-AGB stands for Super-AGB.

Gaudin et al. (2020) derived a younger age of ≈ 0.93 Gyr, using a neural network approach, but we tend to disfavor the Cantat-Gaudin et al. (2020) solution for the reasons provided below.

The two clusters NGC 7789 and NGC 2660 exhibit a similar peculiar morphology of the red clump, that is the locus of core-He burning stars in color-magnitude diagrams. As extensively discussed by Girardi et al. (2009, see also Girardi et al. 2010), the so-called dual clump, that is the coexistence of a faint extension, slightly to the blue of the main concentration of clump stars, is a likely clue that both clusters host, at the same time, stars of low-mass which undergo the helium flash at the RGB tip, and those just massive enough to avoid electron degeneracy in the helium core. An age of $\simeq 1.6$ Gyr derived by Rain et al. (2021); Jeffery et al. (2016) is nicely consistent with this interpretation, while a younger age

(Cantat-Gaudin et al. 2020) hardly accounts for the observed dual clump morphology.

The carbon star Case 588 belongs to the cluster Dias 2, whose parameters (age, distance and extinction) were first derived by Tadross (2009) on the base of 2MASS photometric data (Cutri et al. 2003). Following the systematic revision based on *Gaia* DR2 of Cantat-Gaudin et al. (2020), Dias 2 is assigned an age of $\simeq 1.74$ Gyr. We note that the isochrone fitting of the *Gaia* color-magnitude diagram relies on a small number of stars (44 stars have a membership probability $p > 0.7$), and therefore significant uncertainties may affect this age derivation. Anyhow, it is reassuring that this value is in broad agreement with the age ($\simeq 1.86$ Gyr) independently derived by Kharchenko et al. (2013, MWSC # 0756) from UBV and 2MASS data, and the recent estimate of $\simeq 1.3$

Gyr by [Dias et al. \(2021\)](#). The initial mass of the progenitor should be in the range $1.8 \lesssim M_i^{\text{AGB}}/M_\odot \lesssim 2.0$.

It follows that the carbon stars MSB 75, BM VI 90, and Case 588 sample the region close to the transition mass M_{HeF} , between the classes of low- and intermediate-mass stars. In addition, these carbon stars are extremely interesting objects, as their progenitors fall in the initial mass range where a kink in the initial-final mass relation has been recently detected ([Marigo et al. 2020](#)). This point will be further addressed in Sect. 5.2.

Case 63—This carbon star is a likely member of the cluster Berkeley 9, with an estimated age of $\simeq 1.4 - 1.5$ Gyr. The progenitor initial mass is $M_i^{\text{AGB}} \simeq 2.0 - 2.1 M_\odot$ that is close or just above the transition mass M_{HeF} . The metallicity of the cluster is slightly subsolar, $[\text{Fe}/\text{H}] \simeq -0.17$ ([Carrera et al. 2019](#)).

Case 473—It is a carbon star associated to the cluster Berkeley 53, with an age of $\simeq 0.98$ Gyr. The initial mass of the progenitor is $M_i^{\text{AGB}} \simeq 2.3 M_\odot$. The metallicity of the cluster is close to solar, with $[\text{Fe}/\text{H}] \simeq -0.02$ according to the spectroscopic estimate from APOGEE and GALAH surveys ([Carrera et al. 2019](#)).

Wray 18-47—This carbon star was identified in the field of the open cluster NGC 2533 by [Jorgensen & Westerglund \(1988\)](#). Not present in *Gaia* DR2 catalog of [Cantat-Gaudin & Anders \(2020\)](#), its cluster membership probability turns out relatively good ($p \simeq 0.6$) using the *Gaia* EDR3. The age of NGC 2533 is $\simeq 0.71$ Gyr following [Cantat-Gaudin et al. \(2020\)](#), fully consistent with the study of [Dias et al. \(2021\)](#), as well as of [Siegel et al. \(2019\)](#) based on the Swift UVOT Stars Survey. The initial mass of the progenitor is $M_i^{\text{AGB}} \simeq 2.6 M_\odot$.

BM IV 34—It is a carbon star associated to the relatively young star cluster Haffner 14 ([Jorgensen & Westerglund 1988](#); [Groenewegen et al. 1995](#)), with an estimated age of $\simeq 288$ Myr ([Cantat-Gaudin et al. 2020](#)), or $\simeq 195$ Myr ([Bossini et al. 2019](#)), $\simeq 362$ Myr ([Dias et al. 2021](#)). The relevance of this star lies in the fact that the initial mass of the progenitor is relatively high, $M_i^{\text{AGB}} \simeq 3.3 - 4.0 M_\odot$ and therefore places constraints on the maximum mass for the formation of carbon stars at solar metallicity during the TP-AGB phase.

IRAS 19582+2907, Case 121, Case 49—These 3 carbon stars have a relatively low membership probability, $p = 0.4$, according to [Cantat-Gaudin & Anders \(2020\)](#). We will further investigate this aspect with *Gaia* EDR3 in Sect. 4.3. Looking at the ages of the parent clusters ([Cantat-Gaudin et al. 2020](#)), it turns out that these carbon stars belong to young clusters and their

initial masses suggest them as plausible candidates for the occurrence of HBB, either in the standard TP-AGB phase (IRAS 19582+2907: $M_i \simeq 4.4 M_\odot$) or during the Super-AGB evolution (Case 121: $M_i \simeq 7 M_\odot$, Case 69: $M_i \simeq 9.7 M_\odot$). We note that [Dias et al. \(2021\)](#) derive an older age for Berkeley 72, so that the progenitor mass of Case 121 becomes $\simeq 2.9 M_\odot$, which brings it back into a normal TP-AGB evolution. A more detailed discussion of these stars will be carried out in Sect. 5.

4.1. Variability

Variability is a common feature of AGB stars that can be used to better constrain their physical properties. For all TP-AGB sources listed in Table 2 (with the exception of Case 49, see Sect. 5.1) we searched for variability information in the General Catalog of Variable Stars (GCVS, [Samus' et al. 2017](#)). We found the variability type of five stars, but only for one star (MSB 75) did we find an estimate of the period.

Therefore we extended the search to three ongoing surveys dedicated to time-domain astronomy, namely *Gaia* (see [Holl et al. 2018](#), for information about the variability processing of *Gaia* DR2 data), the All-Sky Automated Survey for SuperNovae (ASAS-SN, [Shappee et al. 2014](#)), and the Zwicky Transient Facility (ZTF, [Bellm et al. 2019](#)). Each one of these surveys provide access to photometric time series for a large number of variable stars, as well as catalogs of variability properties from the processing of the light curves.

As a first step, we crossmatched our list of 19 sources with the variability catalog provided in the framework of each one of the three surveys. The *Gaia* DR2 catalog of LPV candidates ([Mowlavi et al. 2018](#)) provides information for more than 150 000 sources, among which we found seven of the stars in our sample (six with a period). ASAS-SN is an automated, ground-based visual survey aimed at the detection of transient phenomena that also collected a large amount of observations of variable stars. The ASAS-SN catalog of variable stars ([Jayasinghe et al. 2019](#), and references therein) includes more than 660 000 objects automatically processed and classified. In this catalog we found 16 of the stars in our sample, and found a period estimate for ten of them³. ZTF is a ground-based wide-field survey for transients observing at visual and IR wavelengths. [Chen et al. \(2020\)](#) describe the ZTF catalog of periodic variable stars and its content of more than 780 000 sources, in which we found a match for four stars, all of them with

³ We integrated data for a few stars with more recent information from the corresponding dedicated pages at the ASAS-SN Sky Patrol website (<https://asas-sn.osu.edu/>).

period information. We note that [Chen et al. \(2020\)](#) provide an additional catalog of more than 1 380 000 ‘suspected’ variables, with which we matched two further sources from our sample. However we disregarded these matches as the reported periods are shorter than one day.

The periods and variability type we retrieved are summarized in [Table 3](#). We found at least one match for 17 sources, but four of them have no period estimate. There are two sources, HD 292921 and [W71b] 030-01, the we could not find in any of the examined catalogs. For seven stars we found information in more than one of the catalogs, that in most cases are not entirely in agreement. For instance, the two periods reported for 2MASS J00161695+5958115 differ by more than a factor seven, while three different variability types are reported for V* V493 Mon. Such discrepancies can be easily explained in terms of the nature of the observed stars and of the differences in cadence and coverage of the three surveys. Indeed, LPVs can be multi-periodic, in which case different observational strategies can lead to the detection of distinct periods. Even for mono-periodic variables, cycle-to-cycle variations can cause discrepancies associated with the epochs of observation. Moreover, all three catalogs adopted here have been produced by means of automated pipelines, which inevitably leads to spurious results when the number of processed objects is large.

This prompted us to re-examine the light curves of each individual star. Not only this allowed us to select the most reasonable value of the period, but we could also find data for sources not present in the catalogs, or for which a period is not given.

Using the ASAS-SN Sky Patrol service⁴, that gives almost real-time access to ASAS-SN observations, we were able to retrieve *V*-band light curves for all sources in our sample (including the three stars not reported in the ASAS-SN variable stars catalog). For a few sources we also retrieved time series in the *g* band. Similarly, by accessing the ZTF data products ([Masci et al. 2019](#)) through the NASA/IPAC Infrared Science Archive (IRSA⁵), we retrieved *g*-band light curves for the four stars included in the ZTF variable stars catalog, as well as for six additional sources. In some cases we also retrieved time series in the *r* band. The retrieved light curves are displayed in [Fig. 2](#).

For each time series we computed the Lomb-Scargle periodogram (e.g. [VanderPlas 2018](#), and references therein) to determine the variability period, then sub-

tracted the best-fit sine model from the data and repeated the process in order to check for the presence of possible secondary periods. A higher-order Fourier series model was adopted instead in some cases, selected by visual inspection, in which the light curve displays a clearly asymmetric shape (a common feature of Miras and related LPVs).

Many sources present long-term trends, not necessarily periodic, that are nonetheless fitted by the periodic model. Whether or not these are long secondary periods is hard to say given the relatively short observational baselines of the data. Regardless of the nature of these features, their subtraction from the time series during the first step of our processing effectively acts as a detrending, allowing for a better characterization of the true period of each star. We disregard all periods associated with such trends and consider only the periods over shorter timescales. We were not able to identify secondary periods that can be realistically attributed to pulsation, so we consider a single period for each star.

For each source we selected the most realistic period by considering the quality of the light curve in each band of each survey (photometric errors, time sampling and coverage), and by visually inspecting the best-fitting models and the Fourier transform of the window function of the time series. Then we compared our periods with those reported in the literature catalogs. If the literature periods are reasonably similar to the values we obtained, we adopted the former. Otherwise, we employed the periods we derived. We were not able to determine a reliable period for the source HD 292921, for which we also did not find a period in literature, so we exclude it from further analysis. We caution the reader that this does not necessarily mean that HD 292921 is not variable.

For 12 stars (most of the sample) we ended up relying on ASAS-SN data for the period, that was recomputed from the light curve in half of the cases. We adopted ZTF data for four sources, in all cases using the value of period computed by us. Indeed, we found significant differences between the four periods published in the ZTF catalog and the values we derived for the same sources using ZTF time series. Such discrepancies were expected as the catalog of [Chen et al. \(2020\)](#) is based on the ZTF data release 2, while we employed significantly longer time series from the more recent data release 7⁶. Only for two stars we adopted the period published in *Gaia* DR2, whose time series in most cases have insufficient coverage or sampling. We note, however, that

⁴ <https://asas-sn.osu.edu/>

⁵ <https://irsa.ipac.caltech.edu/frontpage/>

⁶ <https://www.ztf.caltech.edu/page/dr7>

Table 3. Period and variability type for the sources in our sample according to the stellar variability catalogs from *Gaia* DR2, ASAS-SN, ZTF, as well as to the GCVS. The final column lists the period adopted in this work.

Star	GCVS Name	<i>Gaia</i> DR2	ASAS-SN		ZTF		GCVS		adopted	
		<i>P</i>	<i>P</i> ^(a)	Type	<i>P</i>	Type	<i>P</i> ^(a)	Type	<i>P</i>	Ref. ^(b)
		[days]	[days]		[days]		[days]		[days]	
V* V493 Mon	V* V493 Mon	317.7	0	L	288.3	Mira	0	SRB:	432.4	Z ^(c)
[W71b] 030-01	-	393.3	460.0	SR	-	-	-	-	460.0	A
C* 908	-	-	517.7	SR	-	-	-	-	235.9	A ^(c)
Case 588	-	0	539.0	SR	-	-	-	-	539.0	A
BM IV 90	V* GV Vel	-	0	L	-	-	0	LB	438.2	A ^(c)
MSB 75	V* V532 Cas	432.5	449.2	SR	-	-	450.0	SRA	432.5	G
Case 63	V* BI Per	-	0	L	-	-	0	LB	163.4	A ^(c)
Case 473	-	-	0	YSO	-	-	-	-	358.4	Z ^(c)
WRAY 18-47	V* V521 Pup	368.9	277.9	SR	-	-	0	SR:	368.9	G
BM IV 34	-	-	136.7	L	-	-	-	-	136.7	A
IRAS 19582+2907	-	-	-	-	201.1	SR	-	-	364.6	Z ^(c)
Case 121	-	-	228.2	SR	-	-	-	-	228.2	A
S1* 338	-	-	43.28	SR	-	-	-	-	43.28	A
[D75b] Star 30	-	-	-	-	-	-	-	-	76.36	A ^(c)
CSS 291	-	-	0	L	-	-	-	-	95.52	A ^(c)
IRAS 23455+6819	-	604.1	0	L	248.1	SR	-	-	85.02	Z ^(c)
HD 292921	-	-	-	-	-	-	-	-	-	-
IRAS 09251-5101	-	148.9	144.4	SR	-	-	-	-	144.4	A
2MASS J00161695+5958115	-	-	801.7	SR	118.1	SR	-	-	95.01	A ^(c)

Notes:

- (a) Zero-day periods under the ASAS-SN or GCVS column indicate that the source is included in the catalog but its period is not reported.
(b) indicates whether the adopted period was taken from *Gaia* DR2 (G), ASAS-SN (A) or ZTF (Z).
(c) means that the adopted period was recomputed from a time series produced by the survey rather than taken from the corresponding variability catalog.

the *Gaia* DR2 G_{BP} -band light curves match remarkably well the ones in the ASAS-SN V -band over the overlapping time interval, an agreement that we often took as confirmation of the results we derived from ASAS-SN data.

Besides the impact of differences in coverage and cadence associated with the three surveys, we did not identify any evident systematic trend associated with the differences between the periods we derived and the ones we found in literature. Two relatively bright sources (MSB 75 and CSS 291) are close to the saturation limit of ASAS-SN (as discussed below), but no other source is at risk of saturation for the surveys we considered.

Below we provide an overview of the results and variability properties of each star.

V V493 Mon*—The shape and regularity of the ZTF light curves, from which we derived the adopted period of 432 days, suggest this object is a Mira, despite it being reported as a SRB star in the GCVS and classified as irregular by ASAS-SN. Overall, the derived light curves suggest this star may be subject to long-term variations.

[W71b] 030-01—This star shows an asymmetric light curve, typical of Miras, that can be appreciated in the ASAS-SN time series. The latter covers two full cycles with good sampling, and the period we computed from it is in good agreement with the automatically-derived

value from the ASAS-SN catalog of 460 days, that we adopted.

C 908*—Most likely a semi-regular variable. The processing of both the ASAS-SN and the g -band ZTF light curves highlighted a long-term trend and a periodicity about half that reported in the ASAS-SN catalog. We adopted the 236 day period we extracted from the ASAS-SN time series.

Case 588—Our analysis is in agreement with the results from the ASAS-SN catalog, from which we take the adopted period of 539 days. Despite its low amplitude, that would be consistent with it being classified as SR, this star displays a relatively long period and regular light curve, being thus similar to Miras.

BM IV 90—Despite being reported in the ASAS-SN catalog as an irregular variable (with no period), this star shows a clear periodicity in its V -band light curve, from which we derive a period of 438 days. It has a rather small amplitude ($\Delta V \lesssim 0.5$ mag), but a rather regular light curve with no clear sign of multi-periodicity.

MSB 75—The *Gaia* DR2 light curves show an asymmetric shape with a secondary maximum that is not evident in the ASAS-SN time series due to its cadence. We note that the latter light curve is flagged with a saturation warning, yet its periodicity and compatibility with *Gaia*

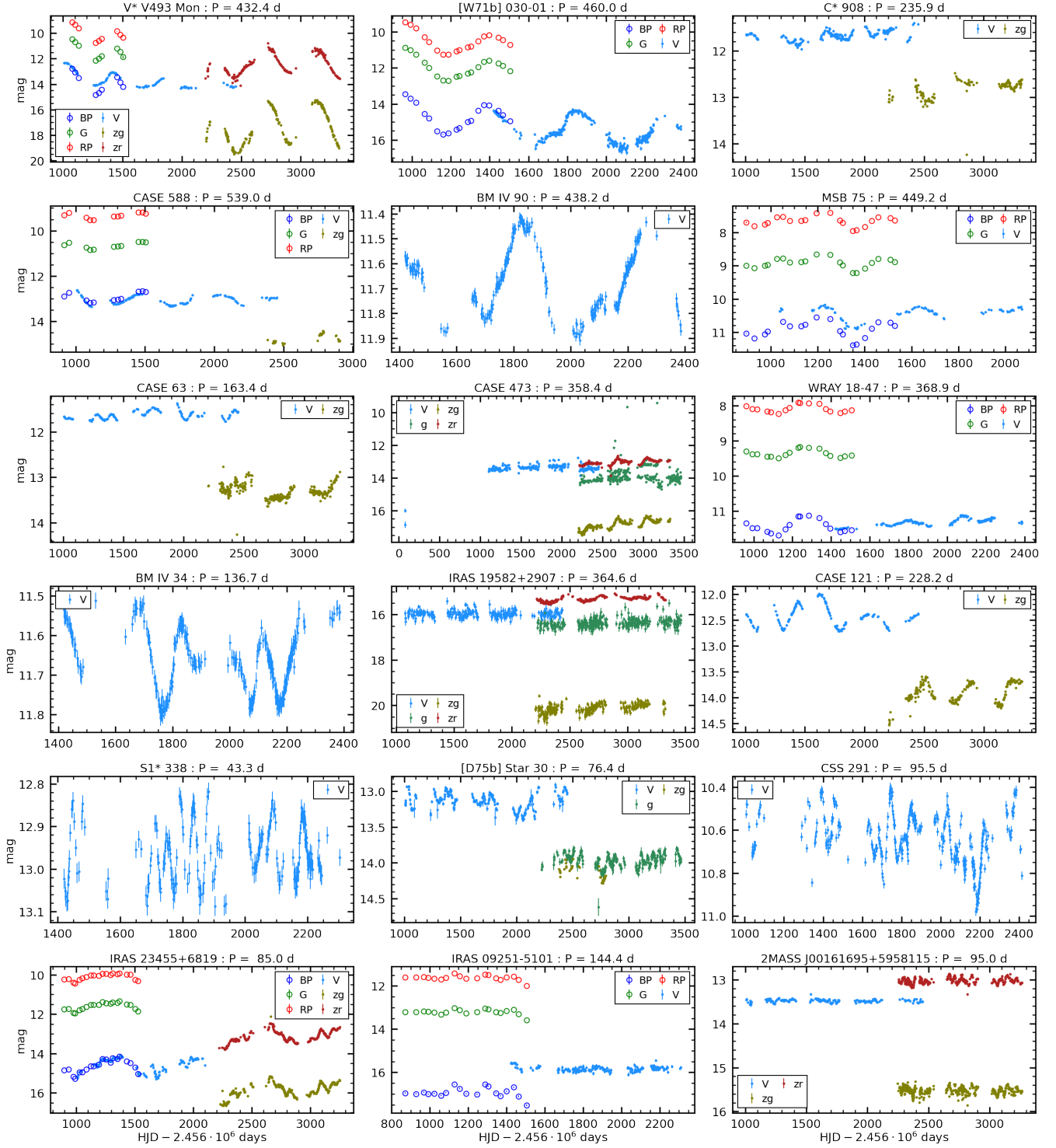


Figure 2. Light curves of the 18 sources for which we determined a period in filters of *Gaia* (G , G_{BP} , G_{RP}), ASAS-SN (V , g), and ZTF (g , r).

data are evident. When modelling the data of both surveys using a two-component Fourier series we obtain a period consistent with the value of 433 days published in *Gaia* DR2, that we adopt. The amplitude and reg-

ularity of the light curve are consistent with the GCVS classification as a SRA variable.

Case 63—While not highly regular, the V -band light curve of this source clearly shows a periodicity that we

constrain to 163 days. This period is not evident in the g -band time series from ZTF, that is rather suggestive of a longer-timescale variability. The latter could be a secondary pulsation period, which would be consistent with identifying this star as a semiregular variable.

Case 473—This source is classified as a young stellar object in the ASAS-SN catalog, with no reported period. This classification is unlikely given the data presented in the previous section and that this is a spectroscopically confirmed C-rich star. From ZTF photometry we identified a period of 358 days, that we adopted, corresponding to asymmetric variability. While close to the one-year alias, visual inspection of the light curve suggest this period to be realistic.

WRAY 18-47—Our analysis is consistent with the *Gaia* DR2 period of 369 days, that we adopt. Since the period is close to 1 yr, the coverage of the ASAS-SN time series is insufficient do confidently derive a period estimate.

BM IV 34—This star shows a clear semiregular behavior with an evident periodicity. We adopt the ASAS-SN estimate of 137 days, consistent with our analysis.

IRAS 19582+2907—ASAS-SN time series for this source do not show any sign of clear periodicity. The ZTF r -band light curve, having smaller errors, allows for the derivation of a period of 365 days. The evident ~ 0.5 mag fluctuations are evidence that this period is unlikely to be attributed to an alias.

Case 121—The periodicity of this star is evident from both the ASAS-SN and ZTF light curves. Our analysis of the former is consistent with the published period of 228 days, that we adopt. We note, however, that the periodogram for the ZTF time series shows a strong peak at 395 days that could be a secondary pulsation period. While this would be consistent with this star being a bi-periodic semiregular variable, this latter period is rather uncertain.

S1 338*—This is the shortest-period star in our sample (43 days adopted from ASAS-SN), and has a V -band amplitude of only ~ 0.2 mag. These features are consistent with this star being a semiregular variable pulsating in an overtone mode. Other pulsation modes are likely active in this star, but the coverage and sampling of the light curve does not allow them to be reliably constrained.

[*D75b*] *Star 30*—We found no published period for this source, that indeed has quite an irregular light curve. Upon subtracting long-term trends, analysis of the three available time series (ASAS-SN V and g band, ZTF g band) lead to consistent results, and we adopt a 76 days

period derived from the ASAS-SN g -band light curve. This star is probably a semiregular variable.

CSS 291—Similar to *S1* 338*, this appears to be a semiregular variable pulsating in one or more overtone modes. In absence of published periods, we derive a value of 96 days from the ASAS-SN V -band time series. This source is flagged with a saturation warning, and indeed is close to the ASAS-SN saturation limit of ~ 10 – 11 mag. However, the ASAS-SN aperture photometry pipeline is capable of recovering saturated sources up to ~ 7 – 8 mag, suggesting that this light curve is likely reliable.

IRAS 23455+6819—The combination of *Gaia* DR2, ASAS-SN and ZTF light curves clearly highlights the presence of two periods with remarkably different timescales in this source. The longer period, easily detected as the primary variability in any automated pipeline, is likely a long secondary period. From the r -band ZTF light curve we derive a value of 631 days for it, in fairly good agreement with the value published in *Gaia* DR2. For the shorter period, more likely associated with pulsation, we derive a value of 85 days from the ZTF data, in good agreement with the result from the ASAS-SN light curve. The sampling of the *Gaia* DR2 time series is insufficient to constrain this period.

HD 292921—For this source we only found a time series in the ASAS-SN V -band, characterized by relatively large photometric errors. The period derived from the periodogram is uncertain, so we do not adopt it here.

IRAS 09251-5101—The good agreement between the periods published in *Gaia* DR2 and ASAS-SN for this source suggests they are correct, although the poor sampling in the time series of the former and relatively large uncertainties in the light curves from of the latter make it difficult to confirm their validity. We adopt the 144 day period from ASAS-SN.

2MASS J00161695+5958115—Visual inspection of the light curves available for this source suggests that its period can be better constrained from ZTF data, from which we derived our adopted value of 95 days. This star is probably a semiregular variable.

4.2. *Gaia* EDR3 parallaxes and zero-point correction

The *Gaia* space mission marks an unprecedented progress in the precision of astrometric parameters of stars. Compared to other types of stars, the parallaxes, π , of AGB stars may be affected by greater uncertainties for two main reasons. First, the errors can be amplified

by the photocentric variability caused by complex surface convection structures (Chiavassa et al. 2018). Second, assuming a constant mean color to compute the parallaxes (Lindgren et al. 2018, 2021b) may introduce an unknown color bias which, in principle, could be substantial for pulsating AGB stars with large color variations over a cycle (Platais et al. 2003). It is therefore possible that these inconsistencies may affect not only the precision, but also the accuracy of the astrometric solution for AGB star parallaxes.

With these caveats in mind, we adopt the *Gaia* EDR3 parallaxes to derive the distances of the 29 AGB star candidates in our spectroscopic sample (see Table 2). The majority of them – 69%, 86%, 93 % – have *Gaia* EDR3 parallax uncertainty, $\epsilon(\pi)/\pi < 10\%, 15\%, 20\%$, where $\epsilon(\pi)$ is the tabulated error. The goodness of the astrometric solution can be checked with the aid of the renormalised unit weight error (RUWE), which should be $\simeq 1$ for a well-behaved *Gaia* EDR3 source (Lindgren et al. 2021b). Most of the stars in our spectroscopic sample (86%) have $\text{RUWE} < 1.1$ and the maximum value, $\text{RUWE} = 1.24$, is associated to the variable M star V* V460 Car. These indicators, therefore, support the good quality of the astrometric data, bearing in mind the issues described above.

To complete the discussion on AGB star parallaxes, another aspect is noteworthy. Recent studies have shown that the *Gaia* EDR3 parallaxes are affected by a systematic offset, the magnitude of which primarily depends on the position in the sky, magnitude, and colour (Groenewegen 2021; Lindgren et al. 2021a; Zinn 2021; Bhardwaj et al. 2021; Stassun & Torres 2021; Huang et al. 2021). Following a standard formalism (see, e.g., Groenewegen 2021), the parallax zero-point offset, ZP, is defined through

$$\pi_t = \pi_0 - \text{ZP}, \quad (1)$$

where π_0 is the observed parallax listed in the published catalog, and π_t denotes the true parallax corrected for the ZP offset. The ZP offset is typically negative; quasars have a median *Gaia* EDR3 parallax of $\approx -17 \mu\text{as}$. Lindgren et al. (2021a) provided the community with a useful tool to compute the parallax ZP as a function of object parameters, which has been used and tested extensively in various works. A few studies have pointed out that the model of Lindgren et al. (2021a) could produce an over-correction, in the sense that the ZP are too much negative and therefore the corrected parallaxes are too large (Riess et al. 2021; Zinn 2021; Huang et al. 2021; Groenewegen 2021). This occurs for classical Cepheids (Riess et al. 2021), RGB stars (Zinn 2021), and RR-Lyrae variables (Bhardwaj

et al. 2021). In light of this, a few different formulations have been proposed that either correct Lindgren’s prescription (e.g., Zinn 2021), or offer alternative approaches (e.g., Groenewegen 2021). In any case it should be noted that the source samples used for the ZP calibration generally do not adequately cover the characteristic intervals of AGB stars for some parameters (for example, the effective wavenumber ν_{eff} , and the color $BP - RP$). In general, AGB stars have smaller ν_{eff} and redder $BP - RP$ colors compared with those of the calibrating objects. It follows that the ZP corrections have not yet been properly validated for AGB stars and must be taken with some caution.

In consideration of the above, in this work we have decided to check three options, namely: no ZP correction (noZP case), and the ZP corrections according to Lindgren et al. (2021a, L21ZP case) and Groenewegen (2021, G21ZP case). As to the L21ZP case, we used the python script provided by the authors, while to implement the G21ZP correction we followed the instructions given by the author at the end of the paper. In this latter case, we used his models 30-34 to extract the spatial correction at $G = 20$ mag for the 5 HEALPix levels (from 0 to 4) and chose the highest level for which the number of calibrating sources, n_{obj} , is not less than 100. As discussed by Groenewegen (2021), forty objects or more are required to maintain a good signal-to-noise and get robust results. With the condition $n_{\text{obj}} > 100$, most stars are attributed HEALPix levels 2 or 3 and not higher. To estimate the magnitude correction to the parallax we adopted his equation 6. Finally, the total ZP is given by the sum of the spatial and magnitude corrections. Figure 3 shows an example of the effect produced by applying the ZP parallax corrections to the carbon star V* V493 Mon and the stars of its candidate hosting cluster Trumpler 5.

4.3. Cluster membership revisited with *Gaia* EDR3

To assess the cluster membership of the TP-AGB stars, we exploit the astrometric data from both *Gaia* DR2 and EDR3. Our analysis is applied only to the sources with known spectral type and classified as TP-AGB or Super-AGB stars (Table 2), as we are primarily interested in the final stages of evolution when surface carbon enrichment due to the 3DU can cause the spectral type change along the sequence $M \rightarrow S \rightarrow C$. We end up with a sample of 18 TP-AGB stars and 2 potential Super-AGB stars. We add also the C star NIKK 3-81 which is not a genuine TP-AGB star, but possibly a R-hot star. In total we examine 21 stars.

For each cluster we first consider the most representative stars, which are those with membership probabil-

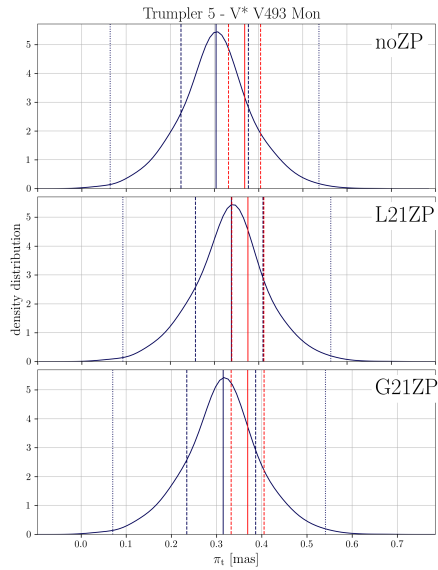


Figure 3. Effect of the *Gaia* EDR3 parallax zero-point corrections considered in this work (no ZP correction, Lindegren et al. 2021a, and Groenewegen 2021) applied to the carbon star $V^* V493$ Mon and its candidate hosting cluster Trumpler 5. The blue curves describe the parallax distributions of the cluster members in form of the density distribution function (calculated using the Kernel Density Estimation method - KDE), normalized by the total area. The solid, dashed, and dotted blue lines mark, respectively, the median, the 68th and the 95th confidence intervals of the distributions. The parallax central value and the $\pm 1 - \sigma$ errors for $V^* V493$ Mon are also shown (red solid and dashed lines).

ity $p > 0.7$ according to Cantat-Gaudin et al. (2020, to which we refer for all details), on the base of a statistical analysis of parallax π and proper motions (μ_α and μ_δ) performed with the UPMASK code (Krone-Martins & Moitinho 2014; Cantat-Gaudin et al. 2018). Using the same sample of stars we then re-determine the global properties of the clusters considering the updated astrometry from *Gaia* EDR3. We then derive the median α , δ , μ_α , μ_δ , and ω of each cluster and assess their 68% and 99% confidence levels (C.L.), accordingly with the 68th and 95th percentiles of each parameter distribution of the members. Figure 4 provides an example of the method applied to the C star $V^* V493$ Mon.

The evaluation of the target star membership is obtained by comparing parameter-by-parameter each individual star with the clusters C.L. (also accounting for the errors on the target star parameters). We consider members only the stars for which *all* the parameters are within the 99% C.L. of the cluster distributions. The results are reported in Table 10 in Appendix A. We list the target stars together with the C.L. they belong to with respect to the parent cluster. Specifically, we indi-

cate if a star lies within the 68% C.L. (i.e. when all the parameters are within this range), or it is found within the 99% C.L. (i.e. when at least one parameter is outside the 68% C.L. but still inside the 99% C.L.), or it is rejected (when at least one parameter is outside the 99% C.L.).

For all the stars and parent clusters for which radial velocity data are available, we also confirm that the two measurements are compatible. However, given the low number of cluster members with measured radial velocities, we do not consider this test stringent for the final membership evaluation.

The same analysis for each star is repeated three times (Sect. 4.2), adopting the *Gaia* EDR3 parallaxes without ZP correction (noZP case), and with the ZP corrections of Lindegren et al. (2021a, L21ZP case) and Groenewegen (2021, G21ZP case). Although the parallax distributions of the host clusters and the parallaxes of the target stars change somewhat, the results of the membership assessment always remain in agreement. Our analysis indicates that out of 21 stars examined, 20 are members of the associated cluster, with the exception of Case 49 whose membership to the cluster NGC 663 is rejected.

4.4. SED fitting: bolometric luminosity and other parameters

The bolometric luminosity is estimated by fitting the observed spectral energy distribution (SED), which typically includes photometry data from *Gaia* EDR3 (Gaia Collaboration et al. 2021), 2MASS (Cutri et al. 2003), WISE (Cutri et al. 2014), MSX (Egan et al. 2003), AKARI (Ishihara et al. 2010), and IRAS (Beichman et al. 1988).

A potential issue with the SED fitting of TP-AGB stars comes from their periodic large-amplitude variability, especially at visual wavelengths. However, the *Gaia* EDR3 photometry we adopt is expected to be well representative of the mean stellar luminosity as it consists of mean magnitudes computed over time series longer than (or at least comparable with) the variability timescales of TP-AGB stars (~ 1000 days, Gaia Collaboration et al. 2021). The variability amplitude decreases rapidly in the IR (Ita et al. 2021; Iwanek et al. 2021), so that even single-epoch survey data can be considered reasonably safe to use.

The SED fitting is performed with the Virtual Observatory SED Analyzer (VOSA; Bayo et al. 2008). The results are reported in Table 5. In VOSA the synthetic photometry is derived from the GRAMS grid of theoretical spectra for M and C stars (Sargent et al. 2011; Srinivasan et al. 2011). These models account for the ra-

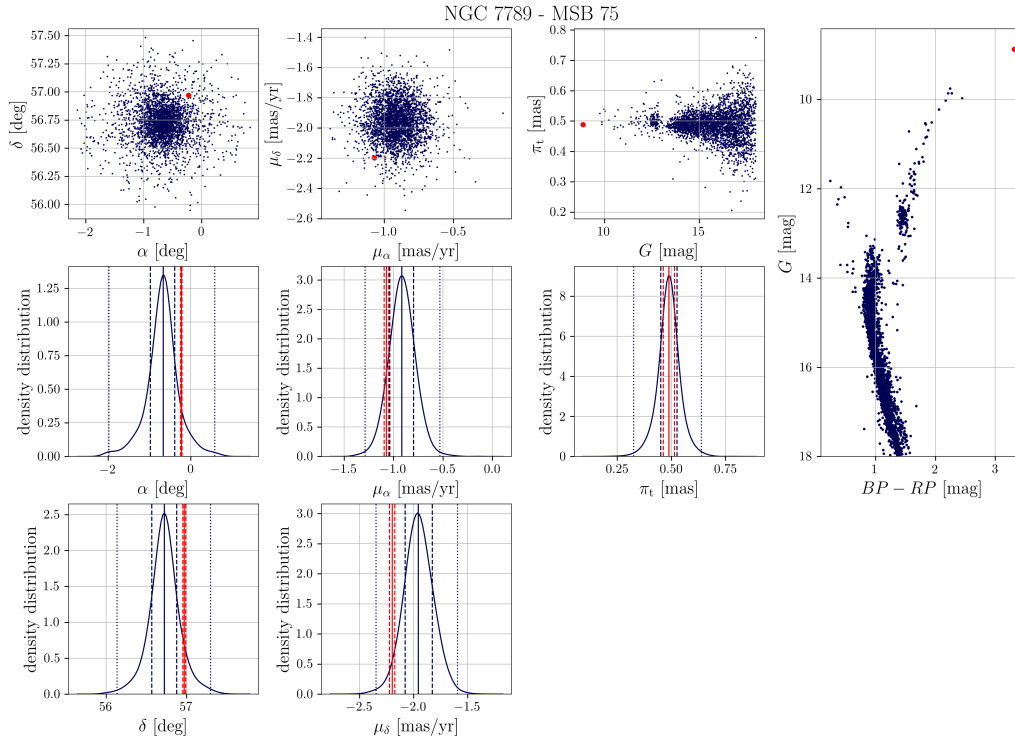


Figure 4. Visual example of membership assessment for the target star MSB 75 with respect to the cluster NGC 7789. The blue dots in the upper panels refer to the cluster members (with $p > 0.7$) according to Cantat-Gaudin et al. (2020), while the red dot marks the target star. The blue curves in the center and lower panels are the density distribution functions of each astrometric parameter (calculated using KDE method, similar to the one adopted in Figure 3), with the solid, dashed, and dotted blue lines indicating the median, the 68th, and the 95th percentiles, respectively. The red lines denote the central values (solid lines) and the $1-\sigma$ errors (dash lines) of MSB 75 parameters. Our analysis indicates that MSB 75 is a member of NGC 7789. The bottom-right panel shows the CMD using the three optical *Gaia* pass-bands. The parameters of each star are updated to *Gaia* EDR3 and the parallaxes corrected for the zero-point offset (in this example using Groenewegen (2021)).

diative transfer of the photospheric emission across the circumstellar dust shell produced by a mass-losing AGB star. The starting hydrostatic atmospheres are taken from the PHOENIX models for M stars (Kućinskas et al. 2005), and from the COMA models for C stars (Aringer et al. 2009).

Each theoretical spectrum in the grid is characterized by a combination of input parameters, namely: stellar mass M , surface gravity $g = GM/R^2$ (G is the gravitation constant and R is the photospheric radius), effective temperature T_{eff} , and photospheric C/O ratio (only for carbon stars).

During the SED fitting procedure these parameters are allowed to vary within selected ranges. In our analysis we used the entire grid of GRAMS models for g , M , T_{eff} , and C/O. To match the observed spectrum we need also to specify the distance D of the source and the visual extinction A_V . Distance and associated uncertainty are derived by inverting the *Gaia* EDR3 parallax, possibly corrected for the zero-point (Lindgren et al. 2021a; Groenewegen 2021). The visual extinction A_V is obtained from the same catalogs we use to date the host

clusters. In the fitting A_V is let vary within a range of ± 0.2 mag around the central value.

To single out the synthetic photometry that best reproduces the observed data we choose the VOSA option of a reduced χ^2 statistical test. In this way the observational errors associated to the different pass-bands are used to weigh the importance of each photometric point when calculating the χ^2 final value for each model. In addition to A_V , g , M , T_{eff} , and C/O, the best-fit model returns other important quantities that contribute to characterize the AGB star, namely: the dust mass-loss rate, \dot{M}_d , the inner radius of the dust shell r_{in} , and the optical depth at 11.3 microns, $\tau_{11.3}$, for C-rich stars, or the optical depth at 10 microns, τ_{10} , for O-rich stars. We note that there are no appropriately calculated spectra for S stars; we treat these cases in the same way as for O-rich stars. For the 3 stars of type MS and S, the quality of the fit is still good.

We set the VOSA option that provides the fit parameter uncertainties using a statistical approach. The best fit is obtained for 100 virtual SEDs by applying a gaussian random noise (proportional to the observational er-

ror) to each photometric point. Then, for each parameter, the reported uncertainty is given by the standard deviation of the derived distribution, if its value is larger than half the grid step for the parameter. Otherwise, the reported uncertainty is just half the grid step.

The best fitting model is then used to infer the total observed flux F_{obs} of the star. Finally, the bolometric luminosity is obtained through the relation $L = 4\pi D^2 F_{\text{obs}}$. It is important to note that the uncertainty in luminosity, σ_L , is obtained through standard error propagation, that is

$$\frac{\sigma_L}{L} = 2\frac{\sigma_D}{D} + \frac{\sigma_{F_{\text{obs}}}}{F_{\text{obs}}} \quad (2)$$

Taking the uncorrected *Gaia* EDR3 parallaxes (noZP case) the typical flux uncertainties are $\sigma_{F_{\text{obs}}}/F_{\text{obs}} \simeq 1 - 7\%$. As to the distance error, we find that the large majority (85%) of the 20 analyzed stars $\sigma_D/D < 15\%$, and the largest uncertainty is $\sigma_D/D \simeq 32\%$. The majority (65%) of the 20 stars analyzed have $\sigma_L/L < 25\%$, and only 2 stars have $\sigma_{\sigma_L}/L \gtrsim 50\%$. Similar results apply for the L21ZP and G21ZP cases. It follows that in all cases under consideration the distance uncertainty, σ_D , dominates the error budget for L .

4.5. Evolutionary models: current core mass

The bolometric luminosity derived from the SED fitting is used to estimate the current mass of the core, M_c , for each TP-AGB star of spectroscopic type M, S, and C in our sample. This is done by using the predictions of TP-AGB stellar models. We adopt the core mass-luminosity (CMLR) relation, that describes a direct proportionality between the mass of the core M_c and the quiescent luminosity L_{CMLR} sustained by the H-burning shell (when the He-shell is almost extinguished). The existence of a positive correlation between the luminosity of a shell-burning star and the mass of its degenerate core – almost independent of the stellar mass, as is the case for RGB and TP-AGB stars –, was explained and extensively investigated in several works carried out in the past (Eggleton 1967; Paczyński 1970; Tuchman et al. 1983; Boothroyd & Sackmann 1988).

As we see in Fig. 6, if we exclude the first few TPs of each sequence (the so-called subluminous pre-pulses), the CMLR relation is well defined by TP-AGB stellar models over the range $0.5 \lesssim M_c/M_\odot \lesssim 0.8$, and a general good agreement is found among stellar models computed with different codes. Conversely, at larger core masses, $M_c > 0.8M_\odot$, the CMLR breaks down due to the possible occurrence of HBB, which makes the models overluminous (Boothroyd & Sackmann 1992; Bloeker & Schoenberner 1991). Moreover, the extreme

dependence of HBB on the adopted treatment of convection in the models causes a significant dispersion of the predictions for the luminosity at the same M_c . Note, for example, the large differences between the FRUITY models (orange) and those computed by Karakas et al. (2002, green) at $M_c \gtrsim 0.85M_\odot$. We also recall that these high-core mass stars are expected to recover the CMLR towards the end of the TP-AGB evolution, when the drastic reduction of the envelope mass by stellar winds makes HBB extinguish (Vassiliadis & Wood 1993; Marigo et al. 2013). This effect produces the bell-shape luminosity curves exhibited by some model sequences with $M_c > 0.8M_\odot$ of Fig. 6. Another possible violation of the CMLR towards higher luminosity may be caused by very deep 3DU episodes, when the efficiency is high (Herwig et al. 1998).

We have paid particular attention to considering all these aspects. First, we do not need to worry about the HBB effect as the luminosities estimated for our stars with $M_i^{\text{AGB}} \gtrsim 3 - 4M_\odot$ lie in the range $8000 \lesssim L/L_\odot \lesssim 15000$, and therefore they are well below the typical values expected when the process is operating ($L > 20000L_\odot$; see Fig. 6). Second, to homogeneously estimate M_c for all our stars we derive a synthetic fit formula for the CMLR, an approach that seems appropriate considering the well-defined and regular behavior of the models, as shown in Fig. 6 for $M_c < 0.8M_\odot$. The quiescent luminosity is expressed as a function of the current core mass, M_c , the core mass at the first thermal pulse, $M_{c,1\text{TP}}$, and the metallicity Z :

$$L_{\text{CMLR}} = (25667 + 481z)(M_c - 0.446) \quad (3a)$$

$$+ 10^{2.684 + 1.643M_c} \quad (3b)$$

$$- 10^{\xi - (M_{c,1\text{TP}} - 0.446)(M_c - M_{c,1\text{TP}})/0.012}, \quad (3c)$$

where $z = Z/Z_\odot$ and $Z_\odot = 0.014$. The relation is valid for $0.50 \lesssim M_c/M_\odot \lesssim 0.95$ and $0.01 \lesssim Z \lesssim 0.02$, in absence of HBB. The metallicity range ($-0.15 \lesssim [\text{Fe}/\text{H}] \lesssim +0.15$) is suitable for the open clusters analyzed in this work, except for Trumpler 5 ($\text{Fe}/\text{H} \simeq -0.37$) and its carbon stars V* V493 Mon that we treat separately.

The functional form for L_{CMLR} is essentially the same as the one proposed by Wagenhuber & Groenewegen (1998, their equation 5), but with some important changes. First, we derive new numerical coefficients by fitting the pre-flash luminosity for a high number (291) of thermal pulses taken from the large FRUITY⁷

⁷ Full-network Repository of Updated Isotopic Tables and Yields: <http://fruity.oa-teramo.inaf.it/>

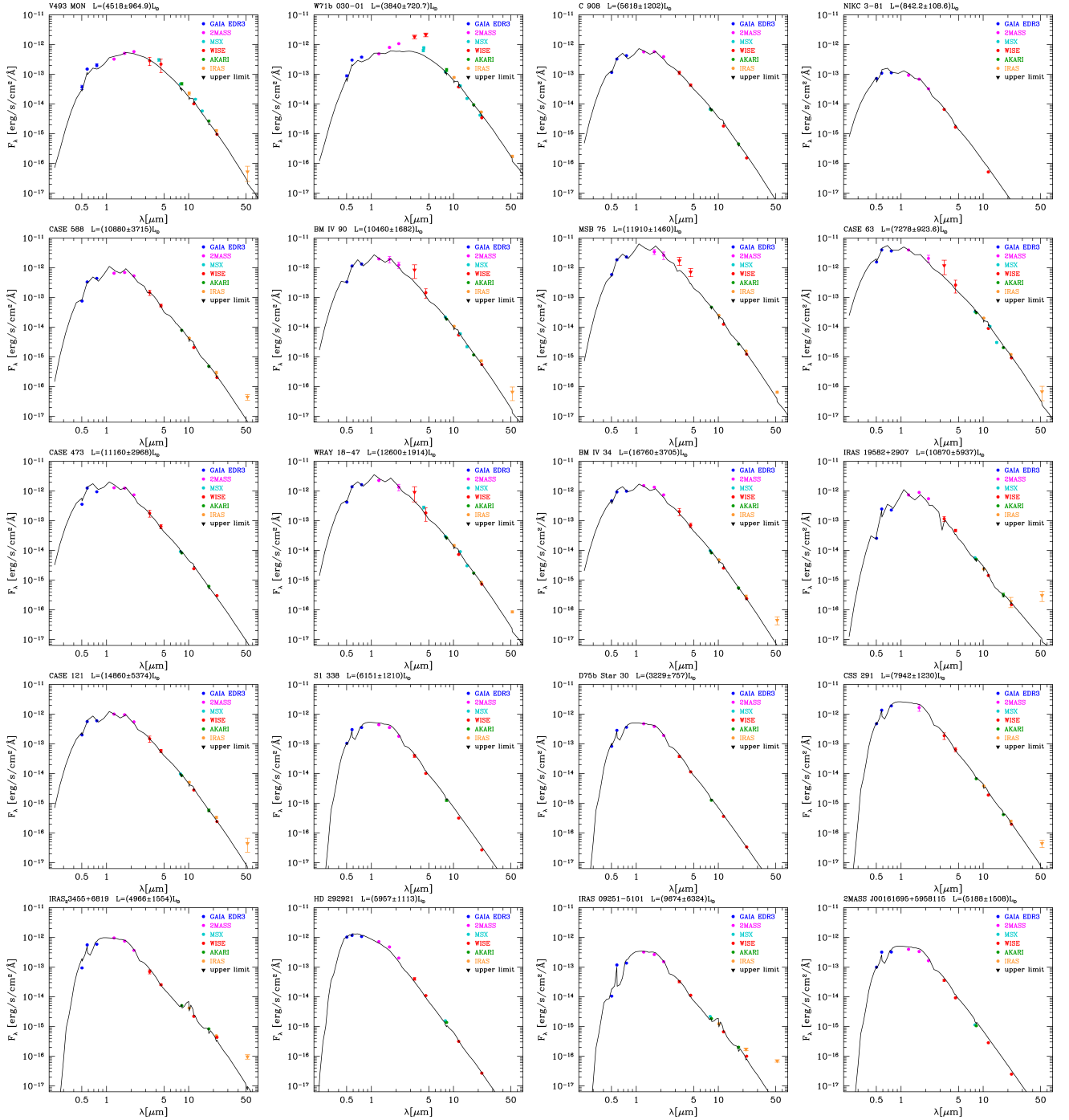


Figure 5. SED fitting of TP-AGB stars of type M, S and C in Milky Way open clusters. Interstellar extinction A_V is taken from the catalog of [Dias et al. \(2021\)](#). Each star is placed at the distance given by its own *Gaia* EDR3 parallax (no ZP correction). Photometric data (with error bars) from various sources are displayed with coloured symbols. Upper limits (denoted with filled triangles) are not considered in the fits. Note that all sources are consistent with being TP-AGB stars, except for NIKC 3-81 which is probably a R-hot star, placed below the RGB tip.

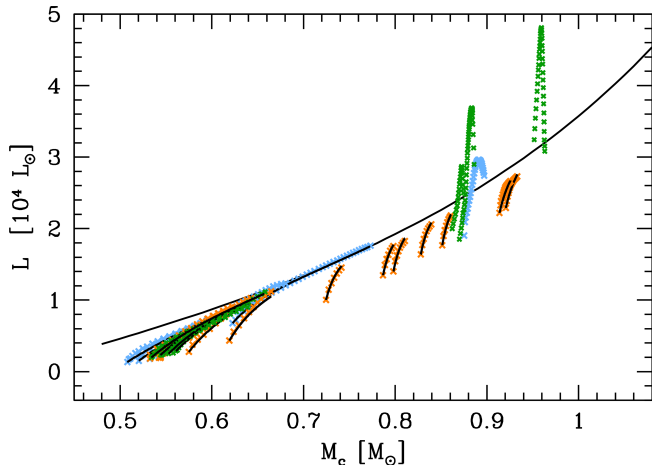


Figure 6. Core mass - luminosity relation of TP-AGB stars. TP-AGB model sequences (crosses) show the evolution of the core mass and luminosity during the quiescent stages of the TP cycles, for a few values of the initial stellar mass in the interval $1.0 \lesssim M_i^{\text{AGB}}/M_\odot \lesssim 6.5$, and metallicities close to the solar value ($0.01 \leq Z \leq 0.02$). Each model (cross) is taken at the pre-flash luminosity maximum, just before the occurrence of a He-shell thermal instability. Various sources are included, namely: Karakas et al. (2002, green); Cristallo et al. (2011, orange - FRUITY database); Addari (2020, blue - models computed with the MESA code). The solid black line running over the entire M_c range is an analytic fit to the asymptotic core mass - luminosity relation for $Z = 0.014$, given by Eq. (3a+3b). Overplotted to the TP-AGB models we show the predictions (black lines) obtained with the synthetic CMLR (Eq. 3a+3b+3c), including the pre-pulses and assuming the same $M_{c,1\text{TP}}$, $L_{1\text{TP}}$, Z , and M_c , as in the stellar models.

database. We select all TP-AGB models with $1.5 \leq M_i^{\text{AGB}}/M_\odot \leq 6.0$ and metallicity $0.01 \leq Z \leq 0.02$. We also add some additional TP-AGB tracks (132 TPs) computed with the MESA code (Paxton et al. 2011) for $M_i^{\text{AGB}} = 1.7, 1.9, 2.0, 2.5, 3.0 M_\odot$ and $Z = 0.014$ (Addari 2020), and the TP-AGB tracks (152 TPs) with $1.0 \leq M_i^{\text{AGB}}/M_\odot \leq 2.5 M_\odot$ and $Z = 0.012, 0.02$ published by Karakas et al. (2002). In total our reference data-set includes 575 models with known M_c , $M_{c,1\text{TP}}$, Z , and L . A standard chi-square minimization technique is adopted to obtain the coefficients. We note that at these solar-like metallicities the most massive FRUITY models do not show evident overluminosity effects due to the occurrence of HBB. This circumstance turns out to be useful as it allows us to map the CMLR at high M_c (where other models predict a strong HBB), which is necessary if we deal with massive TP-AGB stars at the end of their evolution when HBB is off.

The terms (3a) and (3b) describe the asymptotic behavior when thermal pulses have reached the full-amplitude regime, while the negative term (3c) provides

a correction to account for the first sub-luminous pulses. This phase is particularly important for low-mass stars with $M_c \lesssim 0.65 M_\odot$, as their brightening rate is rather slow and they reach the asymptotic regime after a relatively high number of thermal pulses. Neglecting the sub-luminous pulses would therefore lead to underestimating M_c for these stars. We emphasize again that the analytic relation of Eq.(3) is meant to describe the behavior of the quiescent luminosity of a TP-AGB star in absence of HBB and very efficient 3DU.

The CMLR is characterized by a mild dependence on metallicity: at increasing Z the luminosity is somewhat higher at given M_c . In the term (3a) we include linear dependence with the metallicity, expressed through the scaling factor $z = Z/Z_\odot$, where the reference solar metallicity is $Z_\odot = 0.014$ (in place of $Z_\odot = 0.02$ as in Wagenhuber & Groenewegen (1998)).

The parameter ξ in Eq. (3c) deserves some comments. It has a precise physical meaning as it determines the luminosity, $L_{1\text{TP}}$, at the first thermal pulse. In fact, if we set $M_c = M_{c,1\text{TP}}$ in Eq. (3) it is clear that 10^ξ measures the luminosity difference between the CMLR in the asymptotic regime (3a + 3b) and the first thermal pulse. The best fitting returns a global mean value $\xi = 3.596$. However, if we know the values $M_{c,1\text{TP}}$ and $L_{1\text{TP}}$ of a specific TP-AGB model, it is straightforward to derive the corresponding parameter ξ . In this case ξ is not a constant, but it varies as a function of the TP-AGB model under consideration.

We checked the accuracy of our fit relation for L_{CMLR} against the reference data-set of TP-AGB models at solar-like metallicities, as illustrated in Fig. 6. The performance is quite good: not only the relation reproduces satisfactorily the asymptotic behavior, but also recovers well the initial turn-on phase of the pre-pulses. This can be appreciated by comparing the various TP-AGB model sequences (crosses) with the synthetic CMLR (black lines), assuming the same $M_{c,1\text{TP}}$, $L_{1\text{TP}}$ and metallicity Z of the stellar models. As we can see, the formula reproduces the behavior of the different tracks very well, including the initial turn-on part. Considering the whole set of 575 luminosity points, the median relative error of the fit formula is $\simeq 4\%$, while for 70%, 80%, 90% of the cases the synthetic predictions for L deviate from the models less than 7%, 9%, 14%.

In this work, however, we employ the fit formula in the opposite way, that is to infer M_c starting from a known luminosity value. In brief, to estimate M_c from a given observed luminosity, L_{obs} , we proceed as follows. For each TP-AGB star member of an open cluster with known age and metallicity, its initial mass M_i^{AGB} is obtained from the corresponding

Table 4. Comparison of M_c predicted by various sets of full TP-AGB models and with the synthetic CMLR.

	FRUITY	K02	MESA
$L_{1\text{TP}} [L_\odot]$	2346	1982	2208
$M_{c,1\text{TP}} [M_\odot]$	0.533	0.534	0.542
Z	0.014	0.02	0.014
$L [L_\odot]$	$M_c [M_\odot]$		
4000	0.552	0.550	0.550
6000	0.576	0.580	0.577
8000	0.604	0.615	0.610
Results with the fit relation of Eq. (3)			
4000	0.552	0.554	0.558
6000	0.578	0.579	0.581
8000	0.609	0.609	0.610

Notes: Full TP-AGB models are from [Cristallo et al. \(2011, FRUITY\)](#), [Karakas et al. \(2002, K02\)](#), and [Addari \(2020, MESA\)](#).

PARSEC isochrone. Then, we extract $M_{c,1\text{TP}}$ and $L_{1\text{TP}}$ from the PARSEC stellar evolutionary track of initial mass M_i^{AGB} and metallicity Z . Finally, with the aid of a standard root-finding technique we solve the equation $L_{\text{obs}} - L_{\text{CMLR}}(M_c, M_{c,1\text{TP}}, L_{1\text{TP}}, Z) = 0$ and get M_c . We can also compute the error on M_c due to the uncertainty on L_{obs} , obtained with Eq. (2), which depends on both flux and distance errors. Adopting Eq. (3) for L_{CMLR} , it is straightforward to convert σ_L into the statistical uncertainty of the core mass, $\sigma_{M_c, \text{CMLR}}$, by using the standard error propagation law. We find that for the noZP case $\sigma_{M_c, \text{CMLR}}$ varies in the range $\simeq 0.006 - 0.125 M_\odot$, with a median value of $\simeq 0.023 M_\odot$. Among the 19 TP-AGB stars examined, 13 (16) have $\sigma_{M_c, \text{CMLR}} \leq 0.03, (0.05) M_\odot$. The largest uncertainties with $\sigma_{M_c, \text{CMLR}} \gtrsim 0.1 M_\odot$ apply to the C star IRAS 19582+2907 and the M star IRAS 09251-5101. The other two cases, L21ZP and G21ZP, show somewhat different results for individual objects, but the order of magnitude and the typical range for $\sigma_{M_c, \text{CMLR}}$ remain the same.

At this point it is worth analyzing the accuracy of the method to infer M_c . Clearly, intrinsic differences in luminosity and core mass exist among different sets of TP-AGB models, but in the mass range not affected by the occurrence of HBB they appear to be small. For example, let us consider a TP-AGB model with $M_i^{\text{AGB}} = 2.5 M_\odot$ and compare the results from [Karakas et al. \(2002, K02\)](#) for $Z = 0.02$, FRUITY and MESA for $Z = 0.014$. Taking a small grid of luminosity, $L = 4000, 6000, 8000 L_\odot$, the different models⁸ predict the values of M_c reported in Table 4. Overall, the differ-

ences in M_c are modest, ranging within $0.002 - 0.01 M_\odot$. Using our fit relation with $M_{c,1\text{TP}}$ and $L_{1\text{TP}}$ extracted from the three TP-AGB models, we also obtain very similar M_c , the deviations being of the order of few $10^{-3} M_\odot$ in all cases. From these tests we are therefore confident that the formula (Eq. 3) is a reliable tool to derive M_c of the TP-AGB stars in our sample.

Comparing the dispersion in M_c produced by different TP-AGB models at fixed luminosity with $\sigma_{M_c, \text{CMLR}}$ obtained for the observed stars (Eq. 2), it turns out that in many cases the latter uncertainty – due to distance and flux errors – is larger (see Table 5). In other words, differences in M_c among TP-AGB models at solar-like metallicities are mostly washed away by the observational errors.

A further effect is related to the changes in luminosity caused by the occurrence of thermal pulses (see left panel of Fig. 7). The stars in our sample, in principle, may not lie on the CMLR for this reason ([Marigo et al. 1999](#); [Boothroyd & Sackmann 1988](#)). The probability and extent of these deviations from the CMLR were thoroughly quantified ([Wood & Zarro 1981](#); [Boothroyd & Sackmann 1988](#); [Wagenhuber & Groenewegen 1998](#)). Finding a star above the CMLR is always quite unlikely (with a probability $\simeq 1 - 2\%$), as the luminosity rise (up to L_C in Fig. 7) when a TP occurs is extremely short-lived. Instead, the probability increases appreciably to observe TP-AGB stars below the CMLR as they are evolving on the slow luminosity dip following a thermal pulse (from L_D to L_{CMLR}), when the nuclear activity of the H-burning shell starts recovering during the power-down phase of a He-shell flash. At the luminosity minimum, L_D , models predict that the nuclear luminosities produced by the H- and He-burning shells are comparable, $L_H \simeq L_{\text{He}} \simeq 0.5 L_D$. The maximum extent of L_D below the CMLR can be as much as ≈ 1 mag, for the models with the lowest core mass ($M_c \approx 0.5 - 0.6 M_\odot$). But what really matters is the time spent on these fainter stages with respect to the total duration of the pulse cycle, since this controls the probability of observing a star below the CMLR. An example of the probability distribution of the luminosity on the slow dip is given in the top-right panel of Fig. 7.

Using the predictions of TP-AGB models (e.g., [Boothroyd & Sackmann 1988](#); [Wagenhuber & Groenewegen 1998](#)) it turns out that the fraction of the pulse cycle that occurs on the slow luminosity dip becomes smaller at increasing core mass. For example, at solar metallicity, the probability of finding a star with $M_c \simeq 0.55, 0.65, 0.75 M_\odot$ and a luminosity between L_{CMLR} down to $\Delta \log(L) = 0.1$ dex below (i.e. within 0.25 mag fainter), is equal to 57%, 67%, 77% respec-

⁸ In all cases a linear interpolation in L is adopted to get M_c .

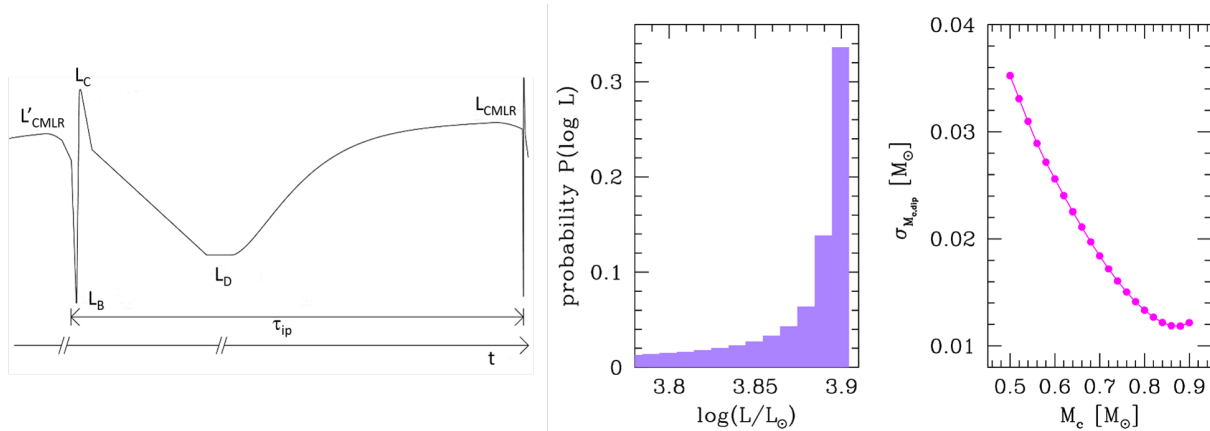


Figure 7. Effects of the slow luminosity dip driven by thermal pulses. *Left panel:* sketch of the luminosity evolution as a function of time between two consecutive thermal pulses, with interpulse period τ_{ip} . The labels indicate a few relevant stages: the quiescent luminosity L_{CMLR} , the rapid dip L_B and peak L_C , and the slow dip L_D . The time axis is stretched around the first TP, from L'_{CMLR} to L_D . These short-lived stages typically covers $\lesssim 0.1$ of the interpulse period. *Middle panel:* probability distribution (purple histogram) of the luminosity along the slow dip from L_D to L_{CMLR} . The width of the luminosity bins is set to 0.01 dex. We consider a TP-AGB star with solar metallicity, $M_c = 0.6 M_\odot$, and $L_{CMLR} \simeq 8000 L_\odot$, and $L_D \simeq 3400 L_\odot$. *Right panel:* statistical (positive only) uncertainty of the core mass derived from the CMLR, due to the probability that a star intercepts the observed luminosity while evolving on a slow dip of a TP at higher M_c . The uncertainty is shown as a function of the core mass in the range $0.5 \leq M_c/M_\odot \leq 0.9$. The corresponding quiescent luminosity in the asymptotic regime spans the interval $4600 \lesssim L_{CMLR}/L_\odot \lesssim 26400$. See the text for more details.

tively. It means that stars with higher M_c stay statistically closer to the CMLR (in absence of HBB).

Given these arguments, we can now ask what is the order of magnitude of the error we commit in using the CMLR to derive M_c , that is under the assumption that the observed luminosity, L_{obs} , lies exactly on the CMLR. The answer is that the CMLR provides a lower limit to the true M_c , as there is always a finite probability that L_{obs} is intercepted while the star is evolving in the slow luminosity dip of a pulse cycle at higher M_c .

To quantify the associated statistical error we proceed as follows. Let us denote with $M_{c,CMLR}$ the core mass predicted by the CMLR for $L_{CMLR} = L_{obs}$. First, we note that the maximum range of M_c , compatible with the observed L_{obs} , goes from $M_{c,CMLR}$ to the maximum core mass, $M_{c,D}$, at which the minimum luminosity, reached during the flash-driven variations, equals the observed luminosity, that is $L_D = L_{obs}$. Second, we compute the probability density function that a star with $M_{c,CMLR} \leq M_c \leq M_{c,D}$ attains L_{obs} during a luminosity dip. Then, we estimate the standard deviation of this distribution, $\sigma_{M_c,dip}$, by extracting the value of the core mass, \tilde{M}_c , such that the probability to intercept L_{obs} from all luminosity dips with $M_{c,CMLR} \leq M_c \leq \tilde{M}_c$ is equal to 68%. Finally we define $\sigma_{M_c,dip} = \tilde{M}_c - M_{c,CMLR}$ as the statistical uncertainty on the estimation of M_c due to the flash-driven luminosity variations, for a given L_{obs} .

We repeated the procedure just described over a range of quiescent luminosities corresponding to $0.5 \leq M_c/M_\odot \leq 0.9$. The results are shown in the right panel of Fig. 7. We find that $\sigma_{M_c,dip}$ decreases at increasing M_c (or equivalently L), and typically ranges from $\approx 0.035 M_\odot$ to $\approx 0.01 M_\odot$. The inverse correlation of $\sigma_{M_c,dip}$ with M_c can be explained as the result of the time spent in the slow luminosity dip, which is shorter at higher M_c .

The final estimate of the core mass is computed as follows

$$M_c = M_{c,CMLR} - \sigma_{M_c,CMLR} + \sqrt{\sigma_{M_c,CMLR}^2 + \sigma_{M_c,dip}^2}. \quad (4)$$

Note that the uncertainty due to the slow luminosity dip, $\sigma_{M_c,dip}$, is only positive and it is combined with $\sigma_{M_c,CMLR}$ through the standard summation in quadrature. The results for the core mass of the TP-AGB stars of the spectroscopic sample are reported in Tables 5 and 6. As expected, we see that the asymmetry of the error-bars increases for the stars with $M_c \lesssim 0.6 M_\odot$ (such as V* V493 Mon, [W71b] 030-31, C* 908, S1* 338, [D75b] Star 30, IRAS 23455-6819, HD 292921), as these objects have a higher probability to be observed while they are evolving on the slow luminosity dip, which corresponds to a larger $\sigma_{M_c,dip}$.

5. ANALYSIS OF THE RESULTS

Our preliminary study provides us with a lot of information for each star which, combined together, can

Table 5. Results from SED fitting and TP-AGB models. Cluster ages and A_V from Cantat-Gaudin et al. (2020).

star	χ^2	$A_V^{(b)}$ [mag]	\dot{M}_{dust} [$M_{\odot} \text{ yr}^{-1}$]	$\tau_{11.3}/\tau_{10}$	$M_i^{\text{AGB}(c)}$ [M_{\odot}]	D [pc]	L [L_{\odot}]	M_c [M_{\odot}]
V* V493 Mon	4.431E+01	1.38 ± 0.10	1.19E-09	2.00E-01	1.328 ± 0.107	2714 ± 268 2661 ± 258 2711 ± 268	4091 ± 867 3933 ± 819 4081 ± 864	0.553 ^{+0.034} _{-0.011} 0.550 ^{+0.034} _{-0.010} 0.553 ^{+0.034} _{-0.011}
[W71b] 030 – 31	5.822E+01	2.53 ± 0.10	3.37E-09	2.00E-01	1.473 ± 0.120	1790 ± 107 1788 ± 106 1698 ± 96	3520 ± 500 3512 ± 498 3167 ± 430	0.545 ^{+0.032} _{-0.006} 0.545 ^{+0.032} _{-0.006} 0.538 ^{+0.035} _{-0.005}
C* 908	1.549E+02	0.36 ± 0.09	1.69E-10	4.00E-02	1.660 ± 0.155	3831 ± 361 3293 ± 267 3735 ± 343	5355 ± 1133 3956 ± 732 5088 ± 1052	0.578 ^{+0.034} _{-0.015} 0.553 ^{+0.034} _{-0.009} 0.573 ^{+0.033} _{-0.014}
Case 588	1.715E+02	0.65 ± 0.10	2.83E-10	2.48E-02	1.834 ± 0.229	4669 ± 748 3706 ± 471 4999 ± 857	9293 ± 3316 5854 ± 1702 10657 ± 4043	0.652 ^{+0.055} _{-0.050} 0.591 ^{+0.037} _{-0.024} 0.675 ^{+0.065} _{-0.061}
BM IV 90	3.418E+01	1.35 ± 0.12	1.59E-10	1.96E-02	1.941 ± 0.224	2884 ± 211 2640 ± 177 2853 ± 207	10421 ± 1874 8730 ± 1463 10196 ± 1819	0.681 ^{+0.034} _{-0.028} 0.652 ^{+0.032} _{-0.022} 0.677 ^{+0.035} _{-0.027}
MBS 75	1.315E+02	1.01 ± 0.10	1.89E-10	2.38E-02	1.977 ± 0.229	2050 ± 107 1871 ± 89 2047 ± 107	11473 ± 2028 9551 ± 1602 11432 ± 2021	0.696 ^{+0.036} _{-0.030} 0.663 ^{+0.032} _{-0.024} 0.695 ^{+0.036} _{-0.030}
Case 63	6.298E+01	2.63 ± 0.07	1.97E-10	1.84E-02	2.063 ± 0.229	1745 ± 95 1594 ± 80 1719 ± 92	6887 ± 907 5750 ± 705 6686 ± 872	0.611 ^{+0.029} _{-0.013} 0.590 ^{+0.030} _{-0.010} 0.607 ^{+0.029} _{-0.013}
Case 473	2.577E+02	4.26 ± 0.04	7.87E-11	8.35E-03	2.326 ± 0.189	3648 ± 443 3414 ± 388 3367 ± 378	11162 ± 2908 9773 ± 2394 9509 ± 2300	0.673 ^{+0.050} _{-0.045} 0.650 ^{+0.043} _{-0.036} 0.646 ^{+0.041} _{-0.034}
WRAY 18-47	5.362E+01	0.98 ± 0.09	2.12E-10	3.41E-02	2.596 ± 0.212	2782 ± 173 2521 ± 142 2452 ± 134	10958 ± 1661 8999 ± 1257 8518 ± 1163	0.665 ^{+0.025} _{-0.017} 0.634 ^{+0.050} _{-0.017} 0.627 ^{+0.029} _{-0.015}
BM IV 34	9.637E+01	1.60 ± 0.11	8.44E-11	1.56E-02	3.540 ± 0.309	4531 ± 433 3848 ± 312 3733 ± 294	15757 ± 3551 11366 ± 2235 ^(a) 10695 ± 2051 ^(a)	0.770 ^{+0.023} _{-0.023} 0.659 ^{+0.052} _{-0.046} 0.645 ^{+0.049} _{-0.044}
IRAS 19582+2907	6.266E+02	3.94 ± 0.05	4.21E-11	9.94E-03	4.420 ± 0.419	4938 ± 1288 3743 ± 740 4139 ± 905	10866 ± 5905 ^(a) 6243 ± 2604 ^(a) 7635 ± 3504 ^(a)	0.648 ^{+0.127} _{-0.125} 0.542 ^{+0.072} _{-0.065} 0.576 ^{+0.089} _{-0.083}
Case 121	1.917E+01	1.63 ± 0.04	1.27E-10	2.08E-02	6.960 ± 0.800	5028 ± 870 3856 ± 512 4454 ± 682	14148 ± 5075 ^(a) 8323 ± 2314 ^(a) 11103 ± 3543 ^(a)	0.714 ^{+0.097} _{-0.095} 0.592 ^{+0.061} _{-0.054} 0.653 ^{+0.078} _{-0.074}
S1* 338	2.009E+02	1.22 ± 0.05	1.67E-12	2.31E-04	1.646 ± 0.150	4708 ± 454 4314 ± 382 4265 ± 373	5012 ± 1107 4209 ± 862 4114 ± 835	0.572 ^{+0.033} _{-0.014} 0.558 ^{+0.034} _{-0.011} 0.556 ^{+0.034} _{-0.010}
[D75b] Star 30	4.446E+02	1.30 ± 0.02	6.70E-12	3.45E-04	1.927 ± 0.224	3427 ± 375 3044 ± 296 3215 ± 330	2988 ± 689 2358 ± 486 2630 ± 571	0.539 ^{+0.036} _{-0.010} 0.523 ^{+0.034} _{-0.007} 0.530 ^{+0.035} _{-0.008}
CSS 291	8.390E+01	0.84 ± 0.09	5.74E-11	2.39E-03	2.130 ± 0.178	2392 ± 141 2190 ± 118 2214 ± 121	7954 ± 1371 6668 ± 1082 6814 ± 1113	0.626 ^{+0.032} _{-0.020} 0.604 ^{+0.030} _{-0.015} 0.606 ^{+0.031} _{-0.016}
IRAS 23455+6819	1.530E+02	2.85 ± 0.00	9.19E-10	2.56E-02	1.310 ± 0.100	3044 ± 445 2816 ± 381 2679 ± 345	4872 ± 1480 4167 ± 1174 3773 ± 1014	0.567 ^{+0.035} _{-0.019} 0.554 ^{+0.035} _{-0.014} 0.547 ^{+0.034} _{-0.012}
HD 292921	1.299E+02	1.48 ± 0.00	2.11E-11	5.59E-04	1.620 ± 0.144	4054 ± 340 3549 ± 261 3925 ± 319	5981 ± 1134 4584 ± 774 5608 ± 1034	0.588 ^{+0.032} _{-0.015} 0.563 ^{+0.031} _{-0.019} 0.581 ^{+0.030} _{-0.014}
IRAS 09251-5101	1.127E+02	2.86 ± 0.00	4.29E-10	2.55E-02	2.721 ± 0.221	6978 ± 2211 4928 ± 1103 6213 ± 1753	9650 ± 6325 4813 ± 2258 ^(a) 7651 ± 4483	0.647 ^{+0.081} _{-0.078} 0.505 ^{+0.069} _{-0.059} 0.620 ^{+0.050} _{-0.044}
2MASS J00161695+5958115	9.889E+02	2.62 ± 0.01	1.67E-12	1.05E-04	2.743 ± 0.222	4439 ± 609 4190 ± 542 3952 ± 483	4924 ± 1381 4387 ± 1163 ^(a) 3903 ± 977 ^(a)	0.508 ^{+0.051} _{-0.036} 0.494 ^{+0.046} _{-0.031} 0.481 ^{+0.042} _{-0.026}

Notes: For each star the distance, luminosity and core mass are given for 3 choices of *Gaia* EDR3 parallax ZP correction (from top to bottom): noZP, L21ZP, and G21ZP. See the text for more details.

(a) Luminosity below the predicted onset of the TP-AGB phase. The core mass is estimated from the asymptotic CMLR (Eq. (3a + 3b)).

(b) In the SED fitting the visual extinction is adjusted within the range ($A_V \pm 0.2$) mag.

(c) The initial mass is obtained from the PARSEC stellar isochrone of the cluster's age; the error bar corresponds to an uncertainty of ± 0.1 dex in $\log(\text{age})$.

Table 6. Results from SED fitting and TP-AGB models. Cluster ages and A_V from Dias et al. (2021).

star	χ^2	$A_V^{(b)}$ [mag]	\dot{M}_{dust} [$M_{\odot} \text{ yr}^{-1}$]	$\tau_{11.3}/\tau_{10}$	$M_i^{\text{AGB}(c)}$ [M_{\odot}]	D [pc]	L [L_{\odot}]	M_c [M_{\odot}]
V* V493 Mon	4.086E+01	2.00 ± 0.12	1.27E-09	2.00E-01	1.423 ± 0.123	2714 ± 268	4518 ± 965	0.563 ^{+0.031} _{-0.012}
						2661 ± 258	4343 ± 911	0.560 ^{+0.035} _{-0.011}
						2711 ± 268	4506 ± 962	0.562 ^{+0.031} _{-0.012}
[W71b] 030 – 31	1.024E+02	3.11 ± 0.07	1.97E-09	2.00E-01	2.315 ± 0.188	1790 ± 107	3840 ± 721	0.550 ^{+0.033} _{-0.009}
						1788 ± 106	3831 ± 717	0.550 ^{+0.033} _{-0.009}
						1698 ± 96	3455 ± 626	0.543 ^{+0.032} _{-0.007}
C* 908	1.474E+02	0.57 ± 0.12	1.69E-10	4.00E-02	1.491 ± 0.122	3831 ± 361	5618 ± 1202	0.581 ^{+0.031} _{-0.015}
						3293 ± 267	4151 ± 778	0.556 ^{+0.034} _{-0.009}
						3735 ± 343	5338 ± 1117	0.577 ^{+0.034} _{-0.014}
Case 588	1.414E+02	1.09 ± 0.08	1.50E-10	2.00E-02	2.119 ± 0.177	4669 ± 748	10880 ± 3715	0.677 ^{+0.056} _{-0.027}
						3706 ± 471	6855 ± 1887	0.608 ^{+0.038} _{-0.027}
						4999 ± 857	12477 ± 4542	0.704 ^{+0.072} _{-0.069}
BM IV 90	3.394E+01	1.40 ± 0.05	1.59E-10	1.94E-02	2.169 ± 0.181	2884 ± 211	10464 ± 1682	0.667 ^{+0.034} _{-0.026}
						2640 ± 177	8766 ± 1302	0.638 ^{+0.032} _{-0.019}
						2853 ± 207	10238 ± 1632	0.663 ^{+0.033} _{-0.025}
MBS 75	1.204E+02	1.20 ± 0.08	1.50E-10	2.02E-02	1.943 ± 0.224	2050 ± 107	11909 ± 1460	0.706 ^{+0.028} _{-0.021}
						1871 ± 89	9913 ± 1127	0.672 ^{+0.027} _{-0.017}
						2047 ± 107	11866 ± 1455	0.705 ^{+0.028} _{-0.021}
Case 63	7.246E+01	2.81 ± 0.03	1.97E-10	1.82E-02	1.992 ± 0.232	1745 ± 95	7278 ± 924	0.621 ^{+0.028} _{-0.013}
						1594 ± 80	6077 ± 716	0.599 ^{+0.030} _{-0.010}
						1719 ± 92	7066 ± 888	0.617 ^{+0.030} _{-0.013}
Case 473	2.577E+02	4.26 ± 0.07	7.87E-11	8.35E-03	2.326 ± 0.189	3648 ± 443	11162 ± 2968	0.673 ^{+0.051} _{-0.046}
						3414 ± 388	9773 ± 2447	0.650 ^{+0.044} _{-0.037}
						3367 ± 378	9509 ± 2351	0.646 ^{+0.042} _{-0.035}
WRAY 18-47	5.634E+01	1.35 ± 0.12	1.59E-10	2.14E-02	2.553 ± 0.209	2782 ± 173	12599 ± 1914	0.693 ^{+0.037} _{-0.031}
						2521 ± 142	10347 ± 1448	0.655 ^{+0.032} _{-0.021}
						2452 ± 134	9794 ± 1341	0.647 ^{+0.030} _{-0.019}
BM IV 34	9.945E+01	1.82 ± 0.07	8.44E-11	1.62E-02	3.252 ± 0.279	4531 ± 433	16764 ± 3705	0.766 ^{+0.052} _{-0.050}
						3848 ± 312	12093 ± 2325	0.716 ^{+0.024} _{-0.014}
						3733 ± 294	11379 ± 2132	0.710 ^{+0.022} _{-0.012}
IRAS 19582+2907	6.266E+02	3.94 ± 0.06	4.21E-11	9.94E-03	2.089 ± 0.175	4938 ± 1288	10866 ± 5937	0.678 ^{+0.092} _{-0.090}
						3743 ± 740	6243 ± 2622	0.598 ^{+0.047} _{-0.037}
						4139 ± 905	7635 ± 3526	0.622 ^{+0.057} _{-0.051}
Case 121	2.643E+01	1.85 ± 0.03	1.27E-10	2.55E-02	2.858 ± 0.232	5028 ± 870	14862 ± 5374	0.731 ^{+0.088} _{-0.087}
						3856 ± 512	8743 ± 2456	0.643 ^{+0.032} _{-0.022}
						4454 ± 682	11663 ± 3755	0.681 ^{+0.053} _{-0.049}
S1* 338	5.090E+02	1.59 ± 0.01	1.67E-12	1.04E-04	1.600 ± 0.140	4708 ± 454	6151 ± 1210	0.590 ^{+0.032} _{-0.016}
						4314 ± 382	5165 ± 933	0.573 ^{+0.032} _{-0.012}
						4265 ± 373	5048 ± 902	0.571 ^{+0.032} _{-0.012}
[D75b] Star30	4.141E+02	1.44 ± 0.03	1.67E-12	1.56E-04	2.068 ± 0.211	3427 ± 375	3229 ± 757	0.540 ^{+0.033} _{-0.010}
						3044 ± 296	2548 ± 535	0.525 ^{+0.034} _{-0.007}
						3215 ± 330	2843 ± 627	0.532 ^{+0.035} _{-0.009}
CSS 291	8.374E+01	0.83 ± 0.00	5.74E-11	1.97E-03	2.119 ± 0.177	2392 ± 141	7942 ± 1230	0.626 ^{+0.030} _{-0.018}
						2190 ± 118	6658 ± 964	0.604 ^{+0.029} _{-0.014}
						2214 ± 121	6803 ± 993	0.607 ^{+0.030} _{-0.014}
IRAS 23455+6819	1.510E+02	2.90 ± 0.00	9.19E-10	2.56E-02	1.410 ± 0.122	3044 ± 445	4966 ± 1554	0.571 ^{+0.036} _{-0.019}
						2816 ± 381	4249 ± 1235	0.558 ^{+0.036} _{-0.015}
						2679 ± 345	3847 ± 1068	0.551 ^{+0.035} _{-0.013}
HD 292921	1.460E+02	1.48 ± 0.00	2.11E-11	5.90E-04	1.620 ± 0.144	4054 ± 340	5957 ± 1113	0.587 ^{+0.031} _{-0.015}
						3549 ± 261	4566 ± 758	0.563 ^{+0.031} _{-0.019}
						3925 ± 319	5586 ± 1014	0.581 ^{+0.030} _{-0.013}
IRAS 09251-5101	1.371E+02	2.86 ± 0.00	4.29E-10	2.56E-02	2.721 ± 0.221	6978 ± 2211	9674 ± 6324	0.647 ^{+0.082} _{-0.078}
						4928 ± 1103	4825 ± 2256	0.506 ^{+0.069} _{-0.059}
						6213 ± 1753	7669 ± 4480	0.620 ^{+0.051} _{-0.044}
2MASS J00161695+5958115	1.166E+03	2.72 ± 0.09	1.67E-12	1.02E-04	2.689 ± 0.218	4439 ± 609	5188 ± 1508	0.515 ^{+0.054} _{-0.039}
						4190 ± 542	4622 ± 1272 ^(a)	0.500 ^{+0.049} _{-0.033}
						3952 ± 483	4112 ± 1072 ^(a)	0.487 ^{+0.044} _{-0.029}

Notes: For each star the distance, luminosity and core mass are given for 3 choices of *Gaia* EDR3 parallax ZP correction (from top to bottom): noZP, L21ZP, and G21ZP. See the text for more details.

(a) Luminosity below the predicted onset of the TP-AGB phase. The core mass is estimated from the asymptotic CMLR (Eq. (3a + 3b)).

(b) In the SED fitting the visual extinction is adjusted within the range ($A_V \pm 0.2$) mag.

(c) The initial mass is obtained from the PARSEC stellar isochrone of the cluster's age; the error bar corresponds to an uncertainty of ± 0.1 dex in $\log(\text{age})$.

help us try to sketch a general view of the TP-AGB phase at solar-like metallicity. There is an important aspect that also needs to be highlighted: the homogeneity of the stellar models. The same PARSEC stellar tracks and isochrones (Bressan et al. 2012) were used to derive the ages of the clusters (Dias et al. 2021; Cantat-Gaudin et al. 2020) and hence M_i^{AGB} , to extract the conditions at the first thermal pulse $M_{c,1\text{TP}}$ and $L_{1\text{TP}}$, and to estimate the initial masses of the white dwarf progenitors that define the initial-final mass relation (Cumings et al. 2018; Marigo et al. 2020). Clearly, this does not safeguard the work from possible systematic errors, but guarantees the internal self-consistency of the results.

For the purposes of the discussion that follows, we invite the reader to refer to Tables 2, 5, 6, and Figs. 8, 9 which show the luminosity and core mass of the stars under examination. They contain the results for two cluster age sets (Dias et al. 2021; Cantat-Gaudin et al. 2020) and three cases of parallax correction (noZP, L21ZP, G21ZP). For simplicity, in the following analysis we will mainly refer to the ages taken from Dias et al. (2021) in conjunction with the noZP case. Whenever major differences emerge with the other combinations, we will report them.

5.1. Evolutionary properties of TP-AGB stars in open clusters

Initial masses of carbon stars—The formation of solar-like metallicity carbon stars is confirmed over an initial-mass range that has the lower extreme, $M_i^{\text{AGB}} \simeq 1.5 M_\odot$, defined by the star C* 908 or [W71b] 030-01 if adopting cluster ages from Dias et al. (2021) or (Cantat-Gaudin et al. 2020). This value agrees with the minimum mass for carbon stars predicted by TP-AGB models with $Z = 0.014$ computed by Cristallo et al. (2011) and Ventura et al. (2018). In our sample there is a carbon star, V* V493 Mon, with a lower initial mass, $M_i^{\text{AGB}} \approx 1.3 - 1.4 M_\odot$, but we observe that the host cluster, Trumpler 5, is relatively metal poor (Carrera et al. 2019, $[\text{Fe}/\text{H}] \simeq -0.37$) and therefore the star does not sample the mass range pertaining to solar metallicity.

As to the upper limit for carbon stars, let us focus on the 3 objects with the most massive progenitors, namely BM IV 34, IRAS 19582+2907 and Case 121 (Case 49 is rejected).

Adopting the age catalog of Cantat-Gaudin et al. (2020), Case 121, member of the cluster Berkeley 72, is assigned $M_i^{\text{AGB}} \simeq 7 M_\odot$. This value is very close or even above the maximum limit, $M_{\text{up}} \approx 6 - 7 M_\odot$, to develop a degenerate C-O core after helium burning. It might

be consistent with a quasi-massive star experiencing the Super-AGB phase once after the completion of the carbon burning in the core (Doherty et al. 2015; Siess 2010). IRAS 19582+2907, hosted in the cluster FSR 0172, corresponds to a progenitor initial mass $M_i^{\text{AGB}} \simeq 4.4 M_\odot$, which points towards a standard double-shell TP-AGB phase.

According to stellar evolution theory, the possibility of forming carbon stars at such high masses requires that two conditions are met: the 3DU process is active while the HBB process is weakly efficient or extinguished. Stellar models (e.g., Frost et al. 1998; Groenewegen et al. 2016; Marigo et al. 2013) indicate that such configuration can be attained towards the end of evolution if, due to the strong reduction of the envelope mass via stellar winds, the temperature at the base of the convective envelope drops so much that the nuclear reactions of the CNO cycle quench, while some last dredge-up episodes still occur, enriching the surface with primary carbon, and eventually making the C/O ratio overcome one. This picture is supported by the detection of very bright carbon stars, typically heavily obscured by dusty envelopes produced by intense mass loss (van Loon et al. 1998; Groenewegen et al. 2016).

May this scenario be reasonably applied to IRAS 19582+2907 and Case 121? We tend to be skeptical about this possibility for the following reasons: Both stars have a luminosity that places them below the first thermal pulse (Fig. 8) for initial masses derived from the age catalog of Cantat-Gaudin et al. (2020). From a theoretical point of view, this involves a severe difficulty in explaining the surface enrichment in carbon. Furthermore, these stars do not appear dust-enshrouded, so the hypothesis of a late transition to C-rich phase, shortly before ending their evolution, is dropped. On the other hand, a natural way out of this inconsistency is provided by a reassessment of the age of the parent clusters. Using Dias et al. (2021) to date Berkeley 72, the initial mass of Case 121 drops to $\simeq 2.9 M_\odot$, so that the values of luminosity and core mass fit well within a standard evolution of TP-AGB, in absence of HBB (see Fig. 9). The cluster FSR 0172 is not present in the Dias et al. (2021) catalog. Adopting the age estimate of $\simeq 1.33$ Gyr provided by Kharchenko et al. (2013, identifier: MWSC 3218), IRAS 19582+2907 is assigned an initial mass of $\simeq 1.9 M_\odot$, which brings the star back into the standard TP-AGB framework. These aspects will need to be verified in future studies.

If we reject the ages of Cantat-Gaudin et al. (2020) for Case 121 and IRAS 19582+2907, it turns out that the most massive and brightest carbon star is BM IV 34, member of the cluster Haffner 14, with an initial mass

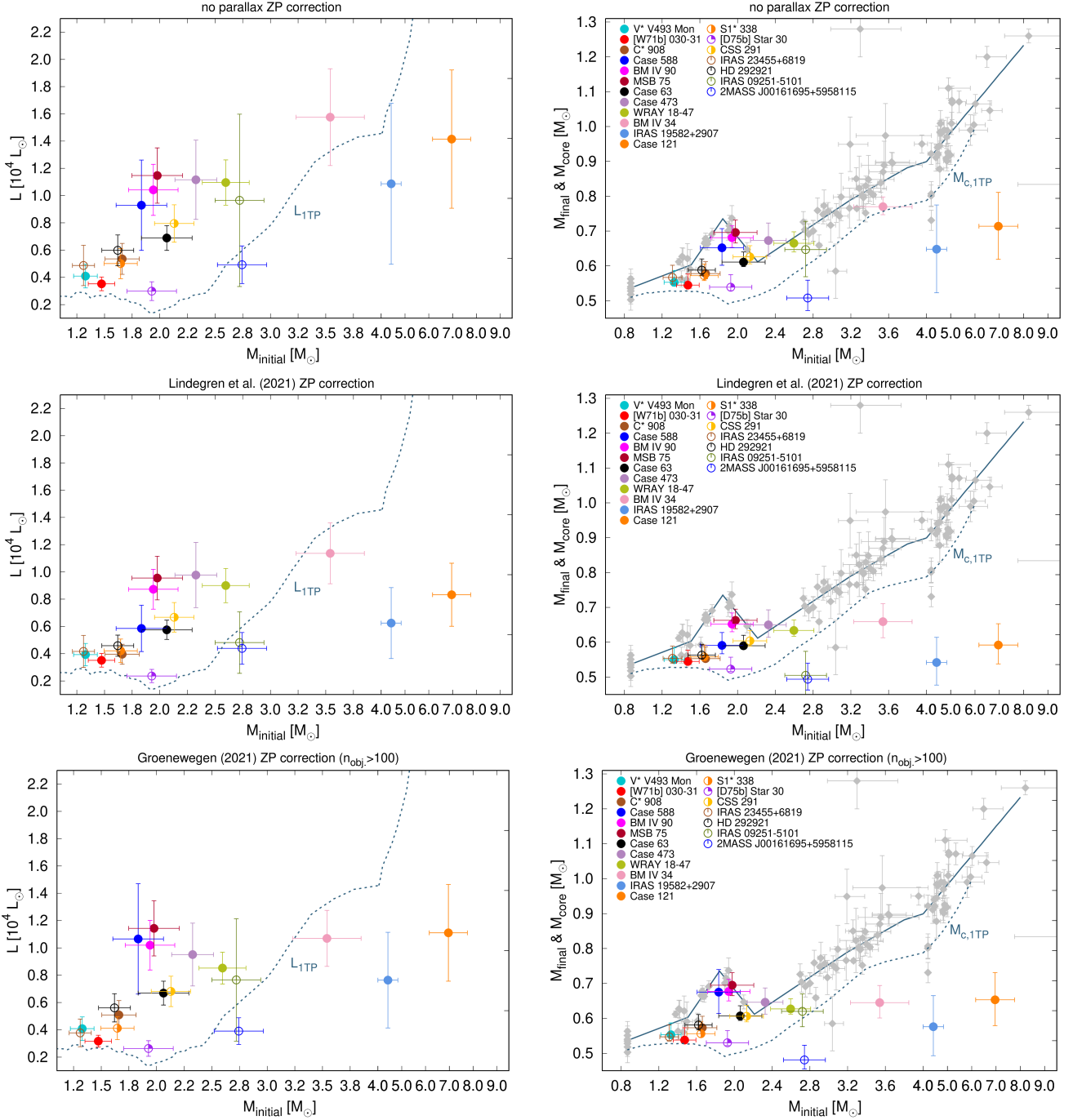


Figure 8. Luminosities and core masses of TP-AGB stars in open clusters as a function of the initial stellar mass. The M, S, and C stars (reported in the legend) are marked with colored symbols and error bars. For comparison we over-plot the luminosity and core mass at the first thermal pulse, $L_{1\text{TP}}$ and $M_{c,1\text{TP}}$, predicted by the PARSEC stellar models at solar metallicity (dashed lines). The cluster ages and visual extinctions are taken from the work of Cantat-Gaudin et al. (2020). Moving downward the panels show the results for three prescriptions of the *Gaia* EDR3 parallax zero-point (ZP), namely: no ZP correction (top), Lindegren et al. (2021a, middle), and Groenewegen (2021, bottom). Note that the X-axis is stretched over the range $0.8 \leq M_i^{\text{AGB}}/M_{\odot} \leq 4.0$. *Left panels:* Bolometric luminosities derived from the fitting of the spectral energy distributions. *Right panels:* The initial-final mass relation of white dwarfs in the Milky Way is compared to the current core masses of TP-AGB stars in open clusters. The semi-empirical IFMR (gray diamonds with error bars) is taken from Marigo et al. (2020) and Cummings et al. (2018). The solid line is a fit to the IFMR data.

$M_i^{\text{AGB}} \simeq 3.3 - 4.0 M_{\odot}$. It is unclear whether BM IV 34 is a plausible candidate for the occurrence of HBB.

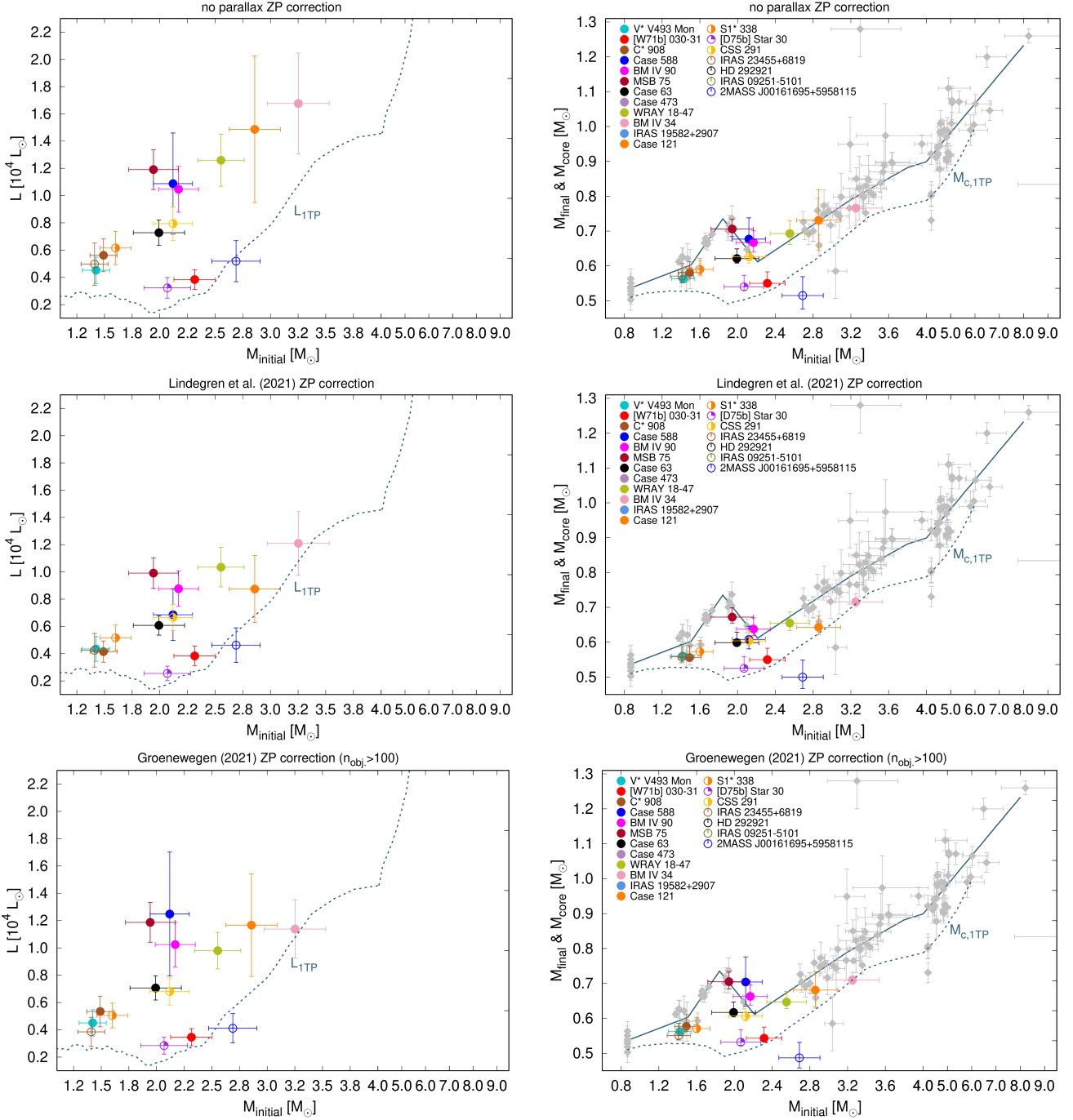


Figure 9. The same as in Fig. 8, but adopting cluster ages and visual extinctions from the work of Dias et al. (2021). Luminosity and core mass of all objects are re-derived accordingly. Note that the stars Case 473, IRAS 19582+2907, HD 292921, and IRAS 09251-5101 are absent, as their host clusters are not included in the catalog.

TP-AGB models do not agree. In order to check this hypothesis, it would be advisable to carry out spectroscopic measurements to verify a possible increase in the abundance of nitrogen or a lowering of the $^{12}\text{C}/^{13}\text{C}$ isotope ratio at the surface. In any case, the SED fitting for BM IV 34 does not indicate the presence of circumstel-

lar dust in significant quantities, nor of large mass-loss rates (see Tables 5 and 6).

Overall, the SED fitting results indicate that the luminosities of the 19 C stars are comprised in the range $3500 - 4000 \lesssim L/L_{\odot} \lesssim 11000 - 16000$, depending on the adopted ZP correction for the *Gaia* EDR3 parallaxes. The corresponding core masses vary in the inter-

val $0.54 \lesssim M_c/M_\odot \lesssim 0.77$. It is worth recalling that the lower limit of M_c can actually extend from $\simeq 0.54 M_\odot$ up to $\approx 0.58 M_\odot$, for the effect of the slow luminosity dip thoroughly discussed in Sect. 4.5.

Adopting the original *Gaia* EDR3 parallaxes (noZP case) the brightest carbon star, BM IV 34, has a core mass $M_c \simeq 0.77 M_\odot$, while with the L21ZP and G21ZP corrections, the star distance becomes shorter and its bolometric luminosity ($L \approx 11\,000 - 12\,000 L_\odot$) approaches the onset the TP-AGB of a star with $M_i^{\text{AGB}} \simeq 3.25 M_\odot$, if we use the cluster ages from [Dias et al. \(2021\)](#). On the other hand, taking the age catalog of [Cantat-Gaudin et al. \(2020\)](#) the mass of the progenitor increases, $M_i^{\text{AGB}} \simeq 3.54 M_\odot$, and its luminosity falls just below the $L_{1\text{TP}}$ with the L21ZP and G21ZP corrections. In both cases it is hard to explain the existence of a carbon star through the standard 3DU channel in a single star. One may perhaps invoke the mass transfer of carbon-enriched material from a companion star in a binary system, but we tend to disfavor such hypothesis. The SED of BM IV 34 is well reproduced by the spectrum of a single carbon star, and we do not detect any sign of recent accretion (e.g., infrared excess due to a circumstellar disk).

M and S stars: the onset of the 3DU.—The 7 stars of spectroscopic type M, MS, and S have luminosities in the range $3\,000 \lesssim L/L_\odot \lesssim 9\,500$, and core masses $0.54 \lesssim M_c/M_\odot \lesssim 0.64$ with the noZP case. As predicted by TP-AGB stellar models, M and S stars are in most cases less bright than carbon stars of similar initial mass, consistent with the fact that the carbon enrichment due to the 3DU drives the variation of the spectral type along the M→S→C sequence. This does not appear to be entirely the case for the M-type low-mass stars HD 292921 and IRAS 23455+6819 which have a higher average luminosity than the carbon stars V* V493 Mon, [W71b] 030-31, and C* 908. However, we note that the error bars in L and M_i^{AGB} for these stars do not allow us to accurately sort their brightness.

Knowing the luminosity of MS and S stars is important as it can place constraints on the 3DU (see, e.g., [Shetye et al. 2021](#)), in particular on the minimum core mass, M_c^{min} , for the occurrence of the mixing events. Solar-metallicity TP-AGB models generally agree that the 3DU is operative at $M_i^{\text{AGB}} \approx 2 M_\odot$ (e.g., [Ventura et al. 2018](#); [Marigo et al. 2013](#); [Cristallo et al. 2011](#)), while predictions may disagree at lower masses, especially in identifying the minimum mass for the occurrence of the 3DU (see the discussion in [Marigo et al. 2013](#); [Karakas & Lugaro 2016](#)). According to current TP-AGB models this critical mass is loosely constrained, taking values in the range from $M_i^{\text{AGB}} \simeq 1.4 M_\odot$ to

$M_i^{\text{AGB}} \simeq 2.0 M_\odot$, mainly depending on the adopted mixing treatment and numerical details.

The new results of this study, based on *Gaia* data, help us to reduce the degree of uncertainty, albeit limited to a narrow range of stellar masses. For example, the MS-type stars [D75b] Star 30 would indicate that for $1.9 \lesssim M_i^{\text{AGB}}/M_\odot \lesssim 2.3$ the onset of the 3DU occurs at $L \simeq 3\,000 \pm 700 L_\odot$, which corresponds to $0.530 \lesssim M_c^{\text{min}}/M_\odot \lesssim 0.575$, taking into account the uncertainties on distance and flux, together with the effect of the slow luminosity dip.

We compared this indication with a few TP-AGB models in the literature that commendably make the relevant quantities available. The FRUITY model of [Cristallo et al. \(2011\)](#) for $M_i^{\text{AGB}} = 2.0 M_\odot$ and $Z = 0.014$ agrees well with the observational data, predicting $M_c^{\text{min}} \simeq 0.56 M_\odot$ with a quiescent luminosity of about $4\,000 L_\odot$. [Weiss & Ferguson \(2009\)](#) find that their TP-AGB model with $M_i^{\text{AGB}} = 2.0 M_\odot$ and $Z = 0.02$ experiences the first mixing episode much earlier, for $M_c^{\text{min}} \simeq 0.49 M_\odot$, but the corresponding luminosity is not indicated. Conversely, a late start of the 3DU seems to characterize the models of [Karakas \(2014\)](#), who reports $M_c^{\text{min}} \simeq 0.62 M_\odot$ at $M_i^{\text{AGB}} = 2 M_\odot$ and $Z = 0.014$.

The S star CSS 291 with $1.9 \lesssim M_i^{\text{AGB}}/M_\odot \lesssim 2.3$ is attributed a type S4/2, which would correspond to C/O $\simeq 0.95$ according to the classification of [Keenan & Boeshaar \(1980\)](#). If confirmed, this star could probe the luminosity, and therefore the core mass, at the transition from the O-rich regime to the C-rich regime. The brightness of CSS 291 is compatible with the range $6\,500 \lesssim L/L_\odot \lesssim 9\,000$ which corresponds to a core mass $0.6 \lesssim M_c/M_\odot \lesssim 0.66$, assuming the noZP case. Somewhat lower values for both L and M_c apply if we take the L21ZP and G21ZP cases. The FRUITY model for $M_i^{\text{AGB}} = 2.0 M_\odot$ and $Z = 0.014$ is broadly consistent with the CSS 291 data: just before becoming a carbon star, the model attains a photospheric C/O $\simeq 0.94$ when $L \approx 6\,700 L_\odot$ and $M_c \simeq 0.59 M_\odot$.

Pulsation.—AGB stars exhibit variability due to stellar pulsation in low-order modes (e.g. [Wood 2015](#)), possibly non-radial ([Yu et al. 2020](#), and references therein). The generally accepted picture (e.g. [Lattanzio & Wood 2004](#); [Wood 2015](#)) is that pulsation is dominated by relatively high-order (third or second overtone) modes during the early stages of the LPV phase, when multi-periodicity is common. Overtone modes become gradually stable as the envelope expands ([Trabucchi et al. 2019](#)), until eventually a star pulsates only in the fundamental mode. As the former acquires large amplitude, a star is identified as a Mira variable.

In order to analyze our sample of LPVs within this picture, we examine them in the period-luminosity diagram (PLD) shown in Figure 10. The absolute magnitude M_{K_s} used to construct it includes the contributions of both interstellar and circumstellar extinction, and we consider the three cases of zero-point correction to the *Gaia* EDR3 parallax discussed in Sect. 4.2. The same is displayed in Fig. 11, except there each source is identified by its name as done in Fig. 9. The corresponding data are reported in Table 7.

By comparison with the pattern seen in the PLD of LPVs in the LMC as observed by OGLE-III (Soszyński et al. 2007, 2009), and following the results of Trabucchi et al. (2017, and references therein) (see also Trabucchi et al. 2021a), we are able to identify the pulsation mode responsible for each period. We identify nine sources with a period due to the fundamental mode, eight sources pulsating predominantly in the first overtone mode, and one star (S1* 338) whose period is most likely due to pulsation in the second overtone mode. Interestingly, the three different approaches adopted for correcting the parallax zero-point lead to the same mode classification, although a few first overtone mode pulsators are shifted towards the region between sequences C' and C, making the identification of their primary period less certain.

Two stars, V* V493 Mon and [W71b] 030-01, are classified as fundamental mode pulsators, but they are located below the period-luminosity (PL) sequence C compared with other stars with similar periods. This is consistent with the fact that these stars have relatively large mass-loss rates, and the resulting circumstellar extinction makes them appear fainter in the K_s band (Ita & Matsunaga 2011; Soszyński et al. 2009; Whitelock et al. 2017).

The M star IRAS 23455+6819 is the only LPV in our sample whose time series show clear evidence of a long secondary period, which lies very nicely on sequence D regardless of the choice of the parallax zero-point correction. We also point out that, having its primary pulsation period in the area between sequences C' and C, this source fits rather well the scenario depicted by Trabucchi et al. (2017). Indeed, they examined data from the OGLE-III catalog of LPVs in the LMC (Soszyński et al. 2009) and notice a large fraction of the sources reported to have a period on sequence D also display a period between sequences C' and C. They suggested that the large amplitude associated with the long secondary periods on sequence D makes so that it is favored over the true pulsation period in the same star when analyzing the PLD, where normally only one period per star is displayed, thus causing the apparent gap between sequences C' and

C. Indeed, that the star IRAS 23455+6819 displays a long secondary period whose amplitude is significantly larger than that of the pulsation period in the same star (cf. Fig. 2).

We note that most of the LPVs in our sample that lie on sequence C, and that we identified as fundamental mode pulsators, have brightness $M_{K_s} \lesssim -8$ mag, consistently with the properties of Miras (see e.g. Fig 1 of Bedding & Zijlstra 1998). Moreover, most of these stars appear to have relatively regular light curves, with little evidence of multi-periodicity, also suggestive of Mira-like behavior. Yet, based on their amplitudes, none of this stars would be classified as a Mira. In fact, only the two relatively dusty sources V* V493 Mon and [W71b] 030-01 have large enough amplitude at visual wavelengths to be possibly identified as Miras, and only the former is classified as such in one of the catalogs we examined (see Table 3).

However, it should be noted that the traditional distinction between Miras and semi-regular variables, according to which the former have visual amplitude $\Delta V > 2.5$ mag, has been criticized by a number of studies (e.g. Kerschbaum & Hron 1992; Kiss et al. 2000; Lebzelter & Hinkle 2002). Recently, Trabucchi et al. (2021a) have shown that semi-regular variables in the LMC that pulsate only in the fundamental mode follow the same sequence as Miras both in the period-luminosity diagram and in the period-amplitude diagram, suggesting that it would be incorrect to assign them different variability types only because their amplitude is smaller than an arbitrary, although reasonable, threshold.

It is also worth noticing that for most of the carbon stars (except for V* V493 Mon and [W71b] 030-31) the small variability amplitude could be linked with the fact that their C/O is just above unity, which is consistent with the absence of powerful dust-driven winds. Indeed, the spectral absorption features of molecules play a crucial role in determining the large visual amplitudes of Miras and related AGB variables (Reid & Goldston 2002). The low surface temperature corresponding to the point of maximum expansion of the pulsation cycle favors the formation of molecules, which in turn effectively block a large fraction of visual light from escaping the photosphere owing to their high opacity. Towards maximum compression the increased temperature causes these molecules to dissociate, and the star appears much brighter at visual wavelengths. In O-rich stars this effect is mainly associated to metallic oxides, primarily TiO, while in C-stars carbon-bearing molecules such as CN and C₂ are the main agents. If C/O is slightly $\gtrsim 1$ almost all oxygen is locked into

CO, while a small excess of carbon, C-O, remains to form other carbon-bearing molecules (Marigo & Aringer 2009). This could explain the relatively low amplitudes of the sources we have examined. This picture is supported by observations of Galactic C-rich low-amplitude semi-regular variables (Schöier & Olofsson 2001) with measured photospheric C/O ratio (Lambert et al. 1986): the majority of them have $1.04 \lesssim \text{C/O} \lesssim 1.3$. Putting all the pieces together we may deduce that as long as the carbon excess is small, (1) stars have low-amplitude pulsation, (2) do not form circumstellar dust in significant amount, and (3) do not experience powerful dust-driven outflows. The three conditions are all met by most of the carbon stars in our sample (Tables 5, 6, 7, Fig. 11), in particular the bright carbon stars MSB 75, BM IV 90 and Case 588. As a consequence, a reasonable expectation is that the carbon enrichment in these stars is modest. This point is relevant for the analysis of their core mass and its link to the IFMR of white dwarfs (Marigo et al. 2020).

Mass loss and dust production.—In addition to the bolometric luminosity, the SED fitting returns information on the present-day dust mass-loss rate, \dot{M}_d , and the optical depth at $10/11.3 \mu\text{m}$ for O-/C-rich stars. All TP-AGB stars analyzed here are optically visible and therefore we do not expect them to be characterized by substantial production of circumstellar dust. In general, in fact, the order of magnitude of \dot{M}_d is very small for most stars, being comprised between $10^{-12} M_\odot \text{yr}^{-1}$ and $10^{-10} M_\odot \text{yr}^{-1}$. Correspondingly, the optical depth τ_{10} or $\tau_{11.3}$ is also low and varies from 10^{-4} and 10^{-2} .

There are 3 stars in the sample that show signs of well-developed stellar winds. One is the M-type low-mass star IRAS 23455+6819, with $1.2 \lesssim M_i^{\text{AGB}}/M_\odot \lesssim 1.4$. It has $\dot{M}_d \simeq 9 \cdot 10^{-10} M_\odot \text{yr}^{-1}$, that may correspond to a total mass-loss rate approaching $\dot{M} = \dot{M}_d/\Psi \approx 10^{-6} M_\odot \text{yr}^{-1}$, assuming a dust-to-gas ratio $\Psi \simeq 10^{-3}$ (Bladh et al. 2019b). Interestingly, this star displays a relatively short pulsation period (85 days), that we attribute to the first overtone mode. This suggests that the star is not a Mira, but more likely a semi-regular variable. However, this is also the only source in our sample clearly showing a long secondary period (631 days) on sequence D, which is consistent with relatively strong mass-loss. Indeed, various works (e.g. Wood & Nicholls 2009; McDonald & Trabucchi 2019) have pointed out the correlation between dust production and the appearance of long secondary periods. More recently, Soszyński et al. (2021) (see also Wood et al. 1999; Soszyński 2007; Soszyński & Udalski 2014) have put forward strong evidence that long secondary peri-

ods are caused by eclipses from a dust cloud dragged probably by a sub-stellar companion.

The other 2 stars with detectable winds are the carbon stars V* V493 Mon and [W71b] 030-31, that have $\dot{M}_d \approx$ few $10^{-9} M_\odot \text{yr}^{-1}$ and $\tau_{11.3} \simeq 0.02$. Both stars have low-mass progenitors, $M_i^{\text{AGB}} \simeq 1.3 - 1.5 M_\odot$. Typical values of the dust-to-gas ratio Ψ for Galactic carbon stars vary in the range $2.5 \cdot 10^{-3} \lesssim \Psi \lesssim 0.01$ (Groenewegen et al. 1998). Assuming a mean value of $\Psi \approx 5 \cdot 10^{-3}$ the total mass-loss rate, \dot{M} , does not exceed some $10^{-8} M_\odot \text{yr}^{-1}$ for most stars, while for V* V493 Mon and [W71b] 030-31 it may reach a few $10^{-7} M_\odot \text{yr}^{-1}$. We recall that $\dot{M} \approx 3 \cdot 10^{-7} M_\odot \text{yr}^{-1}$ is the minimum mass-loss rate for the existence of a radiation-driven wind triggered by carbonaceous dust grains (Bladh et al. 2019a; Eriksson et al. 2014; Mattsson et al. 2010).

Therefore, we can conclude that almost all the C stars in the sample have not yet entered the dust-driven wind regime, while the onset is near or already in progress for V* V493 Mon and [W71b] 030-31. These predictions agree very well with the observed photometric properties of the carbon stars. Looking at the *Gaia*-2MASS diagram (Fig. 1) we see, in fact, that both V* V493 Mon and [W71b] 030-31 are located in the region occupied by the so-called extreme stars, characterized by dusty outflows, and have an intrinsic color $(J - K_s)_0 \approx 3$. We note that there is a third carbon star classified as extreme, Case 49, but it is not considered here as it is rejected from being a member of the cluster NGC 663. All the others are located in the region where dust-free carbon stars are commonly found; as expected they have bluer near-infrared colors, typically $1.5 \lesssim (J - K_s)_0 \lesssim 2$.

5.2. Core mass: comparison with the IFMR of white dwarfs

The following analysis is primarily based on the results for the noZP case; some comparison with the two zero-point parallax corrections (L21ZP and G21ZP) is done at the end of the section. Taking an overall look at the luminosity as a function of the initial mass (top-left panels of Fig. 8 and Fig. 9), we note that among the brightest TP-AGB stars in the sample there are the carbon stars MSB 75 and BM IV 90, members of the clusters NGC 7789 and NGC 2660 ($L \approx 11\,500$ and $10\,400 L_\odot$). Their initial masses are estimated to be in the range $1.94 \lesssim M_i^{\text{AGB}}/M_\odot \lesssim 2.17$. At lower masses, $M_i^{\text{AGB}} < 1.8 M_\odot$ the luminosity drops to $L \lesssim 6\,000 L_\odot$, as shown by the stars [W71b] 030-31, C* 908, S1* 338, IRAS 23455+6819, HD 292921. At $M_i^{\text{AGB}} \simeq 2.1 M_\odot$, we find two stars, - the S star CSS 291 and the carbon star Case 63 -, with a lower luminosity, $L \simeq 7\,000 - 8\,000 L_\odot$. The progenitor mass of

Table 7. Period, pulsation mode, and absolute M_{K_s} magnitude for the LPVs in our sample. We report magnitudes obtained without correcting the parallaxes zero-point, or by using the corrections of L21 and G21.

Star	P	mode ^(a)	noZP	L21ZP	G21ZP
			M_{K_s}	M_{K_s}	M_{K_s}
	[days]		[mag]	[mag]	[mag]
V* V493 Mon	432.4	FM	-7.84	-7.80	-7.84
[W71b] 030-01	460.0	FM	-7.77	-7.77	-7.65
C* 908	235.9	FM	-7.75	-7.42	-7.70
Case 588	539.0	FM	-8.54	-8.04	-8.69
BM IV 90	438.2	FM	-8.39	-8.20	-8.37
MSB 75	449.2	FM	-8.48	-8.28	-8.48
Case 63	163.4	1OM	-7.80	-7.61	-7.77
Case 473	358.4	FM	-8.30	-8.16	-8.13
WRAY 18-47	368.9	FM	-8.35	-8.14	-8.08
BM IV 34	136.7	1OM	-8.75	-8.40	-8.33
IRAS 19582+2907	364.6	FM	-8.68	-8.08	-8.30
Case 121	228.2	1OM	-8.67	-8.10	-8.41
S1* 338	43.28	2OM	-7.29	-7.10	-7.08
[D75b] Star 30	76.36	1OM	-6.70	-6.45	-6.56
CSS 291	95.52	1OM	-7.65	-7.46	-7.48
IRAS 23455+6819	85.02	1OM	-7.15	-6.98	-6.87
HD 292921	-	-	-7.20	-6.91	-7.13
IRAS 09251-5101	144.4	1OM	-8.00	-7.24	-7.75
2MASS J00161695+5958115	95.01	1OM	-7.08	-6.96	-6.83

NOTE—^(a) FM: fundamental mode; 1OM: first overtone mode; 2OM: second overtone mode.

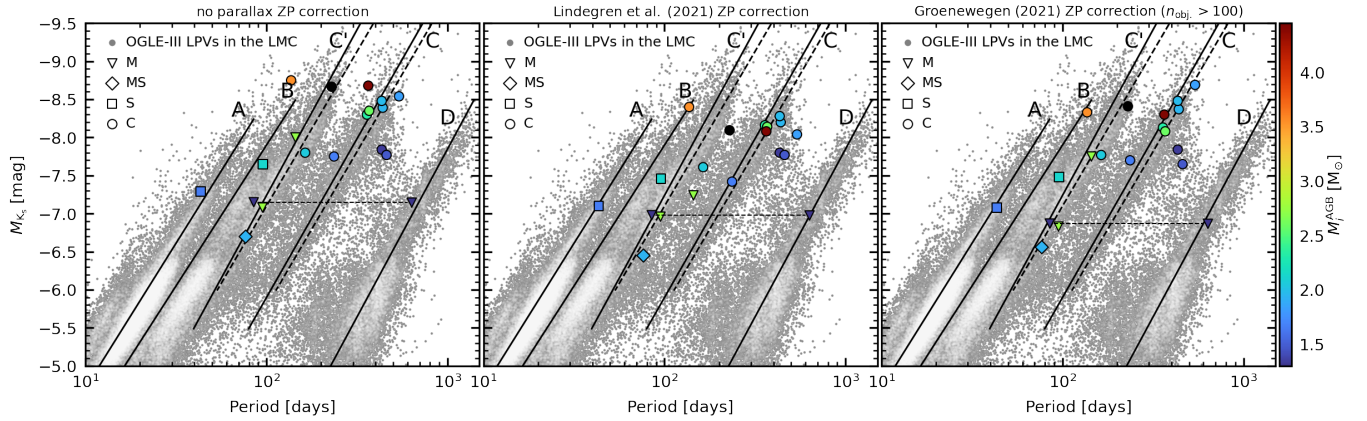


Figure 10. Period-luminosity diagram of the LPVs in open clusters from Table 7, color-coded by initial mass according to Cantat-Gaudin et al. (2020). The source Case 121 is indicated by the black symbol, as its initial mass according to Cantat-Gaudin et al. (2020) ($\sim 7 M_{\odot}$) is substantially larger compared to all other sources. The spectral type is indicated by symbol shapes (triangles: M-type; diamonds: MS-type; squares: S-type; circles: C-type). For the source IRAS 23455+6918 we show both the pulsation period and the long secondary period, connected by a dashed line. For visual reference, primary periods of LPVs in the LMC from OGLE-III (Soszyński et al. 2009) are displayed as gray dots in the background. Solid lines represent the best fits to period-luminosity relations A, B, C', C and D derived by Soszyński et al. (2007) for O-rich LPVs in the LMC, whereas dashed lines correspond to the best fits to C-rich LPVs on sequences C' and C. No parallax correction was applied to sources in the left panel, while in the central and right panels, respectively, we have been adopted the L21 and G21 parallax corrections.

carbon star Case 588, $1.8 \lesssim M_i^{\text{AGB}}/M_{\odot} \lesssim 2.1$, somewhat depends on the adopted cluster age set; independently from that it is one of the most luminous stars, with $L \simeq 9000 - 11000 L_{\odot}$. Then, for $M_i^{\text{AGB}} > 2.4 M_{\odot}$ L increases, reaching a maximum value for the star BM IV 34 with $L \simeq 16000 L_{\odot}$.

At this point it is interesting to compare the initial-final mass relation of the white dwarfs with the core mass of the TP-AGB stars inferred from their luminosity. We recall that the current M_c sets a lower limit to the final mass (right panels of Fig. 8 and Fig. 9). First of all, we note that most sources classified as TP-AGB stars

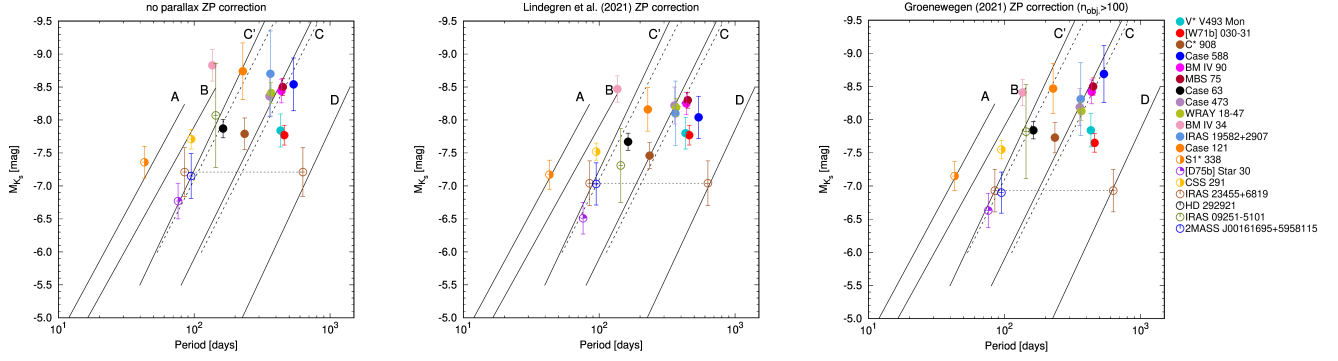


Figure 11. The same as in Fig. 10, but with the TP-AGB stars identified by their names, consistently with other figures in the paper. The absolute magnitude M_{K_s} of each star is corrected for interstellar reddening. The results are shown for the three of options of parallax ZP correction, as indicated on the top of each panel.

have core masses between the values expected at the first thermal pulse and the final mass of white dwarfs. This represents a remarkable agreement between theory and observations. Notable exceptions are the two carbon stars IRAS 19582+2907 and Case 121. Adopting the cluster age estimates from Cantat-Gaudin et al. (2020) their M_c appears located below the expected values at the first thermal pulse (top right panel of Fig. 8)]. As we have already discussed in Sect. 5, Initial masses of carbon stars, the apparent inconsistency is solved if we assign Case 121 the age from Dias et al. (2021). Under this assumption Case 121 is a normal TP-AGB star and the hypothesis that it could be a Super-AGB star is ruled out.

Let us focus now on the $1.8 \lesssim M_i^{\text{AGB}}/M_\odot \lesssim 2.1$ mass range. Here, the study of Marigo et al. (2020) identified a kink in the IFMR, which unexpectedly interrupts the commonly assumed monotonic positive correlation between M_i^{AGB} and the final mass M_f . The kink's peak in white dwarf mass of $\simeq 0.70 - 0.75 M_\odot$ is produced by stars with $M_i^{\text{AGB}} \simeq 1.80 - 1.95 M_\odot$, whereas these final masses are typically associated with more massive stellar progenitors, $M_i^{\text{AGB}} \simeq 3.0 - 3.5 M_\odot$.

In the framework of single-star evolution, the proposed interpretation links this observational fact to the formation of carbon stars and the modest outflows (mass-loss rate $\dot{M} < 10^{-7} M_\odot/\text{yr}$) they should suffer as long as the carbon excess remains too low to produce dust grains in sufficient amount. In other words, the progenitor stars of the IFMR kink would be carbon stars that experienced a shallow 3DU with modest carbon enrichment unable to sustain a powerful dust-driven stellar wind. Under these conditions the mass of the carbon-oxygen core can grow more than is generally predicted by stellar models. We refer to the analysis of Marigo et al. (2020) for all the details.

This scenario now appears strongly supported by the results of this work. Looking at the right panels Figs. 8

and 9 we see that there are indeed some carbon stars that populates the IFMR kink region. In particular MSB 75 (member of NGC 7789), BM IV 90 (belonging to NGC 2660) and Case 588 (hosted in Dias 2) have current core masses $0.67 \lesssim M_c/M_\odot \lesssim 0.70$. These values are comparable with the final masses that draw the IFMR kink. Another important aspect is that the four white dwarfs that define the kink peak belong to NGC 7789, the same cluster that hosts the brightest carbon star, MSB 75. This coincidence is very relevant as MSB 75 precisely defines the TP-AGB progenitor of the observed white dwarfs.

Furthermore, from the SED fitting of MSB 75, BM IV 90, and Case 588 we derive present-day dust mass-loss rates of some $10^{-10} M_\odot/\text{yr}$, which lead to total mass-loss rates of $\dot{M} \approx \text{few } 10^{-8} M_\odot/\text{yr}$ assuming a dust-to-gas ratio $\Psi \simeq 200 - 300$. These values are well below those that characterize a dust-driven wind.

In conclusion, this study confirms the two main hypotheses of the interpretation proposed by Marigo et al. (2020): 1) the progenitors of IFMR kink are carbon stars, 2) they are characterized by modest outflows, with mass-loss rates below the dust-driven regime. Furthermore, a striking agreement is found between the white dwarf masses of the IFMR kink and the current core masses of the progenitor carbon stars, with $0.67 \lesssim M_c/M_\odot \lesssim 0.7$.

5.3. Bright carbon stars in 1-2-Gyr old open clusters

Here we discuss possible formation scenarios of the bright carbon stars MSB 75 and BM IV 90, members of the clusters NGC 7789 and NGC 2660. As shown in Sect. 4.5 and Table 5, their bolometric luminosities indicate current core masses close to $M_c \simeq 0.68 - 0.7 M_\odot$, which are unusually higher than those expected from stellar evolutionary models with initial masses $M_i^{\text{AGB}} \simeq 1.9 - 2.0 M_\odot$ at solar-like metallicity. At the same time, such values of M_c are consistent with the measurements

Table 8. TP-AGB and carbon stars expected from single-star evolution

log(age/yr)	M_{TO}	M_1^{AGB}	M_f	(C/O) _f	$\tau_{\text{TP-AGB}}$	τ_{C}	$N_{\text{TP-AGB}}^{\text{SSP}}$	$N_{\text{C}}^{\text{SSP}}$	NGC 7789 ($N_{\text{G}}^{\text{obs}} = 2275$)		NGC 2660 ($N_{\text{G}}^{\text{obs}} = 376$)			
									$N_{\text{G}}^{\text{SSP}}$	$N_{\text{TP-AGB}}^{\text{cl}}$	N_{C}^{cl}	$N_{\text{G}}^{\text{SSP}}$	$N_{\text{TP-AGB}}^{\text{cl}}$	N_{C}^{cl}
[dex]	[M_{\odot}]	[M_{\odot}]	[M_{\odot}]		[Myr]	[Myr]			Exp	Exp		Exp	Exp	
9.10	1.95	2.13	0.65	2.60	3.72	1.39	882	402	1024958	2.0	0.9	706884	0.3	0.1
9.11	1.93	2.11	0.65	2.56	3.79	1.37	1774	802	2043956	2.0	0.9	1408579	0.3	0.1
9.12	1.92	2.10	0.65	2.52	3.86	1.35	1865	800	2031698	2.1	0.9	1397565	0.3	0.1
9.13	1.90	2.08	0.65	2.44	3.90	1.32	2870	1143	3018628	2.2	0.9	2069930	0.3	0.1
9.14	1.89	2.06	0.65	2.34	3.91	1.28	2772	1050	3000056	2.1	0.8	2052403	0.3	0.1
9.15	1.87	2.05	0.65	2.24	3.93	1.24	875	307	994128	2.0	0.7	678343	0.3	0.1
9.16	1.86	2.03	0.66	2.14	3.94	1.20	881	289	986805	2.0	0.7	672358	0.3	0.1
9.17	1.84	2.01	0.66	2.02	3.96	1.17	2745	826	2936153	2.1	0.6	1997876	0.3	0.1
9.18	1.83	2.00	0.66	1.90	3.97	1.14	1864	537	1949348	2.2	0.6	1325518	0.3	0.1
9.19	1.81	1.98	0.67	1.77	4.05	1.08	1912	446	1919777	2.3	0.5	1298313	0.4	0.1
9.20	1.80	1.96	0.69	1.64	4.16	1.01	2840	652	2870420	2.3	0.5	1938252	0.4	0.1
9.21	1.79	1.94	0.70	1.52	4.26	0.94	928	206	950643	2.2	0.5	639939	0.4	0.1
9.22	1.77	1.93	0.70	1.43	4.34	0.88	941	211	944345	2.3	0.5	633951	0.4	0.1
9.23	1.76	1.91	0.71	1.35	4.43	0.81	8734	1955	1848616	10.7	2.4	1231415	1.8	0.4
9.24	1.74	1.83	0.75	1.32	4.23	1.06	8962	2070	1798429	11.3	2.6	1182242	1.9	0.4
9.25	1.73	1.81	0.74	1.32	4.01	1.06	2249	668	1779231	2.9	0.9	1159680	0.5	0.1
9.26	1.72	1.80	0.74	1.33	3.80	1.05	2841	902	2629329	2.5	0.8	1700064	0.4	0.1
9.27	1.70	1.78	0.73	1.32	3.61	1.01	1761	560	1744256	2.3	0.7	1125162	0.4	0.1
9.28	1.69	1.76	0.71	1.28	3.40	0.88	808	263	859626	2.1	0.7	550197	0.4	0.1
9.29	1.68	1.75	0.69	1.25	3.20	0.75	1508	470	1711477	2.0	0.6	1092995	0.3	0.1
9.30	1.66	1.73	0.67	1.22	3.01	0.62	1341	376	1695549	1.8	0.5	1077948	0.3	0.1

Notes: Predictions based on a simulated SSP with a total mass $M_{\text{SSP}} = 10^7 M_{\odot}$, and solar metallicity, for several values of the age in the interval $9.1 \leq \log(\text{age/yr}) \leq 9.3$. For each age the table reports the turn-off mass, M_{TO} , the initial and final mass of the AGB stars, M_1^{AGB} and M_f , the final surface carbon-to-oxygen ratio, (C/O)_f, the TP-AGB and C-star lifetimes, $\tau_{\text{TP-AGB}}$ and τ_{C} . For both model and observations, $N_{\text{G}}^{\text{SSP}}$ and $N_{\text{G}}^{\text{obs}}$ are the number of stars with apparent magnitude in the interval $12 \leq G \leq 17$, where *Gaia* observations should be complete. Cluster’s visual extinction A_V is taken from [Cantat-Gaudin et al. \(2020\)](#): $A_V = 0.83$ for NGC 7789 and $A_V = 1.12$ for NGC 2660. For each cluster we report the expected (Exp) number of TP-AGB stars, $N_{\text{TP-AGB}}^{\text{cl}}$, and carbon stars, N_{C}^{cl} , computed with Eq. (5). TP-AGB models are taken from [Marigo et al. \(2020\)](#).

of white dwarf masses, $M_f \simeq 0.7 - 0.74 M_{\odot}$, corresponding to progenitors of similar initial mass ([Marigo et al. 2020](#)).

Specifically, we will analyze the probability that these observational facts can be explained by two alternative scenarios relating to 1) the evolution of a single star, or 2) an interacting binary system.

5.3.1. The single-star channel

Under this hypothesis, we estimate the predicted number of TP-AGB and C stars in NGC 7789 and NGC 2660 with the aid of the population synthesis technique. The underlying assumption is that a star cluster can be described with a simple stellar population (SSP) of given age and metallicity.

To build the SSPs we first generate stellar isochrones at solar metallicity; they are the same as in [Marigo et al. \(2017\)](#), except for the TP-AGB phase for which we adopt the recent models computed by [Marigo et al. \(2020\)](#). They successfully reproduce the kink in the IFMR observed at $M_i \simeq 1.7 - 2.0 M_{\odot}$ where white dwarfs have measured masses up to $M_f \simeq 0.70 - 0.74 M_{\odot}$. These TP-AGB models naturally predict carbon stars with

high core masses, as a consequence of a mild carbon enrichment and relatively moderate stellar winds. The new isochrones are then passed to the TRILEGAL code ([Girardi et al. 2005](#)) to generate the SSPs. The initial mass function is from [Kroupa \(2002\)](#).

We compute a fine grid of SSPs with ages in the relevant range for the clusters NGC 7789 and NGC 2660: $9.10 \leq \log(\text{age/yr}) \leq 9.30$, adopting an incremental step of 0.01 dex. An initial total mass of $10^7 M_{\odot}$ is assumed, which ensures a statistically good representation of the short-lived TP-AGB evolution (a few hundreds of TP-AGB stars are present in each SSP). For each cluster, simulated stars are converted to *Gaia* G-band photometry, assuming the distance modulus and visual extinction A_V from [Cantat-Gaudin et al. \(2020\)](#).

The expected number of TP-AGB stars in the cluster is computed with the scaling relation

$$N_{\text{TP-AGB}}^{\text{cl}} \simeq N_{\text{G}}^{\text{obs}} \times \frac{N_{\text{TP-AGB}}^{\text{SSP}}}{N_{\text{G}}^{\text{SSP}}}, \quad (5)$$

where $N_{\text{G}}^{\text{obs}}$ and $N_{\text{G}}^{\text{SSP}}$ are the observed and simulated number of stars within a given apparent G-magnitude

Table 9. TP-AGB and carbon stars expected from the blue-straggler channels

											NGC 7789 ($N_{\text{BSS}}^{\text{obs}} = 16$)		NGC 2660 ($N_{\text{BSS}}^{\text{obs}} = 2$)		
MASS TRANSFER ($f_{\text{ch}} = 0.65, f_{\text{m}} = 0.25$)															
q	M_2	$\tau_{\text{MS},1}$	$\tau_{\text{MS},2}$	M_{BSS}	τ_{MS}	$\tau_{\text{TP-AGB}}$	τ_{C}	M_{f}	$(\text{C/O})_{\text{f}}$	t_{MS}	$N_{\text{TP-AGB}}^{\text{cl}}$	N_{C}^{cl}	$N_{\text{TP-AGB}}^{\text{cl}}$	N_{C}^{cl}	
	[M_{\odot}]	[Myr]	[Myr]	[M_{\odot}]	[Myr]	[Myr]	[Myr]	[M_{\odot}]		[Myr]	Exp	Exp	Exp	Exp	
1.0	1.80	1488	1488	3.00	362	1.74	0.76	0.73	2.90	60	7.5E-02	3.3E-02	9.4E-03	4.1E-03	
0.7	1.26	1488	4454	3.00	362	1.74	0.76	0.73	2.90	800	5.6E-03	2.5E-03	7.1E-04	3.1E-04	
COLLISIONS ($f_{\text{ch}} = 0.15, f_{\text{m}} = 0.25$)															
q	M_2	$\tau_{\text{MS},1}$	$\tau_{\text{MS},2}$	M_{BSS}	τ_{MS}	$\tau_{\text{TP-AGB}}$	τ_{C}	M_{f}	$(\text{C/O})_{\text{f}}$	t_{coll}	t_{MS}	$N_{\text{TP-AGB}}^{\text{cl}}$	N_{C}^{cl}	$N_{\text{TP-AGB}}^{\text{cl}}$	N_{C}^{cl}
	[M_{\odot}]	[Myr]	[Myr]	[M_{\odot}]	[Myr]	[Myr]	[Myr]	[M_{\odot}]		[Myr]	[Myr]	Exp	Exp	Exp	Exp
1.0	1.80	1488	1488	3.33	276	1.06	0.46	0.81	2.61	400	236	2.7E-03	1.2E-03	3.4E-04	1.5E-04
										800	195	3.3E-03	1.4E-03	4.1E-04	1.8E-04
										1200	155	4.1E-03	1.8E-03	5.1E-04	2.2E-04
0.7	1.26	1488	4454	2.84	419	1.87	0.97	0.69	3.31	400	373	3.0E-03	1.6E-03	3.8E-04	1.9E-04
										800	327	3.4E-03	1.8E-03	4.3E-04	2.2E-04
										1200	282	4.0E-03	2.1E-03	5.0E-04	2.6E-04

Notes: Predicted numbers of TP-AGB and C stars are obtained with Eq. (6) for both mass-transfer and collision channels. We assume the primary has a mass $M_1 = 1.80 M_{\odot}$ and consider two values of the mass ratio q . We denote with M_{BSS} the blue straggler mass; $\tau_{\text{MS},1}$, $\tau_{\text{MS},2}$, τ_{MS} are the main sequence lifetimes of the primary, the secondary and the BSS, all derived from single star evolutionary models; $\tau_{\text{TP-AGB}}$ and τ_{C} denote the duration of the TP-AGB and C-star phases of a single star with $M_{\text{f}} = M_{\text{BSS}}$; M_{f} and $(\text{C/O})_{\text{f}}$ are the final mass and photospheric carbon-to-oxygen ratio; t_{coll} is the collision age (only for the collision channel); t_{MS} is the actual remaining main-sequence lifetime of the BSS. Given the observed number of main-sequence BSS, $N_{\text{BSS}}^{\text{obs}}$, the last four columns list the expected numbers of TP-AGB and C stars for the two clusters. The TP-AGB models are taken from Marigo et al. (2020).

range, $12 \leq G \leq 17$, inside which *Gaia* observations should be complete. For both clusters this magnitude interval comprises a large fraction of main-sequence stars and core He-burning stars on the red clump. Specifically, we find $N_G^{\text{obs}} = 2275$ for NGC 7789, and $N_G^{\text{obs}} = 248$ for NGC 2660. The complete results are reported in Table 8.

5.3.2. The blue-straggler channel

An alternative to the carbon-star formation hypothesis proposed by Marigo et al. (2020) is that unusually high core masses of MSB 75 and BM IV 90 are the result of the TP-AGB evolution of blue straggler stars (BSS) hosted in the parent clusters. BSS are main-sequence stars that are observed to be bluer and brighter than the main-sequence turnoff in clusters. Among the various BSS formation pathways proposed in literature we mention: mass transfer from a binary companion (McCrea 1964), mergers of close binary systems, and collisions of single stars (Hills & Day 1976; Leonard 1989). In principle, all these mechanisms can contribute to the production of BSS: the most recent studies indicate that in open clusters the major fraction (55% – 75%) of BSS is produced through mass transfer in an interacting binary system, while a smaller role is to be attributed to collisional (15%) or merging processes (10% – 30%) (e.g., Leiner & Geller 2021; Jadhav & Subramaniam

2021; Gosnell et al. 2015; Geller et al. 2013; Mathieu & Geller 2009).

In the following we attempt to estimate the probability that the BSS channel is at work in the two clusters NGC 7789 and NGC 2660, and compare the results with the predictions from the single-star evolution scenario.

Using the semi-empirical IFMR and the results of stellar evolution models, we expect that core masses $M_{\text{c}} \approx 0.7 M_{\odot}$ should be produced by BSS of masses $M_{\text{BSS}} \approx 3.0 M_{\odot}$ that evolved through the TP-AGB phase and turned into carbon stars following repeated 3DU episodes. Considering that both clusters have a similar turn-off mass ($M_{\text{TO}} \sim 1.80 M_{\odot}$ for $\log(\text{age}/\text{yr}) \simeq 9.2$), the BSS progenitor should have a mass roughly twice the turn-off mass, $M_{\text{BSS}} \approx 2M_{\text{TO}}$. This configuration can be reached through an interacting binary system in which the primary and the secondary companions have similar initial masses ($M_1 \approx M_2 \approx M_{\text{TO}}$), hence a mass ratio not much different from unity ($q = M_1/M_2 \lesssim 1$), provided that no extreme mass loss takes place.

A simple estimate of the expected number of TP-AGB stars progeny from a given BSS formation channel can be obtained with:

$$N_{\text{TP-AGB}}^{\text{cl}} \simeq f_{\text{ch}} \times f_{\text{m}} \times N_{\text{BSS}}^{\text{obs}} \times \frac{\tau_{\text{TP-AGB}}}{t_{\text{MS}}}, \quad (6)$$

where $N^{\text{obs}}(\text{BSS})$ is the number of observed BSS in the cluster, t_{MS} and $\tau_{\text{TP-AGB}}$ denote the remaining main-sequence lifetime and TP-AGB phase duration of the binary product with mass M_{BSS} . A similar equation can be used to compute the expected number of carbon stars, N_{C}^{cl} , by replacing $\tau_{\text{TP-AGB}}$ with the carbon star lifetime, τ_{C} . Stellar lifetimes are obtained from the PARSEC-COLIBRI evolutionary stellar models (Bressan et al. 2012; Marigo et al. 2020). For each cluster the number $N_{\text{BSS}}^{\text{obs}}$ is taken from the new catalog of BSS in open star clusters (Rain et al. 2021), which is based on *Gaia* DR2 data for astrometric, photometric and membership characterisation.

The multiplicative factor f_{ch} denotes the fractional contribution of a given BSS channel. Following the indications reported at the beginning of the section, we take: $f_{\text{ch}} = 0.65$ for the mass-transfer channel, $f_{\text{ch}} = 0.20$ for the merger channel, and $f_{\text{ch}} = 0.15$ for the collisional channel. The other factor f_{m} is the probability that BSS are produced with a specified mass, that in our case we set to $M_{\text{BSS}} \simeq 3.0 M_{\odot}$.

To quantify f_{m} we take advantage of the results of two recent papers (Jadhav & Subramaniam 2021; Leiner & Geller 2021), which investigated the population of BSS in several open clusters as a function of age with *Gaia* DR2. For clusters with $1 \lesssim \text{age}/\text{Gyr} \lesssim 2$, which encompass the range relevant to our test, both studies derived the semi-empirical mass distribution of BSS. Leiner & Geller (2021, see their figure 3) found that, within their sample of 35 open clusters, the difference between the blue straggler mass and the turnoff mass of the cluster ($\delta M = M_{\text{BSS}} - M_{\text{TO}}$) ranges from $-0.2 M_{\odot}$ to $1.5 M_{\odot}$, with a median of $0.4 M_{\odot}$. Therefore, our test combination ($M_{\text{TO}} \simeq 1.8 M_{\odot}$ and $M_{\text{BSS}} \simeq 2.8 - 3.0 M_{\odot}$) gives $\delta M \simeq 1.0 - 1.2 M_{\odot}$. This value belongs to the upper bins of the δM -distribution, and corresponds to an observed frequency of $\simeq 6/35 \approx 17\%$.

Jadhav & Subramaniam (2021) introduced the fractional mass excess for BSSs, $M_{\text{e}} = (M_{\text{BSS}} - M_{\text{TO}})/M_{\text{TO}}$ and grouped the clusters in three classes: low-mass excess with $M_{\text{e}} < 0.5$, high-mass excess with $0.5 < M_{\text{e}} < 1.0$ and extreme-mass excess with $M_{\text{e}} > 1$. The 234 BSS hosted in their sample of 77 open clusters with $9.00 \leq \log(\text{age}/\text{yr}) \leq 9.25$ are distributed in the 3 classes with an observed frequency of 47%, 30% and 23%, respectively (see their table 1). Our BSS test configuration has $M_{\text{e}} \simeq 0.56 - 0.67$, hence it is assigned the high- M_{e} class.

From the above considerations we conclude that the probability of finding BSS with $M_{\text{BSS}} \simeq 3 M_{\odot}$ in NGC 7789 and NGC 2260 is not negligible and may cor-

respond to about 20% – 30%. Accordingly, we set $f_{\text{m}} = 0.25$ in Eq.(6).

In the following we will analyze the predictions from the mass-transfer and collision channels, which overall are expected to contribute to 70% – 90% of the BSS populations in open clusters. To evaluate the impact of the merger channel to a first approximation, we can simply consider the complement to unity of the statistical contribution of the other two formation pathways.

Mass-transfer pathway—Let us start by considering the most probable formation channel, which should be responsible for about 55% – 75% of the BSS population in open clusters. Modeling a stable mass-transfer in a binary system is complex and typically involves several free parameters when an analytic approach is adopted (see, for example, the prescriptions of the BSE code developed by Hurley et al. 2002).

Using the BSE code, Leiner & Geller (2021) carried out a systematic investigation of the mass-transfer process with the aid of synthesis simulations. They pointed out that current binary models tend to underpredict, on average, the number of BSS formed via mass transfer in old open clusters, and concluded that this channel should be more stable than commonly assumed. They explored the performance of different prescriptions for q_{cr} , that is the critical mass ratio below which mass transfer is found to be stable. Among the various cases analyzed, one that comes closest to the observed BSS mass distribution (albeit with persisting defects) is the *L2/L3 Overflow* model, in which the giant donor exceeds its Roche lobe and mass-transfer flows through the outer Lagrange points ($q_{\text{cr}} = 1.8$ is assumed).

In order to apply Eq.(6) we need to know the BSS remaining main sequence lifetime, t_{MS} . For the *L2/L3 Overflow* model Leiner & Geller (2021) computed t_{MS} as a function of the mass ratio q (see their figure 9). For our specific application to the clusters NGC 7789 and NGC 2660, it is appropriate to consider the case with age = 1.5 Gyr (left panel of figure 9). We see that for $1 \gtrsim q \gtrsim 0.7$ the remaining lifetime t_{MS} varies from ≈ 60 Myr to ≈ 800 Myr, also depending on the binary period. We adopt these two extreme values to bracket a wide range of cases. Furthermore, we assume that the mass-transfer process always leads to the formation of a BSS with $M_{\text{BSS}} = 3 M_{\odot}$.

The BSE model accounts in a simple way for the possible rejuvenation of the BSS, if more hydrogen is mixed into the core, which results in a longer t_{MS} . The precise amount of rejuvenation is quite uncertain and recent detailed calculation for the blue straggler binary WOCs 5379 in NGC 188 indicates that the effective prolongation of t_{MS} may be larger than predicted by BSE (Leiner

& Geller 2021; Sun et al. 2021). In this respect we note that higher t_{MS} values tend to lower the expected star counts.

Collisional pathway.—Let us now examine the case in which such a BSS is originated through stellar collisions, which should account for $\simeq 15\%$ of the BSS population in open clusters. Following the results of direct N-body calculations which account for collisions between two main-sequence stars in clusters (Glebbeek & Pols 2008; Hurley et al. 2005, 2001), it turns out that the post-main sequence phases of the merger product have similar duration compared to those of a normal single star with the same initial mass. This implies that in Eq. (6) the quantity $t_{\text{TP-AGB}}$ can be reasonably set equal to the TP-AGB lifetime of a single star with $M_i = M_{\text{BSS}}$.

Conversely, the main sequence lifetime of the collision product, t_{MS} , is shorter than that of a normal single star, τ_{MS} , by an amount that primarily depends on the age of the collision and on how much hydrogen is mixed into the core of the product after the collision (Glebbeek et al. 2013; Sills et al. 2009; Glebbeek & Pols 2008).

According to Glebbeek et al. (2013) and Glebbeek & Pols (2008) the remaining lifetime t_{MS} of the collision product can be expressed as:

$$t_{\text{MS}} = (1 - f_{\text{app}}) \times \tau_{\text{MS}}, \quad (7)$$

where f_{app} is the apparent age of the product, that is the fractional age of a normal main sequence star with the same remaining lifetime t_{MS} .

To estimate f_{app} we adopt the analytic recipe proposed by Glebbeek & Pols (2008), which is a function of M_1 , q , the collision time t_{coll} , and chemical composition. This relation reproduces fairly well the results of N-body simulations designed for old open clusters. As to the collision age, we explore three cases, namely: the collision takes place 1) close to the beginning, $t_{\text{coll}} = 400$ Myr, 2) roughly in the middle, $t_{\text{coll}} = 800$ Myr, and 3) towards the end, $t_{\text{coll}} = 1200$ Myr of the MS phase of the primary star.

In the calculation we take into account the fact that some amount of mass, ΔM_{lost} , is lost through the collision, so that the actual mass of the BSS remnant is

$$M_{\text{BSS}} = (M_1 + M_2) \times (1 - \phi), \quad (8)$$

where $\phi = 0.3q/(1+q)^2$ depends on the mass ratio q , and $\Delta M_{\text{lost}} = \phi \times (M_1 + M_2)$. For the two choices of the mass ratio, $q = 1.0, 0.7$, the blue-straggler mass is $M_{\text{BSS}} \simeq 3.33$, and $2.84 M_{\odot}$, respectively.

5.3.3. Discussion

Tables 8 and 9 present the number of TP-AGB and carbon stars, $N_{\text{TP-AGB}}^{\text{cl}}$ and N_{C}^{cl} , expected from single-star evolution and the BSS channels. For both scenarios we also report the predictions of Marigo et al. (2020) regarding the TP-AGB lifetime ($\tau_{\text{TP-AGB}}$), the duration of the carbon star phase (τ_{C}), the final mass (M_{f}), and the surface carbon-to-oxygen ratio $(\text{C/O})_{\text{f}}$ at the end of the AGB evolution. As to the mass-transfer and collisional pathways, we assume that the primary has a mass $M_1 \simeq M_{\text{TO}} = 1.8 M_{\odot}$, and a MS lifetime $\tau_{\text{MS}} = 1488$ Myr.

In both clusters only one carbon star was identified, which is also the only TP-AGB star detected. The two clusters have very different population size: considering the candidate members with $p \geq 0.5$, NGC 7789 contains 2953 stars, NGC 2660 has 376 stars, about a factor of 10 less. As for NGC 7789, almost over the entire age interval, the stellar evolution channel predicts $N_{\text{TP-AGB}}^{\text{cl}} \approx 2.0 \pm 1.4$, and $N_{\text{C}}^{\text{cl}} \approx 0.5 \pm 0.7$ to $\approx 1 \pm 1$. Taking into account the Poisson uncertainty⁹, this is an excellent agreement with the observational data. As for NGC 2660, the predictions drop to $N_{\text{TP-AGB}}^{\text{cl}} \approx 0.3 - 0.4 \pm 0.6$, and $N_{\text{C}}^{\text{cl}} \approx 0.1 \pm 0.3$. These numbers are still compatible with the detection of 1 TP-AGB star within the uncertainty interval.

We note that in a narrow age range, $9.23 \leq \log(\text{age/yr}) \leq 9.24$, there is a significant increase in the expected numbers. This fact, known as AGB-boosting, is related to the abrupt change in the core He-burning lifetime as soon as stellar populations intercept the ages at which red giant branch stars first appear (all details can be found in Girardi et al. 2013). The boost occurs for $1.74 \lesssim M_{\text{TO}}/M_{\odot} \lesssim 1.76$, and correspondingly for $1.83 \lesssim M_i^{\text{AGB}}/M_{\odot} \lesssim 1.92$. From an evolutionary point of view, these specific ages mark the transition between low-mass stars that develop a degenerate core after the main sequence, and intermediate-mass stars that do not undergo electronic degeneracy. From an observational point of view, clusters with ages $\simeq 1.6$ Gyr show the peculiar morphology of the dual red clump in color-magnitude diagrams (Girardi et al. 2000, 2009; Girardi 2016). Due to their age estimate and elongated red clump, the two clusters are plausible candidates to belong or to be very close to this special class of simple stellar populations. This means that the numbers of TP-AGB stars expected from the single star channel could easily be larger (by factors of a few) than here estimated.

⁹ It is simply computed as $\sqrt{N_{\text{TP-AGB}}^{\text{cl}}}$ and $\sqrt{N_{\text{C}}^{\text{cl}}}$.

Let us now move to analyze the BSS channels. For all cases shown in Table 9 the predicted $N_{\text{TP-AGB}}^{\text{cl}}$ and N_{C}^{cl} are systematically lower than observed, both for the mass-transfer and collision pathways. The expected counts are always of the order of $10^{-2} - 10^{-4}$, the higher values applying to NGC 7789. Given these estimates, we expect that also the merger formation channel, which should statistically account for the remaining 10%–30% of the BSS, helps negligibly to recover the observed counts.

Among all cases explored, the most favorable one seems to be that of a mass transfer with $q \approx 1$ (binary twins), which yields $N_{\text{TP-AGB}}^{\text{cl}} \simeq 0.075$ in NGC 7789. This number could increase up to $\simeq 0.11$ assuming that all the 16 observed BSS formed via Roche-lobe overflow ($f_{\text{ch}} = 1$), and up to $\simeq 0.46$ if we hypothesize that all have the same mass $M_{\text{BSS}} \simeq 3 M_{\odot}$, although this seems rather unrealistic.

From these simple tests, we conclude that the bright carbon stars in NGC 7789 and NGC 2660 can be explained through the TP-AGB evolution of single stars with $1.75 \lesssim M_i^{\text{AGB}}/M_{\odot} \lesssim 2.0$. TP-AGB models that include a carbon-dependent mass loss allow the growth of the core mass up to $M_c \approx 0.7 M_{\odot}$, as inferred from the luminosities of the observed carbon stars and measured from the spectra of their white dwarf progeny (Marigo et al. 2020). On the other hand, the BSS channels do not seem to provide an equally convincing alternative to account for the observational data.

6. CONCLUDING REMARKS

This study provides an in-depth analysis of the AGB star population in open clusters, in light of the new *Gaia* data. We identified 49 AGB candidate stars brighter than the RGB tip. We focused on 19 stars with known spectral types (M, S, C), which should be evolving in the TP-AGB phase. Their cluster membership was reanalyzed using all the astrometric and kinematic information provided by *Gaia* EDR3, also including zero-point corrections based on recent formulations. Combining observations with evolutionary and radiative transport models, we characterized each star by assigning distance, spectral energy distribution from the optical to far infrared, initial mass, bolometric luminosity, core mass, circumstellar extinction, mass-loss rate, period and pulsation mode.

Let us briefly summarize the main conclusions:

- From the bolometric luminosity obtained through the SED fitting we infer the current core mass by using TP-AGB models in the literature. We have paid careful attention to consider the flash-driven luminosity variations and the evolution of

the first pulses occurring below the asymptotic CMLR. These effects are particularly important for low-mass stars, with $M_c \lesssim 0.65 M_{\odot}$. Luminosity and core mass of almost all stars are well explained by TP-AGB evolutionary models, as they lie between the values predicted at the first thermal pulse and the end of the AGB phase.

- For a few specific cases the results differ depending on the adopted catalog of cluster ages and/or parallax correction. The most striking example is the carbon star Case 121 whose initial mass is about $\simeq 7 M_{\odot}$ if we use Cantat-Gaudin & Anders (2020) to date its hosting cluster Berkeley 72, while it drops to $\simeq 3 M_{\odot}$ if we use the age catalog of Dias et al. (2021). With the former age estimate we face great interpretative difficulties (e.g., explaining how a Super-AGB star can have such a low luminosity, $L \approx 14\,000 - 15\,000 L_{\odot}$), whereas in the latter case the data for Case 121 is easily explained with the predictions of a standard TP-AGB phase.
- The minimum initial mass for carbon star formation at solar-like metallicity should not be higher than $\simeq 1.5 M_{\odot}$. The maximum mass should not be lower than $3.0 - 4.0 M_{\odot}$, if we exclude that Case 121 has $M_i \simeq 7 M_{\odot}$ (as discussed in the previous point).
- The 3 stars of type MS and S provide information about the onset of the 3DU and the transition to the C-star domain.
- The 12 carbon stars are all optically visible, and none appear truly dust-enshrouded. The mass-loss rate for most of them is very low ($\dot{M} \approx 10^{-8} M_{\odot}/\text{yr}$), below the typical values that characterize a dust-driven wind, except for two carbon stars of low initial mass (V* V493 Mon and [W71b]) which fall in the region of extreme stars in the *Gaia*-2MASS diagram. For them the estimated mass-loss rate could be of the order of $10^{-7} - 10^{-6} M_{\odot}/\text{yr}$.
- The most massive star in the sample, BM IV 34, is a carbon star, with $M_i^{\text{AGB}} \simeq 3.3 - 4.0 M_{\odot}$. Excluding Case 121 for the reasons discussed above, we did not find plausible candidates for stars with HBB. No M star brighter than the CMLR is identified with $M_i^{\text{AGB}} \gtrsim 4 M_{\odot}$. Among the 4 M stars in the sample the maximum initial mass is $M_i^{\text{AGB}} \simeq 2.7 M_{\odot}$.
- We looked for candidate Super-AGB stars, limiting to the age range $7.38 \lesssim \log(\text{age}/\text{yr}) \lesssim 7.82$,

hence $10 \gtrsim M_i/M_\odot \gtrsim 6$. We have identified 10 stars that satisfy the age criterion, but from the SED fitting the conclusion is negative since all luminosities are too low ($L < 40\,000 L_\odot$).

- The photometric variability data we retrieved suggest the stars in the sample are LPVs. The observed periods, in combination with derived absolute magnitudes, are consistent with Mira-like or semi-regular variability. Most of the C-stars appear to be fundamental mode pulsators, while M-, MS- and S-type stars pulsate predominantly in the first overtone mode (consistent with the fact that they are less evolved), except for the S-star S1* 338 whose primary period is attributed to pulsation in the second overtone mode. The mode identification for this sample of LPVs is not affected by the choice of the parallax zero-point correction method. The two C-stars for which we derive the largest mass-loss rates (V* V493 Mon and [W71b] 030-01) lie below the period-luminosity sequence C compared to LPVs with similar periods, in agreement with previous results for LPVs suffering from self-extinction due to circumstellar dust.
- The comparison of the estimated M_c with the IFMR of the white dwarfs has highlighted a striking fact: the presence of almost dust-free bright carbon stars with $0.65 \lesssim M_c/M_\odot \lesssim 0.70$, and initial masses of $\approx 1.9 - 2.0 M_\odot$. Just in the same mass interval a recent study (Marigo et al. 2020) pointed out the existence of a kink in the IFMR, which breaks its increasing monotonicity, with a peak in white dwarf mass of $\simeq 0.70 - 0.74 M_\odot$.

Therefore, the new findings of this study not only support the existence of the IFMR kink, but also

the underlying interpretative hypotheses: the progenitors are 1) carbon stars that 2) experienced modest outflows for a significant fraction of their C-rich phase, 3) with inefficient dust production. In fact, the carbon stars MSB 75 and BM IV 90 ($L \approx 10\,000 - 13\,000 L_\odot$), have an estimated mass-loss rate of $\approx \text{few } 10^{-8} M_\odot/\text{yr}$, while their variability is characterized by low-amplitude pulsation. Marigo et al. (2020) advanced the hypothesis that these stars are poorly enriched in carbon (following a shallow 3DU) and therefore dust cannot form in sufficient quantities to trigger a powerful wind (Bladh et al. 2019a; Mattsson et al. 2010). Although we do not have photospheric C/O measurements for MSB 75 and BM IV 90, their overall properties seem to fit very well within the suggested picture.

- The above results are particularly intriguing as the open clusters NGC 7789 and NGC 2660 have ages $\approx 1.3 - 1.6$ Gyr and show signs of dual clump morphology (Girardi et al. 2000; Girardi 2016). Therefore, their carbon star progenitors are expected to be close to the initial mass limit, M_{HeF} , at the transition between low-mass stars, that develop degenerate He-cores after the main sequence, and intermediate-mass stars that avoid electron degeneracy.
- Finally, to complete our analysis, we compare two possible pathways for the formation of carbon stars with $M_c \simeq 0.7 M_\odot$ belonging to intermediate-age 1.3 – 1.6 Gyr old clusters. Our calculations suggest that, while the evolution of single stars suggest that, while the evolution of single stars provides a consistent interpretation of the observed star counts, the blue-straggler channel appears rather unlikely.

APPENDIX

A. CLUSTER MEMBERSHIP REVISITED WITH *Gaia* EDR3

Here we include the full table with the results of the new analysis, based on *Gaia* EDR3, to assess the cluster membership of the TP-AGB stars of known spectroscopic type.

REFERENCES

- Abia, C., de Laverny, P., Cristallo, S., Kordopatis, G., & Straniero, O. 2020, *A&A*, 633, A135, doi: [10.1051/0004-6361/201936831](https://doi.org/10.1051/0004-6361/201936831)
- Addari, F. 2020, Master’s thesis, University of Padova, Italy
- Alksnis, A., Balklavs, A., Dzervitis, U., et al. 2001, *Baltic Astronomy*, 10, 1, doi: [10.1515/astro-2001-1-202](https://doi.org/10.1515/astro-2001-1-202)
- Althaus, L. G., Gil-Pons, P., Córscico, A. H., et al. 2021, *A&A*, 646, A30, doi: [10.1051/0004-6361/202038930](https://doi.org/10.1051/0004-6361/202038930)

Table 10. *Gaia* EDR3 astrometric parameters of the C, S, and M stars and their candidate parent clusters. Cluster membership assessment is reported according to the original parallaxes and two cases of zero-point corrections, as indicated.

star cluster	μ_α [mas/yr]	μ_δ [mas/yr]	π_t [mas]			ZP [mas]		membership			type
			noZP	L21	G21	L21	G21	noZP	L21	G21	
V* V493 Mon	-0.48 ± 0.04	$+0.40 \pm 0.03$	$+0.37 \pm 0.04$	$+0.38 \pm 0.04$	$+0.37 \pm 0.04$	-0.007	-0.000	\subseteq	\subseteq	\subseteq	C
Trumpler 5	$[-0.76;-0.48]$ $[-1.07;-0.04]$	$[+0.15;0.40]$ $[-0.24;0.79]$	$[+0.22;0.38]$ $[+0.06;0.54]$	$[+0.26;0.41]$ $[+0.09;0.56]$	$[+0.23;0.39]$ $[+0.07;0.54]$			68% C.L.	68% C.L.	68% C.L.	
[W71b] 030-01	-4.65 ± 0.03	$+6.78 \pm 0.04$	$+0.56 \pm 0.03$	$+0.56 \pm 0.03$	$+0.59 \pm 0.03$	-0.001	-0.030	\subseteq	\subseteq	\subseteq	C
Pismis 3	$[-4.91;-4.66]$ $[-5.15;-4.39]$	$[+6.57;6.83]$ $[+6.30;7.03]$	$[+0.39;0.50]$ $[+0.27;0.61]$	$[+0.42;0.53]$ $[+0.30;0.64]$	$[+0.43;0.54]$ $[+0.31;0.65]$			99% C.L.	99% C.L.	99% C.L.	
C* 908	-1.93 ± 0.02	$+2.15 \pm 0.02$	$+0.26 \pm 0.02$	$+0.30 \pm 0.02$	$+0.27 \pm 0.02$	-0.043	-0.007	\subseteq	\subseteq	\subseteq	C
Ruprecht 37	$[-1.75;-1.61]$ $[-1.92;-1.41]$	$[+2.37;2.48]$ $[+2.13;2.68]$	$[+0.12;0.24]$ $[-0.00;0.32]$	$[+0.16;0.27]$ $[+0.03;0.35]$	$[+0.14;0.25]$ $[+0.01;0.33]$			99% C.L.	99% C.L.	99% C.L.	
Case 588	-0.98 ± 0.04	$+1.28 \pm 0.03$	$+0.21 \pm 0.03$	$+0.27 \pm 0.03$	$+0.20 \pm 0.03$	-0.056	0.014	\subseteq	\subseteq	\subseteq	C
Dias 2	$[-0.89;-0.68]$ $[-1.37;-0.42]$	$[+1.16;1.34]$ $[+1.06;1.81]$	$[+0.15;0.28]$ $[-0.02;0.41]$	$[+0.18;0.32]$ $[+0.01;0.44]$	$[+0.14;0.28]$ $[-0.03;0.39]$			99% C.L.	99% C.L.	99% C.L.	
BM IV 90	-2.77 ± 0.03	$+5.30 \pm 0.03$	$+0.35 \pm 0.03$	$+0.38 \pm 0.03$	$+0.35 \pm 0.03$	-0.032	-0.004	\subseteq	\subseteq	\subseteq	C
NGC 2660	$[-2.83;-2.65]$ $[-2.99;-2.46]$	$[+5.12;5.29]$ $[+4.87;5.55]$	$[+0.29;0.38]$ $[+0.18;0.50]$	$[+0.32;0.41]$ $[+0.20;0.53]$	$[+0.30;0.39]$ $[+0.18;0.51]$			68% C.L.	68% C.L.	68% C.L.	
MSB 75	-1.07 ± 0.02	-2.20 ± 0.02	$+0.49 \pm 0.03$	$+0.53 \pm 0.03$	$+0.49 \pm 0.03$	-0.047	-0.001	\subseteq	\subseteq	\subseteq	C
NGC 7789	$[-1.04;-0.80]$ $[-1.29;-0.53]$	$[-2.08;-1.83]$ $[-2.35;-1.59]$	$[+0.44;0.52]$ $[+0.32;0.63]$	$[+0.47;0.54]$ $[+0.35;0.65]$	$[+0.45;0.53]$ $[+0.33;0.64]$			99% C.L.	99% C.L.	99% C.L.	
Case 63	$+1.54 \pm 0.03$	$+0.08 \pm 0.03$	$+0.57 \pm 0.03$	$+0.63 \pm 0.03$	$+0.58 \pm 0.03$	-0.054	-0.009	\subseteq	\subseteq	\subseteq	C
Berkeley 9	$[+1.41;1.61]$ $[+1.07;1.85]$	$[-0.10;0.10]$ $[-0.37;0.73]$	$[+0.49;0.61]$ $[+0.36;0.76]$	$[+0.52;0.65]$ $[+0.40;0.79]$	$[+0.50;0.63]$ $[+0.37;0.77]$			99% C.L.	99% C.L.	99% C.L.	
Case 473	-3.90 ± 0.04	-5.78 ± 0.04	$+0.27 \pm 0.03$	$+0.29 \pm 0.03$	$+0.30 \pm 0.03$	-0.019	-0.023	\subseteq	\subseteq	\subseteq	C
Berkeley 53	$[-4.00;-3.69]$ $[-4.51;-3.23]$	$[-5.81;-5.55]$ $[-6.31;-5.02]$	$[+0.17;0.33]$ $[+0.01;0.53]$	$[+0.22;0.37]$ $[+0.06;0.56]$	$[+0.19;0.34]$ $[+0.03;0.54]$			68% C.L.	68% C.L.	68% C.L.	
Wray 18-47	-3.26 ± 0.02	$+5.11 \pm 0.02$	$+0.36 \pm 0.02$	$+0.40 \pm 0.02$	$+0.41 \pm 0.02$	-0.037	-0.048	\subseteq	\subseteq	\subseteq	C
NGC 2533	$[-3.21;-3.15]$ $[-3.31;-2.96]$	$[+5.02;5.11]$ $[+4.94;5.24]$	$[+0.33;0.37]$ $[+0.26;0.44]$	$[+0.36;0.41]$ $[+0.29;0.47]$	$[+0.38;0.43]$ $[+0.31;0.50]$			99% C.L.	99% C.L.	99% C.L.	
BM IV 34	-1.77 ± 0.02	$+1.68 \pm 0.02$	$+0.22 \pm 0.02$	$+0.26 \pm 0.02$	$+0.27 \pm 0.02$	-0.039	-0.047	\subseteq	\subseteq	\subseteq	C
Haffner 14	$[-1.87;-1.77]$ $[-2.04;-1.60]$	$[+1.68;1.79]$ $[+1.49;1.96]$	$[+0.21;0.28]$ $[+0.12;0.40]$	$[+0.25;0.31]$ $[+0.15;0.43]$	$[+0.27;0.34]$ $[+0.17;0.46]$			68% C.L.	68% C.L.	68% C.L.	
IRAS 19582+2907	-2.28 ± 0.04	-5.74 ± 0.05	$+0.20 \pm 0.05$	$+0.27 \pm 0.05$	$+0.24 \pm 0.05$	-0.065	-0.039	\subseteq	\subseteq	\subseteq	C
FSR 172	$[-2.61;-2.49]$ $[-3.01;-2.28]$	$[-6.05;-5.86]$ $[-6.12;-5.43]$	$[+0.26;0.33]$ $[+0.10;0.40]$	$[+0.30;0.37]$ $[+0.16;0.43]$	$[+0.29;0.37]$ $[+0.13;0.43]$			99% C.L.	99% C.L.	99% C.L.	
Case 121	$+0.61 \pm 0.04$	-0.10 ± 0.03	$+0.20 \pm 0.03$	$+0.26 \pm 0.03$	$+0.22 \pm 0.03$	-0.060	-0.026	\subseteq	\subseteq	\subseteq	C
Berkeley 72	$[+0.67;0.88]$ $[+0.30;1.26]$	$[-0.35;-0.13]$ $[-0.65;0.24]$	$[+0.07;0.22]$ $[+0.01;0.48]$	$[+0.11;0.25]$ $[+0.04;0.51]$	$[+0.10;0.25]$ $[+0.04;0.51]$			99% C.L.	99% C.L.	99% C.L.	
NIKC 3-81	$+1.31 \pm 0.02$	$+0.43 \pm 0.02$	$+0.25 \pm 0.02$	$+0.26 \pm 0.02$	$+0.26 \pm 0.02$	-0.006	-0.007	\subseteq	\subseteq	\subseteq	C
Berkeley 14	$[+1.29;1.53]$ $[+0.90;1.80]$	$[+0.29;0.51]$ $[+0.02;0.79]$	$[+0.12;0.27]$ $[-0.05;0.40]$	$[+0.15;0.30]$ $[-0.02;0.43]$	$[+0.13;0.29]$ $[-0.03;0.41]$			68% C.L.	68% C.L.	68% C.L.	
Case 49	-1.40 ± 0.02	-0.38 ± 0.02	$+0.43 \pm 0.03$	$+0.44 \pm 0.03$	$+0.45 \pm 0.03$	-0.010	-0.018				C
NGC 663	$[-1.20;-1.07]$ $[-1.32;-0.95]$	$[+0.40;-0.25]$ $[-0.55;-0.08]$	$[+0.31;0.38]$ $[+0.24;0.44]$	$[+0.35;0.40]$ $[+0.28;0.47]$	$[+0.34;0.40]$ $[+0.27;0.47]$			rejected	rejected	rejected	
S1* 338	-4.15 ± 0.02	$+3.19 \pm 0.02$	$+0.21 \pm 0.02$	$+0.23 \pm 0.02$	$+0.23 \pm 0.02$	-0.019	-0.022	\subseteq	\subseteq	\subseteq	S
BH 55	$[-4.03;-3.85]$ $[-4.20;-3.63]$	$[+3.09;3.23]$ $[+2.97;3.34]$	$[+0.16;0.27]$ $[+0.02;0.36]$	$[+0.19;0.30]$ $[+0.05;0.39]$	$[+0.18;0.28]$ $[+0.04;0.38]$			99% C.L.	99% C.L.	99% C.L.	
[D75b] Star 30	$+0.64 \pm 0.04$	-0.20 ± 0.03	$+0.29 \pm 0.03$	$+0.33 \pm 0.03$	$+0.31 \pm 0.03$	-0.037	-0.019	\subseteq	\subseteq	\subseteq	MS
NGC 1798	$[+0.71;0.90]$ $[+0.44;1.19]$	$[-0.44;-0.28]$ $[-0.75;0.08]$	$[+0.15;0.25]$ $[+0.07;0.35]$	$[+0.19;0.28]$ $[+0.09;0.38]$	$[+0.17;0.27]$ $[+0.08;0.37]$			99% C.L.	99% C.L.	99% C.L.	
CSS 291	-2.61 ± 0.02	$+3.72 \pm 0.02$	$+0.42 \pm 0.02$	$+0.46 \pm 0.02$	$+0.45 \pm 0.02$	-0.039	-0.034	\subseteq	\subseteq	\subseteq	S
Tombaugh 1	$[-2.63;-2.49]$ $[-2.83;-2.27]$	$[+3.76;3.91]$ $[+3.64;4.03]$	$[+0.35;0.42]$ $[+0.28;0.50]$	$[+0.39;0.45]$ $[+0.31;0.53]$	$[+0.39;0.46]$ $[+0.31;0.54]$			99% C.L.	99% C.L.	99% C.L.	
IRAS 23455+6819	-3.37 ± 0.05	-0.70 ± 0.05	$+0.33 \pm 0.05$	$+0.36 \pm 0.05$	$+0.37 \pm 0.05$	-0.027	-0.045	\subseteq	\subseteq	\subseteq	M
King 11	$[-3.49;-3.30]$ $[-3.90;-3.00]$	$[-0.76;-0.56]$ $[-0.97;-0.33]$	$[+0.24;0.36]$ $[+0.08;0.58]$	$[+0.27;0.40]$ $[+0.11;0.61]$	$[+0.27;0.40]$ $[+0.11;0.60]$			68% C.L.	68% C.L.	68% C.L.	
HD 292921	-1.17 ± 0.02	$+0.36 \pm 0.02$	$+0.25 \pm 0.02$	$+0.28 \pm 0.02$	$+0.25 \pm 0.02$	-0.035	-0.008	\subseteq	\subseteq	\subseteq	M
Berkeley 34	$[-1.44;-1.27]$ $[-1.78;-0.91]$	$[+0.12;0.29]$ $[+0.06;0.38]$	$[+0.08;0.24]$ $[-0.01;0.34]$	$[+0.12;0.27]$ $[+0.01;0.37]$	$[+0.09;0.24]$ $[-0.00;0.35]$			99% C.L.	99% C.L.	99% C.L.	
IRAS 09251-5101	-3.79 ± 0.05	$+2.90 \pm 0.05$	$+0.14 \pm 0.05$	$+0.20 \pm 0.05$	$+0.16 \pm 0.05$	-0.060	-0.018	\subseteq	\subseteq	\subseteq	M
BH 67	$[-3.74;-3.54]$ $[-4.19;-3.18]$	$[+2.72;2.92]$ $[+2.42;3.01]$	$[+0.04;0.17]$ $[-0.03;0.28]$	$[+0.07;0.20]$ $[+0.00;0.31]$	$[+0.04;0.17]$ $[-0.02;0.29]$			68% C.L.	68% C.L.	68% C.L.	
2MASS J00161695+5958115	-1.79 ± 0.03	-1.56 ± 0.03	$+0.23 \pm 0.03$	$+0.24 \pm 0.03$	$+0.25 \pm 0.03$	-0.013	-0.028	\subseteq	\subseteq	\subseteq	M
Juchert Saloran 1	$[-1.73;-1.55]$ $[-2.17;-1.33]$	$[-1.42;-1.21]$ $[-1.73;-1.07]$	$[+0.13;0.26]$ $[-0.06;0.38]$	$[+0.16;0.29]$ $[-0.03;0.41]$	$[+0.16;0.29]$ $[-0.03;0.41]$			99% C.L.	99% C.L.	99% C.L.	

Notes: For each star, moving leftward we report: designation, μ_α , μ_δ , π_t (for noZP, L21ZP and G21ZP cases) and their uncertainty, the parallax corrections according to Lindegren et al. (2021a) and Groenewegen (2021), the membership assessments, and the spectral type. For each cluster, in correspondence to each parameter the two intervals indicate the extremes of the confidence regions of 68% and 99%, respectively.

- Aringer, B., Girardi, L., Nowotny, W., Marigo, P., & Lederer, M. T. 2009, *A&A*, 503, 913, doi: [10.1051/0004-6361/200911703](https://doi.org/10.1051/0004-6361/200911703)
- Asplund, M., Grevesse, N., Sauval, A. J., & Scott, P. 2009, *ARA&A*, 47, 481, doi: [10.1146/annurev.astro.46.060407.145222](https://doi.org/10.1146/annurev.astro.46.060407.145222)
- Barnett, J. W., Williams, K. A., Bédard, A., & Bolte, M. 2021, arXiv e-prints, arXiv:2107.06373. <https://arxiv.org/abs/2107.06373>
- Bayo, A., Rodrigo, C., Barrado Y Navascués, D., et al. 2008, *A&A*, 492, 277, doi: [10.1051/0004-6361:200810395](https://doi.org/10.1051/0004-6361:200810395)
- Bedding, T. R., & Zijlstra, A. A. 1998, *ApJL*, 506, L47, doi: [10.1086/311632](https://doi.org/10.1086/311632)
- Beichman et al. 1988, *Infrared Astronomical Satellite (IRAS) Catalogs and Atlases. Volume 1: Explanatory Supplement.*, Vol. 1
- Bellm, E. C., Kulkarni, S. R., Graham, M. J., et al. 2019, *PASP*, 131, 018002, doi: [10.1088/1538-3873/aaecbe](https://doi.org/10.1088/1538-3873/aaecbe)
- Bhardwaj, A., Rejkuba, M., de Grijs, R., et al. 2021, *ApJ*, 909, 200, doi: [10.3847/1538-4357/abdf48](https://doi.org/10.3847/1538-4357/abdf48)
- Bladh, S., Eriksson, K., Marigo, P., Liljegren, S., & Aringer, B. 2019a, *A&A*, 623, A119, doi: [10.1051/0004-6361/201834778](https://doi.org/10.1051/0004-6361/201834778)
- Bladh, S., Liljegren, S., Höfner, S., Aringer, B., & Marigo, P. 2019b, *A&A*, 626, A100, doi: [10.1051/0004-6361/201935366](https://doi.org/10.1051/0004-6361/201935366)
- Bloeker, T., & Schoenberner, D. 1991, *A&A*, 244, L43
- Blum, R. D., Mould, J. R., Olsen, K. A., et al. 2006, *AJ*, 132, 2034, doi: [10.1086/508227](https://doi.org/10.1086/508227)
- Boothroyd, A. I., & Sackmann, I. J. 1988, *ApJ*, 328, 641, doi: [10.1086/166322](https://doi.org/10.1086/166322)
- . 1992, *ApJL*, 393, L21, doi: [10.1086/186441](https://doi.org/10.1086/186441)
- Bossini, D., Vallenari, A., Bragaglia, A., et al. 2019, *A&A*, 623, A108, doi: [10.1051/0004-6361/201834693](https://doi.org/10.1051/0004-6361/201834693)
- Boyer, M. L., McDonald, I., van Loon, J. T., et al. 2008, *AJ*, 135, 1395, doi: [10.1088/0004-6256/135/4/1395](https://doi.org/10.1088/0004-6256/135/4/1395)
- Boyer, M. L., Srinivasan, S., van Loon, J. T., et al. 2011, *AJ*, 142, 103, doi: [10.1088/0004-6256/142/4/103](https://doi.org/10.1088/0004-6256/142/4/103)
- Boyer, M. L., Girardi, L., Marigo, P., et al. 2013, *ApJ*, 774, 83, doi: [10.1088/0004-637X/774/1/83](https://doi.org/10.1088/0004-637X/774/1/83)
- Bressan, A., Marigo, P., Girardi, L., et al. 2012, *MNRAS*, 427, 127, doi: [10.1111/j.1365-2966.2012.21948.x](https://doi.org/10.1111/j.1365-2966.2012.21948.x)
- Bruzual, A. G. 2007, in *Stellar Populations as Building Blocks of Galaxies*, ed. A. Vazdekis & R. Peletier, Vol. 241, 125–132, doi: [10.1017/S1743921307007624](https://doi.org/10.1017/S1743921307007624)
- Caffau, E., Ludwig, H. G., Steffen, M., Freytag, B., & Bonifacio, P. 2011, *SoPh*, 268, 255, doi: [10.1007/s11207-010-9541-4](https://doi.org/10.1007/s11207-010-9541-4)
- Cantat-Gaudin, T., & Anders, F. 2020, *A&A*, 633, A99, doi: [10.1051/0004-6361/201936691](https://doi.org/10.1051/0004-6361/201936691)
- Cantat-Gaudin, T., Jordi, C., Vallenari, A., et al. 2018, *A&A*, 618, A93, doi: [10.1051/0004-6361/201833476](https://doi.org/10.1051/0004-6361/201833476)
- Cantat-Gaudin, T., Anders, F., Castro-Ginard, A., et al. 2020, *A&A*, 640, A1, doi: [10.1051/0004-6361/202038192](https://doi.org/10.1051/0004-6361/202038192)
- Cardelli, J. A., Clayton, G. C., & Mathis, J. S. 1989, *ApJ*, 345, 245, doi: [10.1086/167900](https://doi.org/10.1086/167900)
- Carraro, G., & Ortolani, S. 1994, *A&A*, 291, 106
- Carrera, R., Bragaglia, A., Cantat-Gaudin, T., et al. 2019, *A&A*, 623, A80, doi: [10.1051/0004-6361/201834546](https://doi.org/10.1051/0004-6361/201834546)
- Castro-Ginard, A., Jordi, C., Luri, X., Cantat-Gaudin, T., & Balaguer-Núñez, L. 2019, *A&A*, 627, A35, doi: [10.1051/0004-6361/201935531](https://doi.org/10.1051/0004-6361/201935531)
- Castro-Ginard, A., Jordi, C., Luri, X., et al. 2020, *A&A*, 635, A45, doi: [10.1051/0004-6361/201937386](https://doi.org/10.1051/0004-6361/201937386)
- Catchpole, R. M., & Feast, M. W. 1973, *MNRAS*, 164, 11P, doi: [10.1093/mnras/164.1.11P](https://doi.org/10.1093/mnras/164.1.11P)
- Chen, X., Wang, S., Deng, L., et al. 2020, *ApJS*, 249, 18, doi: [10.3847/1538-4365/ab9cae](https://doi.org/10.3847/1538-4365/ab9cae)
- Chen, Y., Bressan, A., Girardi, L., et al. 2015, *MNRAS*, 452, 1068, doi: [10.1093/mnras/stv1281](https://doi.org/10.1093/mnras/stv1281)
- Chiavassa, A., Freytag, B., & Schultheis, M. 2018, *A&A*, 617, L1, doi: [10.1051/0004-6361/201833844](https://doi.org/10.1051/0004-6361/201833844)
- Cioni, M. R. L., Blommaert, J. A. D. L., Groenewegen, M. A. T., et al. 2003, *A&A*, 406, 51, doi: [10.1051/0004-6361:20030707](https://doi.org/10.1051/0004-6361:20030707)
- Costa, G., Bressan, A., Mapelli, M., et al. 2021, *MNRAS*, 501, 4514, doi: [10.1093/mnras/staa3916](https://doi.org/10.1093/mnras/staa3916)
- Cristallo, S., Piersanti, L., Straniero, O., et al. 2011, *ApJS*, 197, 17, doi: [10.1088/0067-0049/197/2/17](https://doi.org/10.1088/0067-0049/197/2/17)
- Cummings, J. D., Kalirai, J. S., Tremblay, P. E., Ramirez-Ruiz, E., & Choi, J. 2018, *ApJ*, 866, 21, doi: [10.3847/1538-4357/aadfd6](https://doi.org/10.3847/1538-4357/aadfd6)
- Cutri, R. M., 1, a., 2, a., et al. 2014, *VizieR Online Data Catalog*, II/328
- Cutri, R. M., Skrutskie, M. F., van Dyk, S., et al. 2003, *VizieR Online Data Catalog*, II/246
- Dalcanton, J. J., Williams, B. F., Seth, A. C., et al. 2009, *ApJS*, 183, 67, doi: [10.1088/0067-0049/183/1/67](https://doi.org/10.1088/0067-0049/183/1/67)
- Dalcanton, J. J., Williams, B. F., Lang, D., et al. 2012, *ApJS*, 200, 18, doi: [10.1088/0067-0049/200/2/18](https://doi.org/10.1088/0067-0049/200/2/18)
- Dell’Agli, F., Ventura, P., Schneider, R., et al. 2015, *MNRAS*, 447, 2992, doi: [10.1093/mnras/stu2559](https://doi.org/10.1093/mnras/stu2559)
- Dias, W. S., Monteiro, H., Moitinho, A., et al. 2021, *MNRAS*, 504, 356, doi: [10.1093/mnras/stab770](https://doi.org/10.1093/mnras/stab770)
- Doherty, C. L., Gil-Pons, P., Siess, L., Lattanzio, J. C., & Lau, H. H. B. 2015, *MNRAS*, 446, 2599, doi: [10.1093/mnras/stu2180](https://doi.org/10.1093/mnras/stu2180)
- Egan, M. P., Price, S. D., Kraemer, K. E., et al. 2003, *VizieR Online Data Catalog*, V/114

- Eggen, O. J., & Iben, Icko, J. 1991, *AJ*, 101, 1377, doi: [10.1086/115773](https://doi.org/10.1086/115773)
- Eggleton, P. P. 1967, *MNRAS*, 135, 243, doi: [10.1093/mnras/135.3.243](https://doi.org/10.1093/mnras/135.3.243)
- El-Badry, K., Rix, H.-W., & Weisz, D. R. 2018, *ApJL*, 860, L17, doi: [10.3847/2041-8213/aaca9c](https://doi.org/10.3847/2041-8213/aaca9c)
- Eriksson, K., Nowotny, W., Höfner, S., Aringer, B., & Wachter, A. 2014, *A&A*, 566, A95, doi: [10.1051/0004-6361/201323241](https://doi.org/10.1051/0004-6361/201323241)
- Feast, M. W., Glass, I. S., Whitelock, P. A., & Catchpole, R. M. 1989, *MNRAS*, 241, 375, doi: [10.1093/mnras/241.3.375](https://doi.org/10.1093/mnras/241.3.375)
- Ferrarotti, A. S., & Gail, H. P. 2006, *A&A*, 447, 553, doi: [10.1051/0004-6361:20041198](https://doi.org/10.1051/0004-6361:20041198)
- Ferreira, F. A., Corradi, W. J. B., Maia, F. F. S., Angelo, M. S., & Santos, J. F. C., J. 2020, *MNRAS*, 496, 2021, doi: [10.1093/mnras/staa1684](https://doi.org/10.1093/mnras/staa1684)
- Fragkou, V., Parker, Q. A., Zijlstra, A., Shaw, R., & Lykou, F. 2019, *MNRAS*, 484, 3078, doi: [10.1093/mnras/stz108](https://doi.org/10.1093/mnras/stz108)
- Freedman, W. L., Madore, B. F., Hoyt, T., et al. 2020, *ApJ*, 891, 57, doi: [10.3847/1538-4357/ab7339](https://doi.org/10.3847/1538-4357/ab7339)
- Frogel, J. A., Mould, J., & Blanco, V. M. 1990, *ApJ*, 352, 96, doi: [10.1086/168518](https://doi.org/10.1086/168518)
- Frost, C. A., Cannon, R. C., Lattanzio, J. C., Wood, P. R., & Forestini, M. 1998, *A&A*, 332, L17. <https://arxiv.org/abs/astro-ph/9710054>
- Frost, C. A., & Lattanzio, J. C. 1996, *ApJ*, 473, 383, doi: [10.1086/178152](https://doi.org/10.1086/178152)
- Gaia Collaboration, Brown, A. G. A., Vallenari, A., et al. 2018, *A&A*, 616, A1, doi: [10.1051/0004-6361/201833051](https://doi.org/10.1051/0004-6361/201833051)
- . 2021, *A&A*, 649, A1, doi: [10.1051/0004-6361/202039657](https://doi.org/10.1051/0004-6361/202039657)
- Gaustad, J. E., & Conti, P. S. 1971, *PASP*, 83, 351, doi: [10.1086/129135](https://doi.org/10.1086/129135)
- Geller, A. M., Hurley, J. R., & Mathieu, R. D. 2013, *AJ*, 145, 8, doi: [10.1088/0004-6256/145/1/8](https://doi.org/10.1088/0004-6256/145/1/8)
- Girardi, L. 2016, *ARA&A*, 54, 95, doi: [10.1146/annurev-astro-081915-023354](https://doi.org/10.1146/annurev-astro-081915-023354)
- Girardi, L., Groenewegen, M. A. T., Hatziminaoglou, E., & da Costa, L. 2005, *A&A*, 436, 895, doi: [10.1051/0004-6361:20042352](https://doi.org/10.1051/0004-6361:20042352)
- Girardi, L., & Marigo, P. 2007, *A&A*, 462, 237, doi: [10.1051/0004-6361:20065249](https://doi.org/10.1051/0004-6361:20065249)
- Girardi, L., Marigo, P., Bressan, A., & Rosenfield, P. 2013, *ApJ*, 777, 142, doi: [10.1088/0004-637X/777/2/142](https://doi.org/10.1088/0004-637X/777/2/142)
- Girardi, L., Mermilliod, J. C., & Carraro, G. 2000, *A&A*, 354, 892. <https://arxiv.org/abs/astro-ph/0001068>
- Girardi, L., Rubele, S., & Kerber, L. 2009, *MNRAS*, 394, L74, doi: [10.1111/j.1745-3933.2008.00614.x](https://doi.org/10.1111/j.1745-3933.2008.00614.x)
- Girardi, L., Williams, B. F., Gilbert, K. M., et al. 2010, *ApJ*, 724, 1030, doi: [10.1088/0004-637X/724/2/1030](https://doi.org/10.1088/0004-637X/724/2/1030)
- Girardi, L., Boyer, M. L., Johnson, L. C., et al. 2020, *ApJ*, 901, 19, doi: [10.3847/1538-4357/abad3a](https://doi.org/10.3847/1538-4357/abad3a)
- Glebbeek, E., Gaburov, E., Portegies Zwart, S., & Pols, O. R. 2013, *MNRAS*, 434, 3497, doi: [10.1093/mnras/stt1268](https://doi.org/10.1093/mnras/stt1268)
- Glebbeek, E., & Pols, O. R. 2008, *A&A*, 488, 1017, doi: [10.1051/0004-6361:200809931](https://doi.org/10.1051/0004-6361:200809931)
- Goldman, S. R., Boyer, M. L., McQuinn, K. B. W., et al. 2019, *ApJ*, 877, 49, doi: [10.3847/1538-4357/ab0965](https://doi.org/10.3847/1538-4357/ab0965)
- Gosnell, N. M., Mathieu, R. D., Geller, A. M., et al. 2015, *ApJ*, 814, 163, doi: [10.1088/0004-637X/814/2/163](https://doi.org/10.1088/0004-637X/814/2/163)
- Goswami, S., Slemmer, A., Marigo, P., et al. 2021, *A&A*, 650, A203, doi: [10.1051/0004-6361/202039842](https://doi.org/10.1051/0004-6361/202039842)
- Groenewegen, M. 2021, arXiv e-prints, arXiv:2106.08128. <https://arxiv.org/abs/2106.08128>
- Groenewegen, M. A. T., & Sloan, G. C. 2018, *A&A*, 609, A114, doi: [10.1051/0004-6361/201731089](https://doi.org/10.1051/0004-6361/201731089)
- Groenewegen, M. A. T., Sloan, G. C., Soszyński, I., & Petersen, E. A. 2009, *A&A*, 506, 1277, doi: [10.1051/0004-6361/200912678](https://doi.org/10.1051/0004-6361/200912678)
- Groenewegen, M. A. T., van den Hoek, L. B., & de Jong, T. 1995, *A&A*, 293, 381
- Groenewegen, M. A. T., Whitelock, P. A., Smith, C. H., & Kerschbaum, F. 1998, *MNRAS*, 293, 18, doi: [10.1046/j.1365-8711.1998.01113.x](https://doi.org/10.1046/j.1365-8711.1998.01113.x)
- Groenewegen, M. A. T., Vlemmings, W. H. T., Marigo, P., et al. 2016, *A&A*, 596, A50, doi: [10.1051/0004-6361/201629590](https://doi.org/10.1051/0004-6361/201629590)
- Gullieuszik, M., Groenewegen, M. A. T., Cioni, M. R. L., et al. 2012, *A&A*, 537, A105, doi: [10.1051/0004-6361/201117493](https://doi.org/10.1051/0004-6361/201117493)
- Hartwick, F. D. A., & Hesser, J. E. 1971, *PASP*, 83, 53, doi: [10.1086/129067](https://doi.org/10.1086/129067)
- . 1973, *ApJ*, 183, 883, doi: [10.1086/152275](https://doi.org/10.1086/152275)
- Herwig, F., Schoenberner, D., & Bloeker, T. 1998, *A&A*, 340, L43. <https://arxiv.org/abs/astro-ph/9811076>
- Hills, J. G., & Day, C. A. 1976, *Astrophys. Lett.*, 17, 87
- Holl, B., Audard, M., Nienartowicz, K., et al. 2018, *A&A*, 618, A30, doi: [10.1051/0004-6361/201832892](https://doi.org/10.1051/0004-6361/201832892)
- Huang, Y., Yuan, H., Beers, T. C., & Zhang, H. 2021, *ApJL*, 910, L5, doi: [10.3847/2041-8213/abe69a](https://doi.org/10.3847/2041-8213/abe69a)
- Humphreys, R. M., & Davidson, K. 1979, *ApJ*, 232, 409, doi: [10.1086/157301](https://doi.org/10.1086/157301)
- Hurley, J. R., Pols, O. R., Aarseth, S. J., & Tout, C. A. 2005, *MNRAS*, 363, 293, doi: [10.1111/j.1365-2966.2005.09448.x](https://doi.org/10.1111/j.1365-2966.2005.09448.x)
- Hurley, J. R., Tout, C. A., Aarseth, S. J., & Pols, O. R. 2001, *MNRAS*, 323, 630, doi: [10.1046/j.1365-8711.2001.04220.x](https://doi.org/10.1046/j.1365-8711.2001.04220.x)

- Hurley, J. R., Tout, C. A., & Pols, O. R. 2002, *MNRAS*, 329, 897, doi: [10.1046/j.1365-8711.2002.05038.x](https://doi.org/10.1046/j.1365-8711.2002.05038.x)
- Ishihara, D., Onaka, T., Kataza, H., et al. 2010, *A&A*, 514, A1, doi: [10.1051/0004-6361/200913811](https://doi.org/10.1051/0004-6361/200913811)
- Ita, Y., & Matsunaga, N. 2011, *MNRAS*, 412, 2345, doi: [10.1111/j.1365-2966.2010.18056.x](https://doi.org/10.1111/j.1365-2966.2010.18056.x)
- Ita, Y., Matsunaga, N., Tanabé, T., et al. 2018, *MNRAS*, 481, 4206, doi: [10.1093/mnras/sty2539](https://doi.org/10.1093/mnras/sty2539)
- Ita, Y., Menzies, J. W., Whitelock, P. A., et al. 2021, *MNRAS*, 500, 82, doi: [10.1093/mnras/staa3251](https://doi.org/10.1093/mnras/staa3251)
- Iwanek, P., Kozłowski, S., Gromadzki, M., et al. 2021, arXiv e-prints, arXiv:2107.03397. <https://arxiv.org/abs/2107.03397>
- Jadhav, V. V., & Subramaniam, A. 2021, *MNRAS*, 507, 1699, doi: [10.1093/mnras/stab2264](https://doi.org/10.1093/mnras/stab2264)
- Jaschek, M., & Keenan, P. C., eds. 1985, Carbon stars and S stars near open clusters -a statistical approach., Vol. 114, 181, doi: [10.1007/978-94-009-5325-3_22](https://doi.org/10.1007/978-94-009-5325-3_22)
- Jayasinghe, T., Stanek, K. Z., Kochanek, C. S., et al. 2019, *MNRAS*, 485, 961, doi: [10.1093/mnras/stz444](https://doi.org/10.1093/mnras/stz444)
- Jeffery, E. J., von Hippel, T., van Dyk, D. A., et al. 2016, *ApJ*, 828, 79, doi: [10.3847/0004-637X/828/2/79](https://doi.org/10.3847/0004-637X/828/2/79)
- Jorgensen, U. G., & Westerlund, B. E. 1988, *A&AS*, 72, 193
- Kalinowski, J. K., Burkhead, M. S., & Honeycutt, R. K. 1974, *ApJL*, 193, L77, doi: [10.1086/181636](https://doi.org/10.1086/181636)
- Kalirai, J. S., Marigo, P., & Tremblay, P.-E. 2014, *ApJ*, 782, 17, doi: [10.1088/0004-637X/782/1/17](https://doi.org/10.1088/0004-637X/782/1/17)
- Kamath, D., Karakas, A. I., & Wood, P. R. 2012, *ApJ*, 746, 20, doi: [10.1088/0004-637X/746/1/20](https://doi.org/10.1088/0004-637X/746/1/20)
- Kamath, D., Wood, P. R., Soszyński, I., & Lebzelter, T. 2010, *MNRAS*, 408, 522, doi: [10.1111/j.1365-2966.2010.17137.x](https://doi.org/10.1111/j.1365-2966.2010.17137.x)
- Karakas, A. I. 2014, *MNRAS*, 445, 347, doi: [10.1093/mnras/stu1727](https://doi.org/10.1093/mnras/stu1727)
- Karakas, A. I., Lattanzio, J. C., & Pols, O. R. 2002, *PASA*, 19, 515, doi: [10.1071/AS02013](https://doi.org/10.1071/AS02013)
- Karakas, A. I., & Lugaro, M. 2016, *ApJ*, 825, 26, doi: [10.3847/0004-637X/825/1/26](https://doi.org/10.3847/0004-637X/825/1/26)
- Keenan, P. C., & Boeshaar, P. C. 1980, *ApJS*, 43, 379, doi: [10.1086/190673](https://doi.org/10.1086/190673)
- Kerschbaum, F., & Hron, J. 1992, *A&A*, 263, 97
- Kharchenko, N. V., Piskunov, A. E., Schilbach, E., Röser, S., & Scholz, R. D. 2013, *A&A*, 558, A53, doi: [10.1051/0004-6361/201322302](https://doi.org/10.1051/0004-6361/201322302)
- Kiss, L. L., Szatmáry, K., Szabó, G., & Mattei, J. A. 2000, *A&AS*, 145, 283, doi: [10.1051/aas:2000353](https://doi.org/10.1051/aas:2000353)
- Krone-Martins, A., & Moitinho, A. 2014, *A&A*, 561, A57, doi: [10.1051/0004-6361/201321143](https://doi.org/10.1051/0004-6361/201321143)
- Kroupa, P. 2002, *Science*, 295, 82, doi: [10.1126/science.1067524](https://doi.org/10.1126/science.1067524)
- Kučinskas, A., Hauschildt, P. H., Ludwig, H. G., et al. 2005, *A&A*, 442, 281, doi: [10.1051/0004-6361:20053028](https://doi.org/10.1051/0004-6361:20053028)
- Lambert, D. L., Gustafsson, B., Eriksson, K., & Hinkle, K. H. 1986, *ApJS*, 62, 373, doi: [10.1086/191145](https://doi.org/10.1086/191145)
- Lattanzio, J. C., & Wood, P. R. 2004, *Evolution, Nucleosynthesis, and Pulsation of AGB Stars*, 23–104, doi: [10.1007/978-1-4757-3876-6_2](https://doi.org/10.1007/978-1-4757-3876-6_2)
- Lebzelter, T., & Hinkle, K. H. 2002, *A&A*, 393, 563, doi: [10.1051/0004-6361:20021085](https://doi.org/10.1051/0004-6361:20021085)
- Lebzelter, T., Lederer, M. T., Cristallo, S., et al. 2008, *A&A*, 486, 511, doi: [10.1051/0004-6361:200809363](https://doi.org/10.1051/0004-6361:200809363)
- Lebzelter, T., Mowlavi, N., Marigo, P., et al. 2018, *A&A*, 616, L13, doi: [10.1051/0004-6361/201833615](https://doi.org/10.1051/0004-6361/201833615)
- Lebzelter, T., Nowotny, W., Hinkle, K. H., Höfner, S., & Aringer, B. 2014, *A&A*, 567, A143, doi: [10.1051/0004-6361/201424078](https://doi.org/10.1051/0004-6361/201424078)
- Lebzelter, T., Trabucchi, M., Mowlavi, N., et al. 2019, *A&A*, 631, A24, doi: [10.1051/0004-6361/201936395](https://doi.org/10.1051/0004-6361/201936395)
- Lebzelter, T., & Wood, P. R. 2005, *A&A*, 441, 1117, doi: [10.1051/0004-6361:20053464](https://doi.org/10.1051/0004-6361:20053464)
- Leiner, E. M., & Geller, A. 2021, *ApJ*, 908, 229, doi: [10.3847/1538-4357/abd7e9](https://doi.org/10.3847/1538-4357/abd7e9)
- Leonard, P. J. T. 1989, *AJ*, 98, 217, doi: [10.1086/115138](https://doi.org/10.1086/115138)
- Lindegren, L., Hernández, J., Bombrun, A., et al. 2018, *A&A*, 616, A2, doi: [10.1051/0004-6361/201832727](https://doi.org/10.1051/0004-6361/201832727)
- Lindegren, L., Bastian, U., Biermann, M., et al. 2021a, *A&A*, 649, A4, doi: [10.1051/0004-6361/202039653](https://doi.org/10.1051/0004-6361/202039653)
- Lindegren, L., Klioner, S. A., Hernández, J., et al. 2021b, *A&A*, 649, A2, doi: [10.1051/0004-6361/202039709](https://doi.org/10.1051/0004-6361/202039709)
- Liu, L., & Pang, X. 2019, *ApJS*, 245, 32, doi: [10.3847/1538-4365/ab530a](https://doi.org/10.3847/1538-4365/ab530a)
- Madore, B. F. 1982, *ApJ*, 253, 575, doi: [10.1086/159659](https://doi.org/10.1086/159659)
- Maraston, C. 2005, *MNRAS*, 362, 799, doi: [10.1111/j.1365-2966.2005.09270.x](https://doi.org/10.1111/j.1365-2966.2005.09270.x)
- Maraston, C., Daddi, E., Renzini, A., et al. 2006, *ApJ*, 652, 85, doi: [10.1086/508143](https://doi.org/10.1086/508143)
- Marigo, P. 2001, *A&A*, 370, 194, doi: [10.1051/0004-6361:20000247](https://doi.org/10.1051/0004-6361:20000247)
- Marigo, P. 2015, in *Astronomical Society of the Pacific Conference Series*, Vol. 497, Why Galaxies Care about AGB Stars III: A Closer Look in Space and Time, ed. F. Kerschbaum, R. F. Wing, & J. Hron, 229. <https://arxiv.org/abs/1411.3126>
- Marigo, P., & Aringer, B. 2009, *A&A*, 508, 1539, doi: [10.1051/0004-6361/200912598](https://doi.org/10.1051/0004-6361/200912598)
- Marigo, P., Bressan, A., Nanni, A., Girardi, L., & Pumo, M. L. 2013, *MNRAS*, 434, 488, doi: [10.1093/mnras/stt1034](https://doi.org/10.1093/mnras/stt1034)
- Marigo, P., & Girardi, L. 2007, *A&A*, 469, 239, doi: [10.1051/0004-6361:20066772](https://doi.org/10.1051/0004-6361:20066772)

- Marigo, P., Girardi, L., & Bressan, A. 1999, *A&A*, 344, 123.
<https://arxiv.org/abs/astro-ph/9901235>
- Marigo, P., Girardi, L., Bressan, A., et al. 2017, *ApJ*, 835, 77, doi: [10.3847/1538-4357/835/1/77](https://doi.org/10.3847/1538-4357/835/1/77)
- Marigo, P., Cummings, J. D., Curtis, J. L., et al. 2020, *Nature Astronomy*, 4, 1102, doi: [10.1038/s41550-020-1132-1](https://doi.org/10.1038/s41550-020-1132-1)
- Masci, F. J., Laher, R. R., Rusholme, B., et al. 2019, *PASP*, 131, 018003, doi: [10.1088/1538-3873/aae8ac](https://doi.org/10.1088/1538-3873/aae8ac)
- Mathieu, R. D., & Geller, A. M. 2009, *Nature*, 462, 1032, doi: [10.1038/nature08568](https://doi.org/10.1038/nature08568)
- Mattsson, L., Wahlin, R., & Höfner, S. 2010, *A&A*, 509, A14, doi: [10.1051/0004-6361/200912084](https://doi.org/10.1051/0004-6361/200912084)
- McCrea, W. H. 1964, *MNRAS*, 128, 147, doi: [10.1093/mnras/128.2.147](https://doi.org/10.1093/mnras/128.2.147)
- McDonald, I., Boyer, M. L., van Loon, J. T., & Zijlstra, A. A. 2011a, *ApJ*, 730, 71, doi: [10.1088/0004-637X/730/2/71](https://doi.org/10.1088/0004-637X/730/2/71)
- McDonald, I., & Trabucchi, M. 2019, *MNRAS*, 484, 4678, doi: [10.1093/mnras/stz324](https://doi.org/10.1093/mnras/stz324)
- McDonald, I., van Loon, J. T., Decin, L., et al. 2009, *MNRAS*, 394, 831, doi: [10.1111/j.1365-2966.2008.14370.x](https://doi.org/10.1111/j.1365-2966.2008.14370.x)
- McDonald, I., van Loon, J. T., Sloan, G. C., et al. 2011b, *MNRAS*, 417, 20, doi: [10.1111/j.1365-2966.2011.18963.x](https://doi.org/10.1111/j.1365-2966.2011.18963.x)
- Meixner, M., Gordon, K. D., Indebetouw, R., et al. 2006, *AJ*, 132, 2268, doi: [10.1086/508185](https://doi.org/10.1086/508185)
- Momany, Y., Saviane, I., Smette, A., et al. 2012, *A&A*, 537, A2, doi: [10.1051/0004-6361/201117223](https://doi.org/10.1051/0004-6361/201117223)
- Monteiro, H., Dias, W. S., Moitinho, A., et al. 2020, *MNRAS*, 499, 1874, doi: [10.1093/mnras/staa2983](https://doi.org/10.1093/mnras/staa2983)
- Mowlavi, N., Lecoœur-Taïbi, I., Lebzelter, T., et al. 2018, *A&A*, 618, A58, doi: [10.1051/0004-6361/201833366](https://doi.org/10.1051/0004-6361/201833366)
- Nanni, A., Bressan, A., Marigo, P., & Girardi, L. 2014, *MNRAS*, 438, 2328, doi: [10.1093/mnras/stt2348](https://doi.org/10.1093/mnras/stt2348)
- Nanni, A., Groenewegen, M. A. T., Aringer, B., et al. 2019, *MNRAS*, 487, 502, doi: [10.1093/mnras/stz1255](https://doi.org/10.1093/mnras/stz1255)
- Nanni, A., Marigo, P., Girardi, L., et al. 2018, *MNRAS*, 473, 5492, doi: [10.1093/mnras/stx2641](https://doi.org/10.1093/mnras/stx2641)
- Noël, N. E. D., Greggio, L., Renzini, A., Carollo, C. M., & Maraston, C. 2013, *ApJ*, 772, 58, doi: [10.1088/0004-637X/772/1/58](https://doi.org/10.1088/0004-637X/772/1/58)
- O'Donnell, J. E. 1994, *ApJ*, 422, 158, doi: [10.1086/173713](https://doi.org/10.1086/173713)
- Paczyński, B. 1970, *AcA*, 20, 47
- Pal, T., & Worthey, G. 2021, *MNRAS*, 506, 3669, doi: [10.1093/mnras/stab1967](https://doi.org/10.1093/mnras/stab1967)
- Pastorelli, G., Marigo, P., Girardi, L., et al. 2019, *MNRAS*, 485, 5666, doi: [10.1093/mnras/stz725](https://doi.org/10.1093/mnras/stz725)
- . 2020, *MNRAS*, 498, 3283, doi: [10.1093/mnras/staa2565](https://doi.org/10.1093/mnras/staa2565)
- Paxton, B., Bildsten, L., Dotter, A., et al. 2011, *ApJS*, 192, 3, doi: [10.1088/0067-0049/192/1/3](https://doi.org/10.1088/0067-0049/192/1/3)
- Paxton, B., Cantiello, M., Arras, P., et al. 2013, *ApJS*, 208, 4, doi: [10.1088/0067-0049/208/1/4](https://doi.org/10.1088/0067-0049/208/1/4)
- Paxton, B., Marchant, P., Schwab, J., et al. 2015, *ApJS*, 220, 15, doi: [10.1088/0067-0049/220/1/15](https://doi.org/10.1088/0067-0049/220/1/15)
- Paxton, B., Schwab, J., Bauer, E. B., et al. 2018, *ApJS*, 234, 34, doi: [10.3847/1538-4365/aaa5a8](https://doi.org/10.3847/1538-4365/aaa5a8)
- Pessev, P. M., Goudfrooij, P., Puzia, T. H., & Chandar, R. 2008, *MNRAS*, 385, 1535, doi: [10.1111/j.1365-2966.2008.12935.x](https://doi.org/10.1111/j.1365-2966.2008.12935.x)
- Piatti, A. E., Angelo, M. S., & Dias, W. S. 2019, *MNRAS*, 488, 4648, doi: [10.1093/mnras/stz2050](https://doi.org/10.1093/mnras/stz2050)
- Platais, I., Pourbaix, D., Jorissen, A., et al. 2003, *A&A*, 397, 997, doi: [10.1051/0004-6361:20021589](https://doi.org/10.1051/0004-6361:20021589)
- Rain, M. J., Ahumada, J., & Carraro, G. 2021, arXiv e-prints, arXiv:2103.06004, <https://arxiv.org/abs/2103.06004>
- Reid, M. J., & Goldston, J. E. 2002, *ApJ*, 568, 931, doi: [10.1086/338947](https://doi.org/10.1086/338947)
- Riebel, D., Boyer, M. L., Srinivasan, S., et al. 2015, *ApJ*, 807, 1, doi: [10.1088/0004-637X/807/1/1](https://doi.org/10.1088/0004-637X/807/1/1)
- Riess, A. G., Casertano, S., Yuan, W., et al. 2021, *ApJL*, 908, L6, doi: [10.3847/2041-8213/abdbaf](https://doi.org/10.3847/2041-8213/abdbaf)
- Rosenfield, P., Marigo, P., Girardi, L., et al. 2014, *ApJ*, 790, 22, doi: [10.1088/0004-637X/790/1/22](https://doi.org/10.1088/0004-637X/790/1/22)
- Salaris, M., Serenelli, A., Weiss, A., & Miller Bertolami, M. 2009, *ApJ*, 692, 1013, doi: [10.1088/0004-637X/692/2/1013](https://doi.org/10.1088/0004-637X/692/2/1013)
- Salaris, M., Weiss, A., & Percival, S. M. 2004, *A&A*, 414, 163, doi: [10.1051/0004-6361:20031578](https://doi.org/10.1051/0004-6361:20031578)
- Samus', N. N., Kazarovets, E. V., Durlевич, O. V., Kireeva, N. N., & Pastukhova, E. N. 2017, *Astronomy Reports*, 61, 80, doi: [10.1134/S1063772917010085](https://doi.org/10.1134/S1063772917010085)
- Sargent, B. A., Srinivasan, S., & Meixner, M. 2011, *ApJ*, 728, 93, doi: [10.1088/0004-637X/728/2/93](https://doi.org/10.1088/0004-637X/728/2/93)
- Schöier, F. L., & Olofsson, H. 2001, *A&A*, 368, 969, doi: [10.1051/0004-6361:20010072](https://doi.org/10.1051/0004-6361:20010072)
- Shappee, B., Prieto, J., Stanek, K. Z., et al. 2014, in *American Astronomical Society Meeting Abstracts*, Vol. 223, American Astronomical Society Meeting Abstracts #223, 236.03
- Shetye, S., Van Eck, S., Jorissen, A., et al. 2021, *A&A*, 650, A118, doi: [10.1051/0004-6361/202040207](https://doi.org/10.1051/0004-6361/202040207)
- Siegel, M. H., LaPorte, S. J., Porterfield, B. L., Hagen, L. M. Z., & Gronwall, C. A. 2019, *AJ*, 158, 35, doi: [10.3847/1538-3881/ab21e1](https://doi.org/10.3847/1538-3881/ab21e1)
- Siess, L. 2010, *A&A*, 512, A10, doi: [10.1051/0004-6361/200913556](https://doi.org/10.1051/0004-6361/200913556)
- Sills, A., Karakas, A., & Lattanzio, J. 2009, *ApJ*, 692, 1411, doi: [10.1088/0004-637X/692/2/1411](https://doi.org/10.1088/0004-637X/692/2/1411)

- Slemer, A., Marigo, P., Piatti, D., et al. 2017, *MNRAS*, 465, 4817, doi: [10.1093/mnras/stw3029](https://doi.org/10.1093/mnras/stw3029)
- Soszyński, I. 2007, *ApJ*, 660, 1486, doi: [10.1086/513012](https://doi.org/10.1086/513012)
- Soszyński, I., & Udalski, A. 2014, *ApJ*, 788, 13, doi: [10.1088/0004-637X/788/1/13](https://doi.org/10.1088/0004-637X/788/1/13)
- Soszyński, I., Wood, P. R., & Udalski, A. 2013, *ApJ*, 779, 167, doi: [10.1088/0004-637X/779/2/167](https://doi.org/10.1088/0004-637X/779/2/167)
- Soszynski, I., Udalski, A., Kubiak, M., et al. 2005, *AcA*, 55, 331. <https://arxiv.org/abs/astro-ph/0512578>
- Soszyński, I., Dziembowski, W. A., Udalski, A., et al. 2007, *AcA*, 57, 201
- Soszyński, I., Udalski, A., Szymański, M. K., et al. 2009, *AcA*, 59, 239. <https://arxiv.org/abs/0910.1354>
- . 2011, *AcA*, 61, 217. <https://arxiv.org/abs/1109.1143>
- Soszyński, I., Olechowska, A., Ratajczak, M., et al. 2021, *ApJL*, 911, L22, doi: [10.3847/2041-8213/abf3c9](https://doi.org/10.3847/2041-8213/abf3c9)
- Srinivasan, S., Sargent, B. A., & Meixner, M. 2011, *A&A*, 532, A54, doi: [10.1051/0004-6361/201117033](https://doi.org/10.1051/0004-6361/201117033)
- Stassun, K. G., & Torres, G. 2021, *ApJL*, 907, L33, doi: [10.3847/2041-8213/abdaad](https://doi.org/10.3847/2041-8213/abdaad)
- Suárez, O., García-Lario, P., Manchado, A., et al. 2006, *A&A*, 458, 173, doi: [10.1051/0004-6361:20054108](https://doi.org/10.1051/0004-6361:20054108)
- Sun, M., Mathieu, R. D., Leiner, E. M., & Townsend, R. H. D. 2021, *ApJ*, 908, 7, doi: [10.3847/1538-4357/abd402](https://doi.org/10.3847/1538-4357/abd402)
- Tadross, A. L. 2009, *NewA*, 14, 200, doi: [10.1016/j.newast.2008.08.004](https://doi.org/10.1016/j.newast.2008.08.004)
- Trabucchi, M., Mowlavi, N., & Lebzelter, T. 2021a, arXiv e-prints, arXiv:2109.04293. <https://arxiv.org/abs/2109.04293>
- Trabucchi, M., Wood, P. R., Montalbán, J., et al. 2017, *ApJ*, 847, 139, doi: [10.3847/1538-4357/aa8998](https://doi.org/10.3847/1538-4357/aa8998)
- . 2019, *MNRAS*, 482, 929, doi: [10.1093/mnras/sty2745](https://doi.org/10.1093/mnras/sty2745)
- Trabucchi, M., Wood, P. R., Mowlavi, N., et al. 2021b, *MNRAS*, 500, 1575, doi: [10.1093/mnras/staa3356](https://doi.org/10.1093/mnras/staa3356)
- Tuchman, Y., Glasner, A., & Barkat, Z. 1983, *ApJ*, 268, 356, doi: [10.1086/160958](https://doi.org/10.1086/160958)
- van Loon, J. T., Zijlstra, A. A., Whitelock, P. A., et al. 1998, *A&A*, 329, 169. <https://arxiv.org/abs/astro-ph/9709119>
- VanderPlas, J. T. 2018, *ApJS*, 236, 16, doi: [10.3847/1538-4365/aab766](https://doi.org/10.3847/1538-4365/aab766)
- Vassiliadis, E., & Wood, P. R. 1993, *ApJ*, 413, 641, doi: [10.1086/173033](https://doi.org/10.1086/173033)
- Ventura, P., & D’Antona, F. 2005, *A&A*, 431, 279, doi: [10.1051/0004-6361:20041917](https://doi.org/10.1051/0004-6361:20041917)
- Ventura, P., D’Antona, F., & Mazzitelli, I. 2000, *A&A*, 363, 605. <https://arxiv.org/abs/astro-ph/0101374>
- Ventura, P., Karakas, A., Dell’Agli, F., García-Hernández, D. A., & Guzman-Ramirez, L. 2018, *MNRAS*, 475, 2282, doi: [10.1093/mnras/stx3338](https://doi.org/10.1093/mnras/stx3338)
- Ventura, P., Karakas, A. I., Dell’Agli, F., et al. 2015, *MNRAS*, 450, 3181, doi: [10.1093/mnras/stv918](https://doi.org/10.1093/mnras/stv918)
- Wagenhuber, J., & Groenewegen, M. A. T. 1998, *A&A*, 340, 183. <https://arxiv.org/abs/astro-ph/9809338>
- Wagstaff, G., Miller Bertolami, M. M., & Weiss, A. 2020, *MNRAS*, 493, 4748, doi: [10.1093/mnras/staa362](https://doi.org/10.1093/mnras/staa362)
- Weiss, A., & Ferguson, J. W. 2009, *A&A*, 508, 1343, doi: [10.1051/0004-6361/200912043](https://doi.org/10.1051/0004-6361/200912043)
- Wenger, M., Ochsenbein, F., Egret, D., et al. 2000, *A&AS*, 143, 9, doi: [10.1051/aas:2000332](https://doi.org/10.1051/aas:2000332)
- Whitelock, P. A., Feast, M. W., & Van Leeuwen, F. 2008, *MNRAS*, 386, 313, doi: [10.1111/j.1365-2966.2008.13032.x](https://doi.org/10.1111/j.1365-2966.2008.13032.x)
- Whitelock, P. A., Kasliwal, M., & Boyer, M. 2017, in *European Physical Journal Web of Conferences*, Vol. 152, *European Physical Journal Web of Conferences*, 01009, doi: [10.1051/epjconf/201715201009](https://doi.org/10.1051/epjconf/201715201009)
- Wood, P. R. 2000, *PASA*, 17, 18, doi: [10.1071/AS00018](https://doi.org/10.1071/AS00018)
- . 2015, *MNRAS*, 448, 3829, doi: [10.1093/mnras/stv289](https://doi.org/10.1093/mnras/stv289)
- Wood, P. R., & Nicholls, C. P. 2009, *ApJ*, 707, 573, doi: [10.1088/0004-637X/707/1/573](https://doi.org/10.1088/0004-637X/707/1/573)
- Wood, P. R., & Sebo, K. M. 1996, *MNRAS*, 282, 958, doi: [10.1093/mnras/282.3.958](https://doi.org/10.1093/mnras/282.3.958)
- Wood, P. R., & Zarro, D. M. 1981, *ApJ*, 247, 247, doi: [10.1086/159032](https://doi.org/10.1086/159032)
- Wood, P. R., Alcock, C., Allsman, R. A., et al. 1999, in *Asymptotic Giant Branch Stars*, ed. T. Le Bertre, A. Lebre, & C. Waelkens, Vol. 191, 151
- Yu, J., Bedding, T. R., Stello, D., et al. 2020, *MNRAS*, 493, 1388, doi: [10.1093/mnras/staa300](https://doi.org/10.1093/mnras/staa300)
- Zhong, J., Chen, L., Wu, D., et al. 2020, *A&A*, 640, A127, doi: [10.1051/0004-6361/201937131](https://doi.org/10.1051/0004-6361/201937131)
- Zinn, J. C. 2021, *AJ*, 161, 214, doi: [10.3847/1538-3881/abe936](https://doi.org/10.3847/1538-3881/abe936)

ACKNOWLEDGMENTS

We acknowledge the support from the ERC Consolidator Grant funding scheme (project STARKEY, grant agreement n. 615604), and from PRD 2021, University of Padova. This work has made use of data from the European Space Agency (ESA) mission *Gaia* (<https://www.cosmos.esa.int/gaia>), processed by the *Gaia* Data Processing and Analysis Consortium (DPAC, <https://www.cosmos.esa.int/web/gaia/dpac/consortium>). Funding for the DPAC has been provided by national institutions, in particular the institutions participating in the *Gaia* Multilateral Agreement. This research has made use of the Virtual Observatory Sed Analyzer (VOSA), developed under the Spanish Virtual Observatory project supported by the Spanish MINECO through grant AyA2017-84089. This research has made use of "Aladin sky atlas" developed at CDS, Strasbourg Observatory, France. DB acknowledges supported by FCT through the research grants UIDB/04434/2020, UIDP/04434/2020 and PTDC/FIS-AST/30389/2017, and by FEDER - Fundo Europeu de Desenvolvimento Regional through COMPETE2020 - Programa Operacional Competitividade e Internacionalização (grant: POCI-01-0145-FEDER-030389).

Software: VOSA (Bayo et al. 2008), MESA (Paxton et al. 2011, 2013, 2015, 2018), TRILEGAL (Girardi et al. 2005), PARSEC (Bressan et al. 2012), COLIBRI (Marigo et al. 2013), AESOPUS (Marigo & Aringer 2009).